REPUBLIQUE ALGERIENNE DEMOCRATIQUE ET POPULAIRE

MINISTERE DE L'ENSEIGNEMENT SUPERIEUR ET DE LA RECHERCHE SCIENTIFIQUE

UNIVERSITE ECHAHID HAMMA LAKHDAR D'EL OUED

Faculté de la Technologie

Département de Génie Electrique

Laboratoire de Valorisation des Technologies des Ressources Sahariennes (VTRS)

Thèse de Doctorat

Présentée par :

MERAH Hana

En vue de l'obtention du diplôme de DOCTORAT LMD en :

Option: Réseaux Electriques

Contribution à l'optimisation de l'énergie des réseaux électriques par les méthodes métaheuristiques en présence des systèmes FACTS et des énergies renouvelables

Soutenue le …./ …./ ……., devant le jury composé de :

BENCHOUIA Mohamed Toufik	Professeur	Université de Biskra	Président
BENATTOUS Djilani	Professeur	Université d'El Oued	Directeur de thèse
GACEM Abdelmalek	MCA	Université d'El Oued	Co-Directeur de thèse
RABHI Boualaga	Professeur	Université de Biskra	Examinateur
ZELLOUMA Laid	Professeur	Université d'El Oued	Examinateur

Année Universitaire 2023/2024

PEOPLE'S DEMOCRATIC REPUBLIC OF ALGERIA

MINISTRY OF HIGHER EDUCATION AND SCIENTIFIC RESEARCH

UNIVERSITY OF ECHAHID HAMMA LAKHDAR EL OUED

Faculty of Technology

Laboratory of Valorisation and Technology of Sahara Resources (VTRS)

Doctoral Thesis

Presented by:

MERAH Hana

With a view to obtaining the **LMD DOCTORATE** diploma in:

Specialty: Electrical Networks

Contribution to the Optimization of Electrical Network Energy using Metaheuristic Methods in the Presence of FACTS Systems and Renewable Energies

Defended on …./ …./ ……., before the jury composed of:

Dissertation Committee:

BENCHOUIA Mohamed Toufik	Professor	University of Biskra	President
BENATTOUS Djilani	Professor	University of El Oued	Supervisor
GACEM Abdelmalek	MCA	University of El Oued	Co-supervisor
RABHI Boualaga	Professor	University of Biskra	Examiner
ZELLOUMA Laid	Professor	University of El Oued	Examiner

Academic year 2023/2024

Acknowledgments

*I want to convey my gratitude to **ALLAH** for giving me the strength to finish my thesis after years of hard labour. First and foremost, praise be to him.*

*I would like to express my heartfelt appreciation and gratitude to my supervisor, **Mr. BENATTOUS Djilani**, Professor at the University of El Oued, for his guidance, support, and determination to see this project through to completion.*

*I would like to thank **Dr. GACEM Abdelmalek**, Lecturer A at the University of El Oued, for his involvement in proposing the doctoral topic, as well as his ongoing support, unlimited encouragement, and guidance throughout my years of work.*

*I would also like to thank all of the jury members: **Prof. BENCHOUIA Mohamed Toufik** at the University of Biskra, and **Prof. RABHI Boualaga** at the University of Biskra, **Prof. ZELLOUMA Laid** at the University of El Oued, for their interest in my work and acceptance of discussing this thesis, as well as those in charge of the Department of Electrical Engineering at the University of the EL Oued, including administration and faculty members.*

*I would also like to thank all members of the **VTRS** laboratory for their welcome and assistance throughout this research project.*

*I would like to express my sincere appreciation to **Prof. Mariam AHMAD SAMEH** from Egypt for her unwavering support and encouragement throughout my research career.*

*I'd like to express my gratitude to **Professors BELOUL Said** and **KHECHEKHOUCHE Abderrahmane** in particular for their continuous encouragement and assistance throughout the project's completion.*

Finally, I want to express my heartfelt gratitude to my family, particularly my parents and friends, for their consistent encouragement, compassion, and emotional support throughout my academic path.

This research would not have been possible without the invaluable help and encouragement from these exceptional individuals and groups. Thank you for being a part of this journey.

Dedication

I dedicate this thesis to the most important persons in my life

my beloved mother and father.

For my sisters and brother.

To all of my teachers.

To all my dear friends, particularly Ilham, Soumeia, Mariam, Zineb, and Ikram.

My path to this Ph.D. was not easy, but I was able to complete it because of your constant encouragement and support.

MERAH Hana

INTERNATIONAL PUBLICATIONS

1. **H. Merah**, A. Gacem, D. Benattous, A. Lashab, F. Jurado, M. Sameh, “Sizing and sitting of static VAR compensator (SVC) using hybrid optimization of combined Cuckoo search (CS)and Antlion Optimization (ALO) Algorithms”. Energies 2022, 15(13).

INTERNATIONAL COMMUNICATIONS

1. **H. Merah**, A. Gacem, D. Benattous, Y. Labbi, M. Om Parkash, “Solving Economic Dispatch Problem Using a New Hybrid PSO-ALO Algorithm”, CCSSP'2020, March 16-17,2020, University of El Oued.
2. **H. Merah**, A. Gacem, D. Benattous, “Economic Dispatch Solution of Renewable Integrated Micro-Grid using Multi-verse optimizer “, fmcrea21, October 27-28, 2021, University of El Oued.
3. **H. Merah**, A. Gacem, D. Benattous, Y. Labbi, Z. Driss, “Combined Economic and Emission Dispatch Solution Using Hybrid PSO-ALO Algorithm”, ICME'2019, December 19-21, 2019, University of Monastir, TUNISIA.

NATIONAL COMMUNICATIONS

1. **H. Merah**, A. Gacem, D. Benattous, Y. Labbi, “Coordinated Design of SVC and PSS Controllers Using PSO Algorithm for Damping Power System Oscillations”, ISTSID'2019, February 24-26, 2019, University of El Oued.

ملخص

في هذه الأطروحة، قدمنا استراتيجية لتحسين كفاءة الشبكة الكهربائية من خلال الجمع بين نظام نقل التيار المتردد المرن (FACTS) ومصادر الطاقة المتجددة، مثل طاقة الرياح والطاقة الشمسية. يعالج هذا المسعى تحديًا كبيرًا يتطلب التخطيط الدقيق للتشغيل الأمثل للنظام. ولمواجهة هذا التحدي، استخدمنا نهج تدفق الطاقة الأمثل (OPF) باستخدام خوارزمية دبور العنكبوت (SWO). كان هدفنا هو المعالجة الفعالة لمختلف المشكلات المتعلقة بالشبكة، بما في ذلك تقليل فقدان الطاقة، وخفض تكاليف الوقود والانبعاثات البيئية، وتحسين مستويات الجهد. علاوة على ذلك، لمعالجة المشكلات متعددة الأهداف، قمنا بتوسيع الخوارزمية إلى خوارزمية متعددة الأهداف (خوارزمية الدبور العنكبوتية المتعددة الأهداف (MOSWO)) والتحقق من صحة أدائها بعناية باستخدام كل من الوظائف الرياضية والهندسية. عند مقارنتها بالحلول الموجودة في الأدبيات، توضح النتائج التي توصلنا إليها بلا منازع الأداء المتفوق لكل من الخوارزميات الفردية والمتعددة الأهداف. من ناحية أخرى، في التكامل الاقتصادي للطاقة المتجددة، مع أو بدون تحديد المواضع والقيم المناسبة للمعوضات الاستاتيكية للقدرة غير الفعالة (SVCs)، فإن هدفنا الرئيسي هو تقليل تكاليف التوليد الإجمالية من خلال الجدولة الفعالة للوحدات الحرارية وطاقة الرياح والطاقة الشمسية. توضح نتائج خوارزمية SWO بشكل لا لبس فيه أن تحديد المواقع والقيم المثالية لأجهزة FACTS بالتزامن مع توربينات الرياح والألواح الشمسية يحسن أداء النظام بشكل كبير من الناحيتين التقنية والاقتصادية، كل ذلك مع الالتزام بالقيود التشغيلية المفروضة.

الكلمات مفتاحية: مصادر الطاقة المتجددة, تدفق الطاقة الأمثل, المعوضات الاستاتيكية للقدرة غير الفعالة, أنظمة مرنة للنقل بالتيار المتناوب, SWO, MOSWO.

abstract

In this thesis, we presented a strategy to improve the efficiency of the electrical network by combining a Flexible AC transmission system (FACTS) with renewable energy sources, such as wind and solar power. This endeavour addresses a substantial challenge that necessitates meticulous planning for the optimal operation of the system. To address this challenge, we employed an Optimal Power Flow (OPF) approach utilizing the Spider Wasp Optimizer (SWO) algorithm. Our objective was to effectively address various network-related issues, including minimizing power losses, reducing fuel costs and environmental emissions, and optimizing voltage levels. Furthermore, to tackle multi-objective problems, we expanded the algorithm to a multi-objective algorithm (Multi-Objective Spider Wasp (MOSWO) algorithm) and carefully validated its performance using both mathematical and geometric functions. When compared to existing solutions in the literature, our findings indisputably illustrate the superior performance of both single- and multi-objective algorithms. On the other hand, in the economic integration of renewable energy, with or without the determination of appropriate placements and values of Static Var Compensators (SVCs), our main objective is to minimize overall generation costs through efficient scheduling of thermal, wind, and solar units. The SWO algorithm results unmistakably demonstrate that identifying optimal locations and values for

FACTS devices in conjunction with wind turbines and solar panels significantly improves system performance from both a technical and economic standpoint, all while adhering to the imposed operational constraints.

Keywords: Renewable energy sources, Optimal Power Flow, Static Var Compensators, FACTS devices, SWO, MOSWO

Résumé

Dans cette thèse, nous avons présenté une stratégie pour améliorer l'efficacité du réseau électrique en combinant un système de transmission flexible en courant alternatif (FACTS) avec des sources d'énergie renouvelables, telles que l'énergie éolienne et solaire. Cet effort répond à un défi de taille qui nécessite une planification méticuleuse pour le fonctionnement optimal du système. Pour relever ce défi, nous avons utilisé une approche écoulement de puissance optimale (OPF) utilisant l'algorithme de guêpe araignée (SWO). Notre objectif était de résoudre efficacement divers problèmes liés au réseau, notamment en minimisant les pertes de puissance, en réduisant les coûts de carburant et les émissions environnementales, et en optimisant les niveaux de tension. De plus, pour résoudre des problèmes multi-objectifs, nous avons étendu l'algorithme à un algorithme multi-objectif (Algorithme de guêpe-araignée multi-objectifs (MOSWO)) et soigneusement validé ses performances à l'aide de fonctions mathématiques et géométriques. Par rapport aux solutions existantes dans la littérature, nos résultats illustrent incontestablement les performances supérieures des algorithmes à objectif unique et multi-objectif. D'autre part, dans l'intégration économique des énergies renouvelables, avec ou sans détermination de l'emplacement et des valeurs appropriés des compensateurs de var statique (SVC), notre objectif principal est de minimiser les coûts globaux de production grâce à une planification efficace des unités thermiques, éoliennes et solaires. Les résultats de l'algorithme SWO démontrent sans équivoque que l'identification des emplacements et des valeurs optimaux pour les dispositifs FACTS en conjonction avec des éoliennes et des panneaux solaires améliore considérablement les performances du système d'un point de vue technique et économique, tout en respectant les contraintes opérationnelles imposées.

Mots Clés : Sources d'énergie renouvelables, écoulement de puissance optimale, compensateurs de var statique, dispositifs FACTS, SWO, MOSWO.

Table of Contents

List of Figures

Chapter IV

Chapter V

List of Tables

Chapter IV

Chapter V

List of Abbreviations and Symbols

Abbreviation	
OPF	Optimal power flow.
MOOPF	Multi-objective optimal power flow.
MOO	Multi-objective optimization.
IEEE	Institute of Electrical and Electronics Engineers.
NOx	Nitrogen oxides.
p.u.	Per unit.
PF	¨Pareto front.
SOx	Sulfur oxides.
Symbols	
f	Fitness function.
x	State variables.
u	Control variables.
$g(x,u)$	Equality constraints.
$h(x,u)$	Inequality constraints.
NG	The number of generators.
NC	The number of shunt capacitors
NT	The number of transformers tapping.
NL	Total number of load buses.
NTL	Total number of power transmission lines.

ECHT-DE	An ensemble of these two constraint handling techniques with differential evolution.
GA	Genetic Algorithm.
HFPSO	Hybrid firefly particle swarm optimization.
HGS	Hunger games search.
HHO	Harris hawks optimization.
IBSA	Improved bird swarm algorithm.
IEO	Improved equilibrium optimizer.
ISSA	Improved salp swarm algorithm algorithm.
MAOA	Multi-objective arithmetic optimization Algorithm.
MOEA/D	A multi-objective evolutionary algorithm based on decomposition.
MOEA/D DAE	Multi-objective evolutionary algorithm with detect-and-escape constraint technique.
MOEMA	Multi-objective electromagnetism-like algorithm.
MOGOA	Multi-objective grasshopper optimization algorithm.
MOHCS	Multi-objective hunger game search.
MOHHO	Multi-objective harris hawks Optimization.
MO-IPSO	Multi-objective improved particle swarm optimisation.
MOJaya	Multi-objective jaya.
MOMICA	Multi-mbjective modified imperialist competitive algorithm
MOPSO	Multi-mbjective particle Swarm optimization.
MOSMA	Multi-objective slime mould algorithm.

N_{PQ}	Total number of load buses.	NSGA2	Non-dominated sorting genetic algorithm.
NB	Total number of buses.	PSO	Particle swarm optimization.
P_{Gi}	Active power produced by generator i.	PSO–Fuzzy	particle swarm optimization and Fuzzy satisfaction maximization approach.
P_{Di}	Active power requested at bus i	rNSGA2	Reference solution-based NSGA2.
P_{Gi}^{max}	Lower and upper limits of active power generation at i-th bus.	SF-DE	superiority of feasibly solutions with differential evolution.
Q_{Gi}	Reactive power produced by generator i.	SMA	Slime mould algorithm.
Q_{Di}	Reactive power requested at bus i.	SSA	Sparrow search algorithm.
$Q_{Gi}^{min}, Q_{Gi}^{max}$	Lower and upper limits of reactive power generation at i-th bus.	TiGEA-2	A tri-goal evolution.
Q_{Ci}	The reactive power compensator at the i-th bus.	TS	Tabu search.
Q_{Ci}^{max}	The lowest and maximum values of the reactive power compensator at the i-th bus.	**Symbols for SWO**	
S_{li}	Transmission line loading of i-th branch.	$r, r_1, r_2, r_3, r_5, r_6, p$	Randomly generated values within the interval [0, 1].
S_{li}^{max}	Maximum transmission line load capacity.	a, b	Two indices selected at random from the population.
T_i	Transformer tap setting of i-th branch.	l	Random value created within the range of 1 to -2.
T_i^{min}, T_i^{max}	The lower and upper limits of the Transformer tap setting value at the i th branch.	C	Distance control factor.
V_i	Voltage magnitude at bus i.	TR	Tradeoff rate.
V_j	Voltage magnitude at bus j.	c	An index chosen randomly from the population.
V_{Gi}	Voltage magnitude at the i-th generator bus.	γ	Number created using the levy flight CR.
$V_{Gi}^{min}, V_{Gi}^{max}$	Lower and upper limits of Voltage magnitude at the i-th generator bus.	X_m^t	Male spider wasp.
V_{Li}	Load voltage value at i-th bus	X_i^t	Female spider wasp.
V_{Li}^{max}	Voltage magnitude boundaries at load buses.	CR	The crossover rate.
a_i, b_i, c_i	Coefficients of the cost function of each generator i.	β, β_1, rn	Random number created utilizing the normal distribution

$\alpha_i, \beta_i, \gamma_i, \delta_i, \varepsilon_i$	The pollution emission coefficients for unit i.

Abbreviation of algorithms

GTLBO	Adaptive Gaussian Teaching–learning-based optimization.
BB-MPSO	bare- bones modified particle swarm optimization.
BSOA	Beetle swarm optimization algorithm.
CS-GWO	Crisscross search based grey wolf optimizer.
DE	Differential evolution.

T_{max}	A maximum iteration count.
N_{pop}	Population sizes.
$Arch\_size$	The maximum size of the archive.
ns_i	Number of solutions in the ith hypercube.
μ_2	The proposed parameter for determining the search direction.
nGrid	The number of grids per dimension.

GENERAL

INRODUCTION

General introduction

The power grid plays a crucial role in supplying electricity to meet the growing energy demands of modern society. However, traditional power grids face several challenges that hinder their efficient and reliable operation. These challenges include the reliance on fossil fuels, environmental pollution, grid instability, and the need for grid expansion to accommodate increasing energy demands. To address these issues and move towards a sustainable energy future, renewable energy sources and Static Var Compensators (SVCs) have emerged as enabling solutions for the power grid.

Renewable energy sources, such as solar power and wind power, offer a clean and abundant alternative to traditional fossil fuel-based generation. They harness natural resources that are renewable and do not deplete over time. By integrating renewable energy sources into the power grid, we can reduce carbon emissions, mitigate climate change, and minimize the environmental impact of electricity generation. Moreover, the decentralization of renewable energy generation allows for localized power production, reducing transmission losses and enhancing grid resilience.

However, the intermittent nature of renewable energy sources poses challenges to the power grid. The variability of solar and wind power generation can cause imbalances in the supply-demand equation, leading to grid instability and voltage fluctuations. To address these issues, SVCs have gained prominence as devices that can enhance the integration of renewable energy sources in the power grid.

Static Var Compensators (SVCs) are one of the types of flexible AC transmission system (FACTS) devices that regulate voltage levels, improve power factor, and provide reactive power support to the grid. bad positioning and sizing of FACTS can lead to a malfunction of the system. SVCs can help maintain grid stability and voltage quality by dynamically adjusting their reactive power output. By deploying SVCs strategically in the power grid, the voltage fluctuations caused by intermittent renewable energy sources can be mitigated, ensuring a more stable and reliable power supply.

The problem of integrating renewable energies and SVC sources is related to achieving an ideal balance between renewable energy production and consumption, and providing electrical stability and energy quality in the grid. This problem is complex and includes technical, economic and operational challenges.

To solve this complex problem, the optimal power flow (OPF) approach can be used. Where it is considered an optimization technique that seeks to reach the best scheduling of control variables to decrease a particular objective function taking into account the achievement of the permissible limits in the system. The objective functions that are reduced in the OPF problem are fuel cost, environmental pollutant emissions, active power losses, voltage deviation, stability of voltage, while taking into account the constraints of equality and inequality.

To solve the OPF problem with the presence of renewable energy sources and SVCs, a metaheuristic optimization algorithm is utilized. Metaheuristic algorithms are powerful optimization techniques inspired by natural phenomena or human behavior, capable of exploring large solution spaces and finding near-optimal solutions for complex problems.

This thesis proposes a new approach to address the problem of OPF in power grids, taking into account the incorporation of renewable energy sources such as solar and wind energy, as well as the integration of SVC devices in the appropriate places and with suitable values. The proposed strategy is based on the exceptional mating, nesting, and hunting behavior found in female spider wasps in nature, as well as their ability to explore and exploit prey beneficially.

The suggested method intends to produce significant energy loss reductions, voltage stability improvements, environmental homeostasis, and, eventually, an overall improvement in system performance.

Main contributions of the thesis

The major contribution of this dissertation can be presented in the following key points:

- The Multi-Objective Spider Wasp Optimization (MOSWO) method was developed as an extension to the nature-inspired Spider Wasp Optimizer (SWO) method. The MOSWO algorithm includes efficient methods such as archive, leader selection, and the Grid mechanism, which allow it to handle several targets at the same time.
- The performance of MOSWO was evaluated using nine test functions, five of which were unrestricted and four of which were restricted. The findings were compared to the Multi-Objective Arithmetic Optimization Algorithm (MAOA) [1] and the Multi-Objective Grasshopper Optimization Algorithm (MOGOA) [2]. MOSWO's effectiveness in handling multi-objective optimization problems is demonstrated by three commonly recognized performance indicators.
- The proposed approach in this study has been applied to address the problem of optimal power flow, which is one of the real-world issues. The performance of the

proposed approach was evaluated in seven different scenarios, including single-objective and multi-objective scenarios. These scenarios have been implemented and evaluated on an IEEE 30-bus system.

- Four scenarios out of seven are single objective approaches including reduction of fuel costs, reducing air pollution by minimizing Nitrogen oxide (NOx) emissions, reducing the active power transmission loss, and improving the voltage profile. Equally, the multi-objective approach focuses on three scenarios including minimizing the total generation costs besides the NOx emissions, decreasing total generation costs along with the active power losses, and the last scenario involving minimizing the total generation costs together with the voltage magnitude deviation.
- The spider wasp algorithm (SWO) investigates OPF with renewable energy sources such as solar and wind energy. It considers the total renewable energy costs, which include direct cost, the penalty cost that result from underestimation, and the reserve cost that result from overestimation of available renewable energy. A carbon price has also been incorporated to calculate emissions.
- The proposed approach was used to determine the optimal placements and values for the Static Var Compensators (SVCs) in the IEEE 30-bus system, to improve network performance and efficiency while minimizing losses.

The structure of the thesis

The dissertation is divided into five chapters, as shown in Figure 1.1, with each chapter covering a different aspect of the proposed research. The first chapter begins with an overview of modeling the components of the power grid, followed by a review of the problem of economic dispatch and the formulation of the power flow problem, as well as an examination of the various objective functions.

Chapter 2 introduces the fundamental concepts of FACTS devices and provides an overview of the features that these devices offer to the electric grid, as well as a review of previous studies on the search for optimal location and sizing of FACTS devices using different metaheuristic optimization techniques.

In Chapter 3, an overview of renewable energy systems is offered, followed by an explanation of the foundations of wind and solar energy conversion systems. Chapter 4 explains the fundamental notions of the optimization process and describes the aspects of the problem to be addressed in the optimization process, as well as how to frame the problem as a

single-objective or multi-objective problem. Some natural-inspired optimization methods and a new multi-objective algorithm based on the contemporary spider wasp algorithm are also described. The emphasis in Chapter 5 shifts to the practical application and modeling of the proposed work. A thorough explanation of how the modern optimization method can be effectively used to address the power flow problem is provided, with an emphasis on its seamless integration with solar and wind energy sources, as well as the incorporation of shunt FACTS devices.

Finally, we offer a thorough conclusion that summarizes the research strengths presented in this thesis. Furthermore, we highlight potential future approaches and perspectives that could enrich and supplement our research.

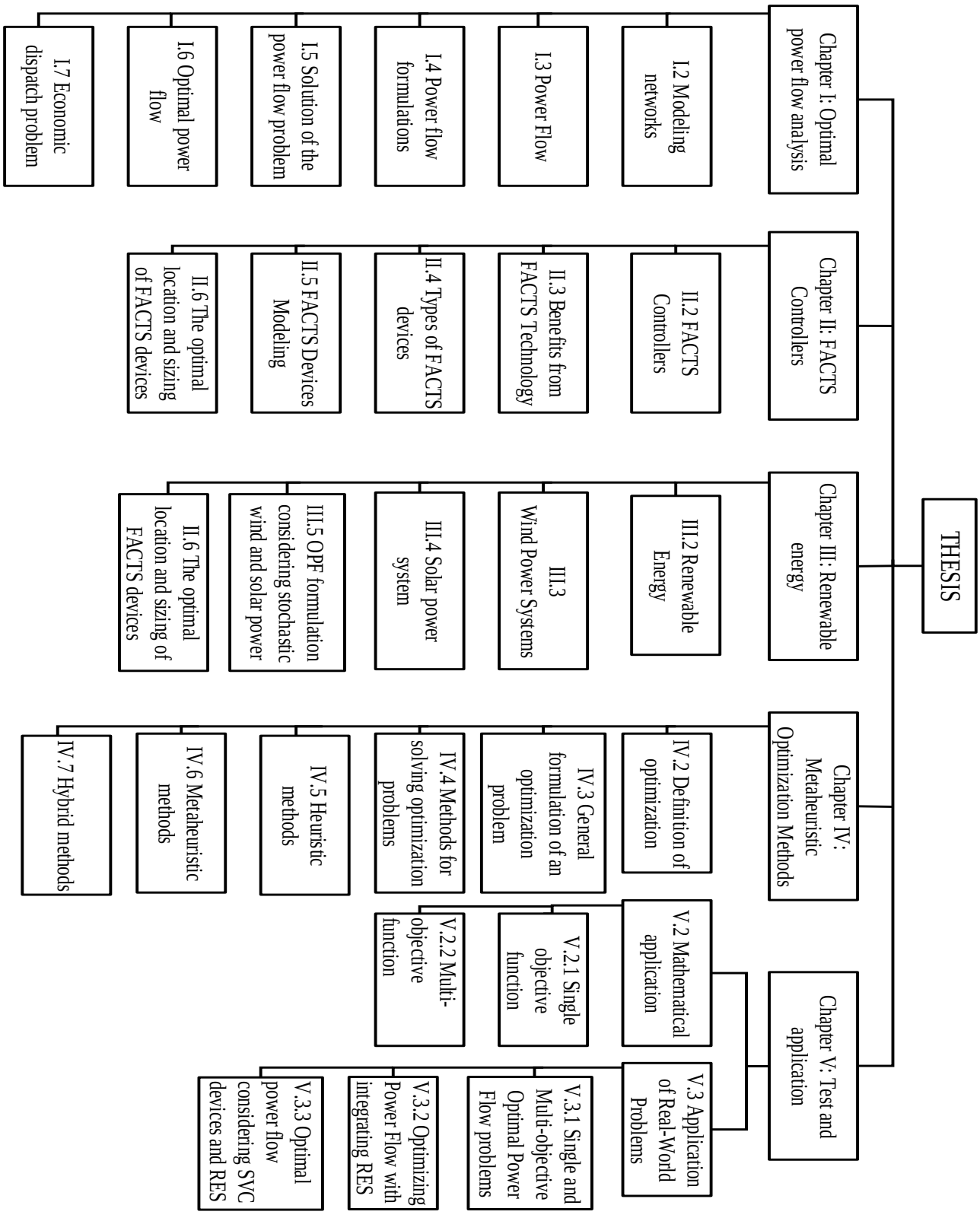

Figure 1.1. Synopsis of the Thesis

Reference

[1] M. Premkumar, P. Jangir, B. S. Kumar, R. Sowmya, H. H. Alhelou, L. Abualigah*, et al.*, "A new arithmetic optimization algorithm for solving real-world multiobjective CEC-2021 constrained

optimization problems: diversity analysis and validations," *IEEE Access,* vol. 9, pp. 84263-84295, 2021.

[2] S. Z. Mirjalili, S. Mirjalili, S. Saremi, H. Faris, and I. Aljarah, "Grasshopper optimization algorithm for multi-objective optimization problems," *Applied Intelligence,* vol. 48, pp. 805-820, 2018.

CHAPTER I

OPTIMAL POWER FLOW

ANALYSIS

I.1 Introduction

Today, rising energy demand and dwindling fossil resource reserves have resulted in a sharp increase in the cost of energy production. As a result, power plants strive to meet demand in the most cost-effective and reliable manner possible. Where it has become necessary to plan the amount of output that will be produced by the current production unit. This problem is defined to minimize operating cost while taking into account system constraints and is known as the optimal power flow problem in power systems.

This chapter provides an overview of power component modeling in the power grid, as well as a brief review of the economic distribution problem, the load flow problem, and a comprehensive model representation of the OPF problem with different objective functions are presented.

I.2 Modeling networks

I.2.1 Generator model

The generator is regarded as the beating heart of the electrical network. It ensures that the consumer's requested electrical energy is produced. In the power flow analysis, the generator is represented as a constant voltage source V_G that injects active P_G and reactive power. Each unit's power is limited in an interval defined as follows:

$$P_{Gi\,min} \leq P_{Gi} \leq P_{Gi\,max} \quad (I.1)$$

$$Q_{Gi\,min} \leq Q_{Gi} \leq Q_{Gi\,max} \quad (I.2)$$

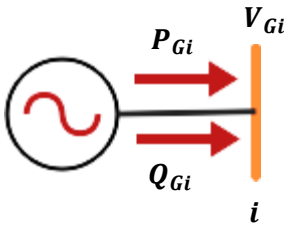

Figure I.1. Generator model.

I.2.2 Line model

The transmission line is generally represented by an π equivalent circuit with a series impedance $Z_{ij} = R_{ij} + jX_{ij}$ (R_{ij} is total resistance between line i and j, and X_{ij} is total

inductive reactance between line i and j) and a shunt admittance $Y_{ij} = jB_{ij}/2$ (B_{ij} is a capacitive susceptance), as shown in Figure I.2.

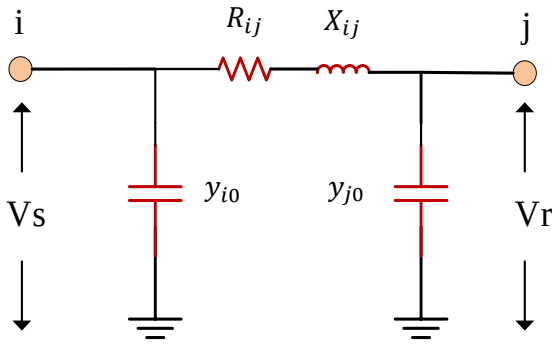

Figure I.2. π model of a transmission line.

The series admittance of transmission line i and j is given by the relation [1]:

$$Y_{ij} = \frac{1}{Z_{ij}} = \frac{1}{R_{ij}+jX_{ij}} \tag{I.3}$$

I.2.3 Transformer model

Power transformers are primarily used in power systems to connect different voltage levels of transmission and distribution systems. Figure I.3 depicts the transformer model that connects buses i and j, which consists of an impedance connected in series with an ideal transformer.

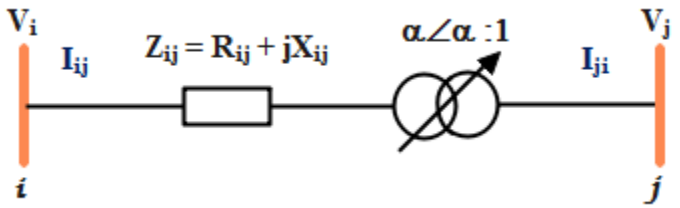

Figure I.3. Power transformer model.

The relationship between bus voltages and line currents in a transformer branch is given as:

$$Y.V = I \tag{I.4}$$

$$\begin{bmatrix} \bar{Y}_{ij} & -\bar{\alpha}\bar{Y}_{ij} \\ -\bar{\alpha}^{*}\bar{Y}_{ij} & \alpha^{2}\bar{Y}_{ij} \end{bmatrix} \begin{bmatrix} \bar{V}_i \\ \bar{V}_j \end{bmatrix} = \begin{bmatrix} \bar{I}_{ij} \\ \bar{I}_{ji} \end{bmatrix} \tag{I.5}$$

Where Y_{ij} denotes the admittance of the transformer inserted between nodes i and j.

$$Y_{ij} = \frac{1}{Z_{ij}} = 1/(R_{ij} + jX_{ij}) \tag{I.6}$$

$$\bar{\alpha} = ae^{j\alpha} = a\angle\alpha \quad \text{(I.7)}$$

With a the complex transformation ratio [1].

I.2.4 Load model

Load modeling is critical in the study and analysis of the problem of reactive energy compensation. In an electrical network, a load is represented by an impedance that consumes a constant amount of active and reactive power.

$$S_{\mathrm{Di}} = P_{\mathrm{Di}} + \mathrm{j}Q_{\mathrm{Di}} \quad \text{(I.8)}$$

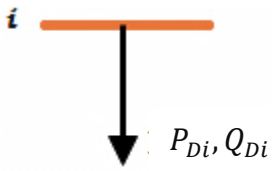

Figure I.4. Load model in power system.

I.2.5 Shunt element

Shunt devices, such as capacitor banks, fixed inductors, and static compensators (SVC), are commonly used for reactive power compensation (consuming reactive power by indicator or supplying reactive power by capacitor) and voltage adjustment. The modeling of these elements will be carried out by an equivalent admittance or by power injection.

I.3 Power Flow

The power flow is defined as the transmission of power from a generator (the source) to a load and is carried out through it with knowledge of the voltage values, the real and reactive power generated and absorbed, and the line losses, and thus it provides an evaluation overview of the power system to determine whether it is working properly or not. Power flow analysis is useful for planning the future expansion of power systems and as well as for determining the best operation of existing systems.

I.3.1 The classification of buses

I.3.1.1 Load Buses

The load bus, also known as the PQ bus, is a bus that is not connected to a generator (i.e., $P_G = Q_G = 0$), and its presence in the power system as a whole is approximately 80%. In this

bus, the real power P_i and reactive power Q_i are known values, whereas the voltage phase angle δ_i and its magnitude $|V_i|$ are calculated by solving power flow equations using various methods (Newton-Raphson, Gauss-Seidel…).

I.3.1.2 Voltage Controlled Buses

These are buses that are linked to generators. The active power P_i and voltage magnitude $|V_i|$ are known to specific values in this bus, but the reactive power Q_i and phase angle δ_i of the voltage are unknown and must be calculated. That is why it is referred to as the PV bus. This bus can also be connected to a VAR device to keep the voltage magnitude constant.

I.3.1.3 Slack Bus

The slack bus is a bus that does not carry any load. Each network has only one bus, and we cannot analyze the load flow without it. This type of bus is typically linked to a large capacity generator capable of balancing power within the grid. In this bus, the known variables are voltage magnitude $|V_i|$and phase angle δ_i, while the unknown variables, P_i and Q_i are calculated using power flow analysis.

I.4 Power flow formulations

The power flow calculation, also known as the load distribution calculation, determines the following: the complex voltages at the different node levels, the conditions given to the buses, such as the capacitive or inductive loads that must be supplied, powers injected at a node, and the active and reactive losses in the power system. To determine the power flow equations in the general case, we assume that the powers at the bus i are balanced; thus, the balance of the electrical powers at a bus i of a power system of N buses is the difference between the complex power of the generator S_{Gi} and the consumed power S_{Di} of the same bus (Figure I.5). The power balance for any bus i can be formulated as:

$$S_i = S_{Gi} - S_{Di} = P_{Gi} - P_{Di} + j(Q_{Gi} - Q_{Di}) \quad \text{(I.9)}$$

$$S_i = S_{Gi} - S_{Di} = \sum_{\substack{j=1 \\ j \neq i}}^{N} S_{ij} \forall i = 1, \dots, N \quad \text{(I.10)}$$

$$P_i = P_{Gi} - P_{Di} \quad \text{(I.11)}$$

$$Q_i = Q_{Gi} - Q_{Di} \quad \text{(I.12)}$$

Where P_i and Q_i represent the injected active and reactive power at bus i, P_{Gi} and Q_{Gi} represent the generated active and reactive power at bus i, and P_{Di} and Q_{Di} represent the active and reactive power load at bus i.

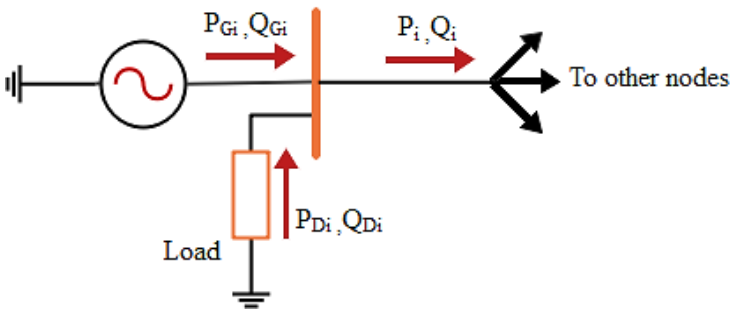

Figure I.5. Power balance at node i.

Eq. (I.3) defining the relationships between currents and voltages at various buses is as follows:

$$I_{BUS} = Y_{BUS} * V_{BUS} \tag{I.13}$$

Where:

I_{BUS}: Current vector for buses.

$$\begin{bmatrix} I_1 \\ I_2 \\ \vdots \\ I_N \end{bmatrix} \tag{I.14}$$

V_{BUS}: Voltage vector for buses.

$$\begin{bmatrix} V_1 \\ V_2 \\ \vdots \\ V_N \end{bmatrix} \tag{I.15}$$

Y_{BUS}: The admittance matrix for the electrical network is defined as:

$$\begin{bmatrix} Y_{11} & Y_{12} & \cdots & Y_{1N} \\ Y_{21} & Y_{22} & \cdots & Y_{2N} \\ \vdots & \vdots & \ddots & \vdots \\ Y_{N1} & Y_{N2} & \cdots & Y_{NN} \end{bmatrix} \tag{I.16}$$

This matrix contains two kinds of elements:

Diagonal elements: Y_{ii} are obtained by summing the admittances connected to node i.

$$Y_{ii} = y_{i0} + \sum_{\substack{j=0 \\ j \neq i}}^{N} y_{ij} \tag{I.17}$$

y_{i0}: The shunt element.

y_{ij}: The off-diagonal element of the Y_{BUS} matrix.

Off-diagonal elements: They are determined by the negative admittance of the line connecting point i to j.

$$Y_{ij} = -\sum_{j\neq i}^{N} y_{ij} \quad \text{(I.18)}$$

Thus, Eq. (I.13) can be reformulated for a system with n nodes as:

$$\begin{bmatrix} I_1 \\ I_2 \\ \vdots \\ I_N \end{bmatrix} = \begin{bmatrix} Y_{11} & Y_{12} & \cdots & Y_{1N} \\ Y_{21} & Y_{22} & \cdots & Y_{2N} \\ \vdots & \vdots & \ddots & \vdots \\ Y_{N1} & Y_{N2} & \cdots & Y_{NN} \end{bmatrix} * \begin{bmatrix} V_1 \\ V_2 \\ \vdots \\ V_N \end{bmatrix} \quad \text{(I.19)}$$

According to Eq. (I.19), the net current that will be injected into a bus i is denoted as follows:

$$I_i = \sum_{j=1}^{N} Y_{ij} * V_j \quad , \quad i = 1,2,3,\dots,N \quad \text{(I.20)}$$

Where:

$$\overline{Y_{ij}} = G_{ik} + j * B_{ij} = Y_{ij}\left(cos\,\theta_{ij} + sin\,\theta_{ij}\right) \quad \text{(I.21)}$$

$$\overline{V_j} = Re_j + j * Im_j = V_j\left(cos\,\theta_j + sin\,\theta_j\right) \quad \text{(I.22)}$$

G_{ij} and B_{ij} are the conductance and succeptance of the admittance $\overline{Y_{ij}}$, respectively.

Re_j and Im_j are the real and imaginary parts of the voltage $\overline{V_j}$, respectively.

θ_j denotes the phase of the voltage at the bus j;

θ_{ij} denotes the phase of the element ij.

The apparent power S injected into a bus can be expressed as follows:

$$S_i = P_i + jQ_i = V_i I_i^* = V_i\left(\sum_{j=1}^{N} Y_{ij}^* * V_j^*\right) \quad \text{(I.23)}$$

P_i and Q_i are the active and reactive powers at bus i respectively.

By substituting Eqs. (I.21) and (I.22) into Eq. (I.23), we obtain:

$$S_i = \sum_{j=1}^{N} V_i|Y_{ij}|V_j\cos\left(\theta_{ij} + \theta_j - \theta_i\right) + j\sum_{j=1}^{N} V_i|Y_{ij}|V_j\sin\left(\theta_{ij} + \theta_j - \theta_i\right) \quad \text{(I.24)}$$

When the real and imaginary parts of Eq (I.24) are separated, we get Eqs. (I.25) and (I.26), which yield:

$$P_i = \sum_{j=1}^{N} V_i|Y_{ij}|V_j\cos\left(\theta_{ij} + \theta_j - \theta_i\right) \quad \text{(I.25)}$$

$$Q_i = \sum_{j=1}^{N} V_i|Y_{ij}|V_j\sin\left(\theta_{ij} + \theta_j - \theta_i\right) \quad \text{(I.26)}$$

Where:

V_i, θ_i: The magnitude and phase of the voltage at node i.

P_i, Q_i: The active and reactive powers injected at the node i.

$\theta_{ij} = \theta_i - \theta_j$: The phase difference between nodes i and j.

I.5 Solution of the power flow problem

I.5.1 Newton-Raphson technique

The Gauss-Seidel method was used at first, which has the disadvantage of converging in a number of iterations proportional to the size of the network, making it unsuitable for large systems. The Newton-Raphson method is currently the most widely used method for solving this problem due to its faster convergence and lower number of iterations when compared to the other methods (Gauss-Seidel). The Taylor series expansions of Eqs. (I.25) and (I.26), respectively, are as follows:

$$\begin{bmatrix} \Delta P \\ \Delta Q \end{bmatrix} = J * \begin{bmatrix} \Delta \theta \\ \Delta V \end{bmatrix} \Rightarrow \begin{bmatrix} \Delta P \\ \Delta Q \end{bmatrix} = \begin{bmatrix} J_1 & J_2 \\ J_3 & J_4 \end{bmatrix} * \begin{bmatrix} \Delta \theta \\ \Delta V \end{bmatrix} \quad \text{(I.27)}$$

Such as:

$$J_1 = \frac{\partial P_i}{\partial \theta_j},\ J_2 = \frac{\partial P_i}{\partial V_j},\ \ J_3 = \frac{\partial Q_i}{\partial \theta_j},\ J_4 = \frac{\partial Q_i}{\partial V_j}$$

$J_1, J_2, J_3,$ and J_4 are the Jacobian submatrices, and they are determined by:

J_1:

$$\frac{\partial P_i}{\partial \theta_i} = \sum_{\substack{j=1 \\ i \neq j}} |Y_{ij}||V_i||V_j| sin(\theta_{ij} + \theta_j - \theta_i) \quad \text{(I.28)}$$

$$\frac{\partial P_i}{\partial \theta_j} = -|Y_{ij}||V_i||V_j| \sin(\theta_{ij} + \theta_j - \theta_i), i \neq j \quad \text{(I.29)}$$

J_2:

$$\frac{\partial P_i}{\partial |V_i|} = 2|Y_{ij}||V_j| cos(\theta_{ii}) + \sum_{i \neq j} |Y_{ij}||V_j| cos(\theta_{ij} + \theta_j - \theta_i) \quad \text{(I.30)}$$

$$\frac{\partial P_i}{\partial |V_j|} = |Y_{ij}||V_i| cos(\theta_{ij} + \theta_j - \theta_i), i \neq j \quad \text{(I.31)}$$

J_3:

$$\frac{\partial Q_i}{\partial \theta_i} = \sum_{i \neq j} |Y_{ij}||V_i||V_j| cos(\theta_{ij} + \theta_j - \theta_i) \quad \text{(I.32)}$$

$$\frac{\partial Q_i}{\partial \theta_j} = -|V_i||V_j||Y_{ij}| cos(\theta_{ij} + \theta_j - \theta_i), i \neq j \quad \text{(I.33)}$$

J_4:

$$\frac{\partial Q_i}{\partial |V_i|} = -2|V_i||Y_{ij}|\,sin(\theta_{ii}) - \sum_{i\neq j}|Y_{ij}||V_j|sin(\theta_{ij}+\theta_j-\theta_i) \quad (I.34)$$

$$\frac{\partial Q_i}{\partial |V_j|} = -|V_i||Y_{ij}|\,sin(\theta_{ij}+\theta_j-\theta_i), i\neq j \quad (I.35)$$

The terms ΔQ and ΔP are defined as the difference between the specified and calculated values, which can be calculated as follows:

$$\Delta P_i^{(k)} = P_i^{spec} - P_i^{(k)} \quad (I.36)$$

$$\Delta Q_i^{(k)} = Q_i^{spec} - Q_i^{(k)} \quad (I.37)$$

The new estimates for bus voltages are given as follows:

$$\delta_i^{(k+1)} \& = \delta_i^{(k)} + \Delta\delta_i^{(k)} \quad (I.38)$$

$$\left|V_i^{(k+1)}\right| \& = \left|V_i^{(k)}\right| + \Delta\left|V_i^{(k)}\right| \quad (I.39)$$

I.6 Optimal power flow

Carpentier first introduced the optimal power flow problem (OPF) in 1962, and it has since become an important and widely studied research topic in electrical power systems research [2]. The OPF aims to reduce total operating cost while meeting system constraints (equality and inequality) and ensuring demand is satisfied.

I.6.1 OPF formulation

The optimal power flow problem is formulated as a nonlinear minimization problem with equality and inequality constraints. The OPF can be solved using one or more objective functions.

The OPF can be expressed mathematically as a single-objective optimization problem as follows:

$$Min: \{f(x,u)\} \quad (I.40)$$

Under the constraints:

$$g_i(x,u) = 0, i = 1,2,3,\dots,m \quad (I.41)$$

$$h_j(x,u) \leq 0, j = 1,2,3,\dots,p \quad (I.42)$$

With: $f(x,u)$ is the objective function to be minimized, x is the state vector, u is the control vector, $g_i(x,u)$ represents equality constraints, and $h_j(x,u)$ represents inequality constraints, and m and p are the equality and inequality constraints numbers, respectively.

I.6.2 Design variables

I.6.2.1 Control variables

Control variables are parameters that can be altered or optimized to meet the intended goal of the power system, and they can be represented as a vector u as follows:

$$u = \left[P_{G_2} \dots P_{G_{NG}}, V_{G_1} \dots V_{G_{NG}}, Q_{C_1} \dots Q_{C_{NC}}, T_1 \dots T_{NT}\right] \quad \text{(I.43)}$$

Where P_{G} stands for the active power outputs at the PV buses (generating buses), excluding the slack bus, V_{G} stands to the magnitude voltage at generator buses. Additionally, NG, NT, and NC denote the number of generators, transformer tapping, and shunt capacitors.

I.6.2.2 State variables

State variables in optimal power flow (OPF) are the variables that result from adjusting control variables and are used to describe the state of a power system grid, and they may be described in the form of a vector x as follows:

$$x = \left[P_{G_1}, V_{L_1} \dots V_{L_{NL}}, Q_{G_1} \dots Q_{G_{NG}}, S_{l_1} \dots S_{l_{NTL}}\right] \quad \text{(I.44)}$$

Where P_{G_1} represents the real power output of the slack or reference bus, V_{L} represents the load voltage value, Q_{G} represents the reactive power released by all generators, and S_{l} denotes line loading. In addition, NL and NTL represent the total number of load buses and power transmission lines, respectively.

I.6.2.3 Disturbance variables

They are variables that cannot be controlled or improved since they depend only on power users. It can be expressed as a vector P as follows:

$$P = \left[P_{D_1} \dots P_{D_{NL}}, Q_{D_1} \dots Q_{D_{NL}}\right] \quad \text{(I.45)}$$

Where P_D and Q_D indicate the demanded active and reactive power, respectively.

I.6.3 Objectives functions

The primary goal of optimal power flow problems is to find the steady-state operating point of the generation-transmission grid, which reduces the predetermined function. The

objective function is also known as the optimization criterion, the adaptive function, or the performance function (the fitness function), and among the most significant target functions in power systems are as follows:

I.6.3.1 Minimization of Fuel Cost of Generation

The first objective function is known as the reduction in total fuel production cost for the system, and it is mathematically modeled as follows:

$$F_1 = \sum_{i=1}^{NG} F_i(P_{Gi}) = \sum_{i=1}^{NG} (a_i + b_i P_{Gi} + c_i P_{Gi}^2) \quad \text{(I.46)}$$

Where P_{Gi} is the active power produced by generator i, a_i, b_i, and c_i are the coefficients of the cost function of each generator i and NG is the number of generating generators.

I.6.3.2 Minimization of Voltage Deviation

Voltage deviation calculation is the most important indicator of service quality and safety in power systems, and it is formulated as reducing the voltage deviations of load buses from a specified value as follows:

$$F_3 = VD = \sum_{i=1}^{NPQ} |(V_i - 1)| \quad \text{(I.47)}$$

Where V_i indicates the voltage magnitude at bus i and NPQ indicates the total number of load buses.

I.6.3.3 Minimization of Active Power Transmission Loss

Active power transmission loss is another objective function of the OPF problem, and its primary goal is to reduce overall real power loss in the power grid. This function is denoted as follows:

$$P_L = \sum_{i=1}^{N_g} P_{Gi} - P_D \quad \text{(I.48)}$$

Where, P_L denotes total active losses, and P_D denotes active power requested.

I.6.3.4 Minimization of Emission

The second objective function seeks to protect the environment by lowering emissions (nitrogen oxides (NOx) and sulfur oxides (SOx)) resulting from the combustion of fossil fuels in electrical plants. The objective function of these emitted gases can be formulated as a quadratic and an exponential function as follows [1, 3]:

$$F_2(x) = \sum_{i=1}^{NG} \left(\alpha_i + \beta_i P_{Gi} + \gamma_i P_{Gi}^2 + \delta_i exp(\varepsilon_i P_{Gi})\right) \quad (I.49)$$

Where: α_i, β_i, γ_i, δ_i, and ε_i are the pollution emission coefficients for unit i.

I.6.4 Objective constraints

The optimal power flow (OPF) problem has two fundamental constraints, namely equality and inequality constraints. Without these constraints, the power delivery to users will be less efficient at a time of need, potentially resulting in problems in the power system.

I.6.4.1 Equality constraints

These constraints are represented by non-linear power flow equations that represent the balance of active and reactive power at each bus.

$$P_{Gi} - P_{Di} - V_i \sum_{j=1}^{NB} V_j\left(G_{ij} cos\,\theta_{ij} + B_{ij} sin\,\theta_{ij}\right) = 0 \quad (I.50)$$

$$Q_{Gi} - Q_{Di} - V_i \sum_{j=1}^{NB} V_j\left(G_{ij} sin\,\theta_{ij} - B_{ij} cos\,\theta_{ij}\right) = 0 \quad (I.51)$$

I.6.4.2 Inequality constraints

Inequality constraints in the OPF include the system operational and security limits such as branch flow boundaries, load bus voltage magnitude boundaries, and generator reactive power output boundaries.

Voltages in all generators, as well as active and reactive powers, should be restricted by the following lower and upper limits:

$$V_{Gi}^{min} \le V_{Gi} \le V_{Gi}^{max}, i = 1, \dots, NG \quad (I.52)$$

$$P_{Gi}^{min} \le P_{Gi} \le P_{Gi}^{max}, i = 1, \dots, NG \quad (I.53)$$

$$Q_{Gi}^{min} \le Q_{Gi} \le Q_{Gi}^{max}, i = 1, \dots, NG \quad (I.54)$$

Limitations of transformer tap settings are represented as follows:

$$T_i^{min} \le T_i \le T_i^{max}, i = 1, \dots, NT \quad (I.55)$$

The reactive compensation power is restricted as follows:

$$Q_{Ci}^{min} \le Q_{Ci} \le Q_{Ci}^{max} i = 1,2, \dots, NC \quad (I.56)$$

Security constraints involve voltage magnitude boundaries at load buses and transmission line loadings as follows:

$$V_{Li}^{min} \leq V_{Li} \leq V_{Li}^{max}, i = 1, \dots, N_{PQ} \quad (I.57)$$

$$S_{li} \leq S_{li}^{max}, i = 1, \dots, NL \quad (I.58)$$

I.7 Economic dispatch problem

The trouble of the economic distribution of energy has garnered considerable importance with the appearance of the energy crisis demanding increasingly costly fuels. It is, therefore, necessary to plan the power output of each power plant, so that the total cost of operation of the entire network is minimal. In another way, the active power of the generators must be varied within certain limits in order to satisfy the particular demand of the load with a minimum cost of fuel. This process is called the Economic Dispatch (ED) problem [4].

I.7.1 Formulation of economic dispatch problem

According to Figure I.6, there are two types of economic distribution problems that have been extensively covered in the power system literature:

- Static Economic Dispatch.
- Dynamic economic dispatch.

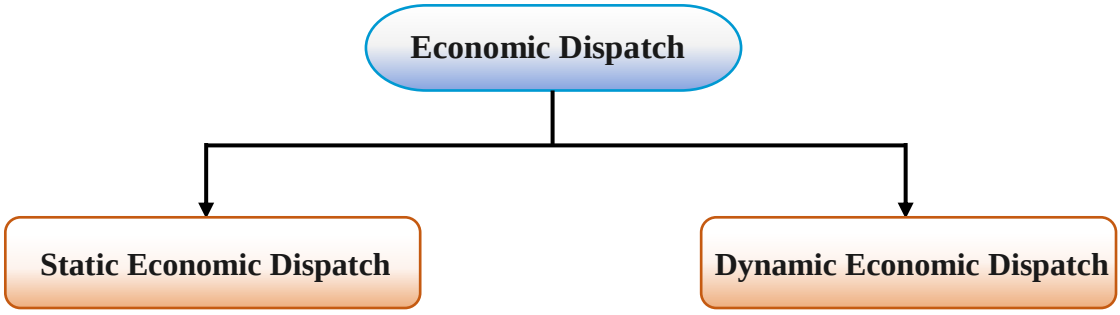

Figure I.6. Divisions of the economic dispatch problem.

I.7.2 Static economic dispatch

The primary goal of economic dispatch is to determine the power contribution of each generation unit in an electrical system so that the total cost of generation is as low as possible for any load condition while respecting the physical constraints of these generators.

I.7.2.1 Objective function

The production cost of a power plant is generally modeled by a second-degree polynomial function as a function of P_G, as shown in Eq. (I.59):

$$F(P_{Gi}) = \sum_{i=1}^{NG} (a_i + b_i P_{Gi} + c_i P_{Gi}^2) \quad \text{(I.59)}$$

Where

F: The fuel cost.

P_{Gi}: Active power output of i-th generator.

a_i, b_i, and c_i denote constants of generator [5].

I.7.2.2 Constraints

a. Equality constraints

— **Case of a System without losses:**

In this case, the only constraint is that the total system load equals the sum of all active powers generated.

$$\sum_{i=1}^{NG} P_{Gi} = P_D \quad \text{(I.60)}$$

— **b) case of a System with losses**

In real systems, the transport of electrical energy to the load buses is frequently accompanied by transmission losses. When compared to the previous case, the problem of economic dispatch becomes a little more complicated. When we denote total active power losses by P_L, the equality constraint becomes:

$$\sum_{i=1}^{NG} P_{Gi} = P_D + P_L \quad \text{(I.61)}$$

b. Inequality constraints

The generated power is constrained by the lower and upper bounds as follows:

$$P_{Gi}^{min} \leq P_{Gi} \leq P_{Gi}^{max} \quad \text{(I.62)}$$

I.7.2.3 Mathematical Formulation of the Static Economic Dispatching Problem

The economic dispatch problem of an interconnected power system can be modeled as the sum of the quadratic cost models for each generator, considering the equality and inequality constraints as follows:

$$\begin{cases} Min\ F(P_{Gi}) = \sum_{i=1}^{NG} F_i = \sum_{i=1}^{NG} (a_i + b_i P_{Gi} + c_i P_{Gi}^2) \\ Sous: \quad g(x): \sum_{i=1}^{NG} P_{Gi} - (P_D + P_L) = 0 \\ \quad\quad h(x): P_{Gi}^{min} \le P_{Gi} \le P_{Gi}^{max} \end{cases} \quad (I.63)$$

$g(x)$: Equality constraints.

$h(x)$: Inequality constraints.

I.7.3 Economic dispatch with generated power boundaries "Economic dispatch without losses"

The Lagrange multiplier is used to solve the economic dispatch problem (For minimizing (or maximizing) total cost function) where the problem linked above is transformed into an unconstrained problem as follows [6]:

$$L = \sum_{i=1}^{NG} F_i(P_{Gi}) + \lambda(P_D - \sum_{i=1}^{N} P_{Gi}) \quad (I.64)$$

The derivative of the Lagrange function for each independent variable (P_{Gi} and λ) must be zero for the total fuel cost to be minimum, as shown by the following equation [7]:

$$\begin{cases} \frac{\partial L}{\partial P_{Gi}} = a_{i1} + 2a_{i2}P_{Gi} - \lambda = 0 \\ \frac{\partial L}{\partial \lambda} = P_D - \sum_{i=1}^{NG} P_{Gi} = 0 \quad ; i = 1, NG \\ P_{Gi}^{min} \le P_{Gi} \le P_{Gi}^{max} \end{cases} \quad (I.65)$$

And

$$\frac{\partial L(P_{Gi},\lambda)}{\partial \lambda} = \sum_{i=1}^{NG} P_{Gi} - P_D = 0 \rightarrow \sum_{i=1}^{NG} P_{Gi} = P_D \quad (I.66)$$

We can calculate the value of P_G using Eq. (I.65) as follows:

$$\lambda = 2c_i P_{Gi} + b_i \rightarrow P_{Gi} = \frac{1}{2c_i}(\lambda - b_i) \quad (I.67)$$

By substituting Eq. (I.67) into Eq. (I.66), we obtain:

$$\sum_{i=1}^{NG} \frac{(\lambda - b_i)}{2c_i} = P_D \quad \text{(I.68)}$$

The optimal lambda value determined from Eq. (I.68) is formulated as follows:

$$\lambda = \lambda_{opt} = \left(P_D + \sum_{i=1}^{NG} \frac{b_i}{2c_i}\right) / \sum_{i=1}^{NG} \frac{1}{2c_i} \quad \text{(I.69)}$$

The optimal numerical value of lambda extracted from the previous equation can be substituted into Eq. (I.67) to obtain all of the optimal values for the generated powers in each bus.

$$P_{Gi} = \frac{1}{2c_i}\left(\left(\sum_{i=1}^{NG} \frac{1}{2c_i}\right)^{-1}\left(P_D + \sum_{i=1}^{NG} \frac{b_i}{2c_i}\right) - b_i\right); i = 1, NG \quad \text{(I.70)}$$

I.7.4 Economic dispatch with losses based on generated powers

Transmission losses are ignored in the case of very high load density and very short transmission distances, but when power is transmitted over long distances and with low load, losses must be considered because they affect the economic scheduling of generators [7].

$$\sum_{i=1}^{NG} P_{Gi} = \sum_{i=1}^{NG} P_{Di} + P_L \quad \text{(I.71)}$$

Transmission loss is expressed as a function of generated power with the help of β coefficients.

The simple formula for transmission loss in terms of β coefficients is given as:

$$P_L = \sum_{i=1}^{NG} \sum_{j=1}^{NG} P_{Gi} B_{ij} P_{Gj} \quad \text{(MW)} \quad \text{(I.72)}$$

Another form of transmission loss is termed Kron's formula, which is expressed as follows [8]:

$$P_L = B_{00} + \sum_{i=1}^{NG} B_{i0} P_{Gi} + \sum_{i=1}^{NG} \sum_{j=1}^{NG} P_{Gi} B_{ij} P_{Gj} \ \text{(MW)} \quad \text{(I.73)}$$

Where

B_{ij}, B_{i0} et B_{00} transmission loss coefficient.

P_{Gi}, P_{Gj} real power outputs at the ith and jth buses.

NG total number of generators.

To solve the problem of economic dispatch with losses, we formulate the Lagrangian as follows:

$$L = \sum_{i=1}^{NG} F_i(P_{Gi}) + \lambda\left(P_D + P_L - \sum_{i=1}^{NG} P_{Gi}\right) \quad \text{(I.74)}$$

For optimization

$$\frac{\partial L}{\partial P_{Gi}} = \frac{\partial F_i(P_{Gi})}{\partial P_{Gi}} + \lambda\left(0 + \frac{\partial P_L}{\partial P_{Gi}} - 1\right) = 0 \quad \text{(I.75)}$$

$$\frac{\partial F_i(P_{Gi})}{\partial P_{Gi}} = \lambda\left(1 - \frac{\partial P_L}{\partial P_{Gi}}\right) \quad \text{(I.76)}$$

$$\lambda = \left(\frac{1}{(1-\partial P_L/\partial P_{Gi})}\right)\frac{\partial F_i(P_{Gi})}{\partial P_{Gi}} = L_i\frac{\partial F_i(P_{Gi})}{\partial P_{Gi}} \quad \text{(I.77)}$$

$$\frac{\partial L}{\partial \lambda} = \sum_{i=1}^{NG} P_{Gi} - P_L - PD = 0 \quad \text{(I.78)}$$

Where L_i is known as a penalty factor of plant i.

In this case, we can use the same method as in the case of no losses, but we will adjust the generated power as follows:

$$P_{Gi} = \frac{1}{2c_i}\left(\left(\sum_{i=1}^{NG}\frac{1}{2c_i}\right)^{-1}\left(P_D + P_L + \sum_{i=1}^{NG}\frac{b_i}{2c_i}\right) - b_i\right); i = 1, NG \quad \text{(I.79)}$$

I.7.5 Practical constraints

I.7.5.1 Characteristic with the effect of opening the valves

Usually large thermal power plants have several steam inlet valves, which are used to control the power output. Each time you begin to open an intake valve, there is a sudden increase in losses and this results in ripples in the fuel cost curve. With the gradual opening of the valve, these losses gradually decrease until the valve is fully open. Figure I.7 shows the typical cost curve of a thermal unit with three steam inlet valves. Points A, B and C are operating points when the valves are open. The valve opening effect is often modeled as a rectification of the basic quadratic function by adding a sinusoidal component [9].

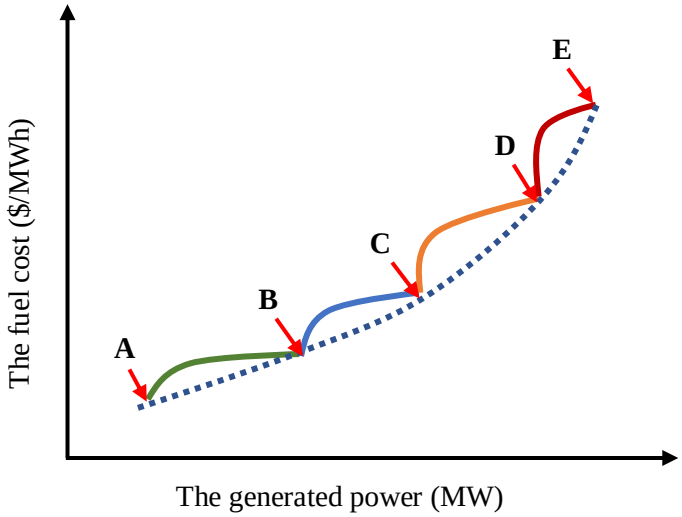

A: First valve **D:** Fourth valve
B: Second valve **E:** Fifth valve
C: Third valve

Figure I.7. Fuel cost curve of a thermal unit with valve-point effects.

I.7.5.2 Prohibited Zone Constraint

In general, thermal units can provide continuous power between the upper and lower values, but in practice, these stations can have undesirable operating zones due to unit stability issues, and significant vibrations are felt in the machine bearings when operating in these areas. As a result, grid operators seek to generate power outside of these areas, resulting in a discontinuous fuel cost curve. The following equation expresses the mathematical formula relating to the effect of restricted [10]:

$$P_i \in \begin{cases} P_{G_i}^{min} \le P_{Gi} \le P_{G_i,1}^{1} \\ P_{G_i,k-1}^{u} \le P_{G_i} \le P_{G_i,k}^{1} \quad k = 2, \dots\dots, z_i \\ P_{G_i,z_i}^{u} \le P_{G_i} \le P_{G_i}^{max} \end{cases} \tag{I.80}$$

$P_{G_i,1}^{1}$ and $P_{G_i,k-1}^{u}$ are the lower and upper bounds of the prohibited operating zone k, respectively, and z_i is the number of prohibited zones of unit i.

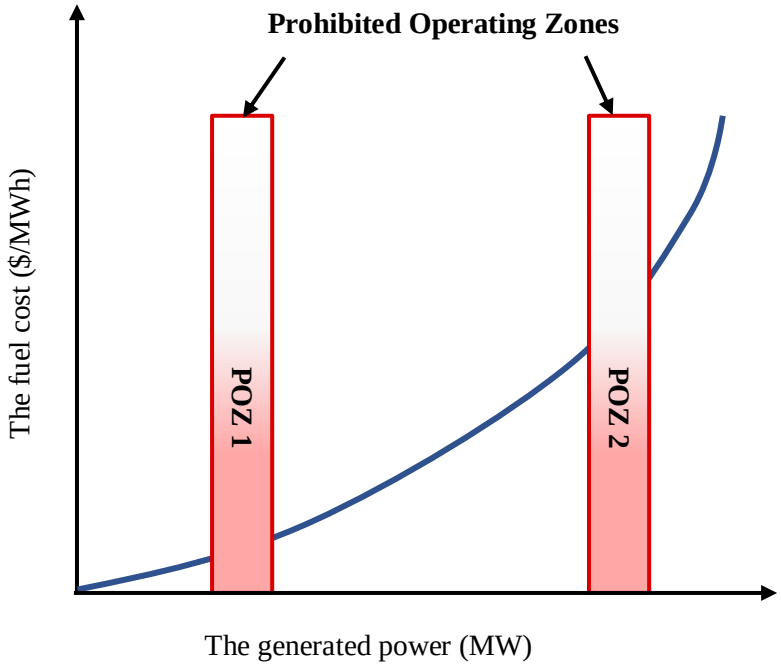

Figure I.8. Fuel cost function with prohibited zones limitations.

I.7.5.3 Characteristics of various types of fuel

Thermal units can sometimes operate on a variety of fuels. Under these conditions, the cost characteristic is composed of several quadratic functions (Figure II.8), which are written as follows:

$$F_i(P_{Gi}) = \begin{cases} a_{i1} + b_{i1} \cdot P_{Gi} + c_{i1} \cdot P_{Gi}^2 P_{Gi,1}^{min} \le P_{Gi} \le P_{Gi,1} \\ a_{i2} + b_{i2} \cdot P_{Gi} + c_{i2} \cdot P_{Gi}^2 P_{Gi,1} \le P_{Gi} \le P_{Gi,2} \\ \cdot \\ \cdot \\ \cdot \\ a_{ik} + b_{ik} \cdot P_{Gi} + c_{ik} \cdot P_{Gi}^2 P_{Gi,2} \le P_{Gi} \le P_{Gi}^{max} \end{cases} \quad (\$/hr) \qquad \text{(I.81)}$$

Where a_{ik}, b_{ik}, and c_{ik} are the cost coefficients of unit i with fuel k.

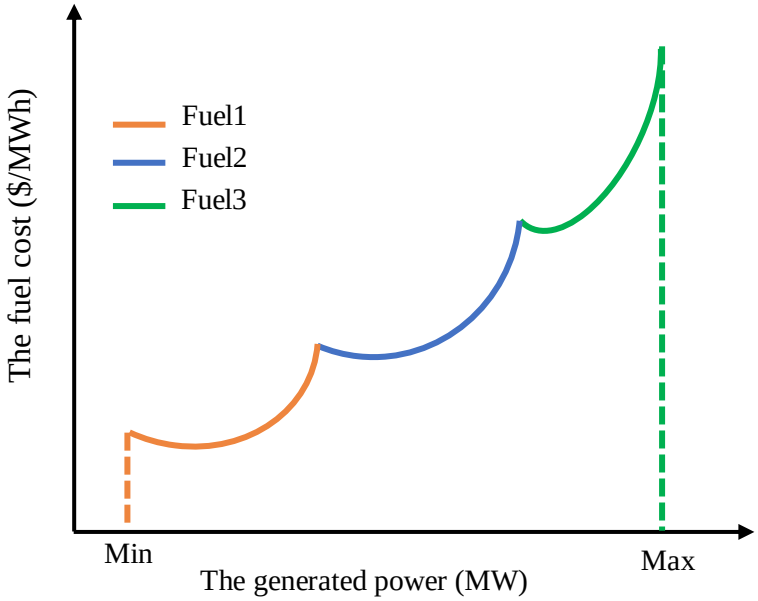

Figure I.9. Cost curve for a thermal unit powered by three different types of fuel.

I.7.6 Dynamic Economic Dispatch

Dynamic economic dispatch (DED) is regarded as the primary component in energy system planning in order to achieve optimal power system operation and control [11]. This problem entails minimizing the fuel costs of thermal power units over a given time period while keeping operational constraints in mind. The overall fuel cost is determined as follows [12]:

I.7.6.1 Mathematical formulation of the dynamic economic dispatch problem

Moreover, the optimization problem can be formulated mathematically by the Eq (I.82):

$$F(P_{Gi,t}) = \sum_{i=1}^{NG} \left(a_i + b_i P_{Gi,t} + c_i P_{Gi,t}^2\right) \quad \text{(I.82)}$$

I.7.6.2 Constraints related to DED

a. Equality Constraints

$$\sum_{i=1}^{NG} \mathrm{P}_{it} = \mathrm{P}_D(t), t = 1,2,3,\dots,T \quad \text{(I.83)}$$

i =1,2,3…… NG (Total number of generators producing electricity), P_D: is the total power demand.

b. Inequality constraints

$$P_{i,t}^{min} \leq P_{Gi,t} \leq P_{i,t}^{max} \quad \text{(I.84)}$$

$P_{i,t}^{min}$ and $P_{i,t}^{max}$ are the maximum and minimum power delivered by the production units.

c. Ramp Constraints of Generators

Ramp restrictions in thermal power plants are defined as the amount of increase (ramp up) or decrease (ramp down) in generator power output from hour to hour that cannot be exceeded in any way, or else the thermal units will be exposed to high stresses at the level of their rotors, potentially causing dangerous damage to the power systems. These constraints are described by the following equations [13]:

$$P_{it} - P_{i(t-1)} \leq UR_i \quad (I.85)$$

$$P_{i(t-1)} - P_{it} \leq DR_i \quad (I.86)$$

Where UR and DR are the ramp-up and ramp-down limitations of the i-th generator and are expressed in MW/h.

I.7.7 Emission dispatch

During the combustion of fossil fuels to generate electrical power, thermal units emit a variety of polluting emissions into the environment [14]. Sulfur oxides (SO2), nitrogen oxides (NOx), and carbon dioxide (CO2) are among the pollutants released [9]. The total amount of pollution emitted can also be expressed as the sum of a quadratic and an exponential function. This function is explained as follows [15]:

$$E = \sum_{i=1}^{NG} \left(\alpha_i + \beta_i P_{Gi} + \gamma_i P_{Gi}^2 + \delta_i * \exp(\varepsilon_i * P_{Gi})\right) \quad (I.87)$$

Where E is the total sum of emissions (Kg/h), α_i, β_i, γ_i, δ_i and ε_i are the emission coefficients of the ith unit.

I.7.8 Combined Economic Emission Dispatch

The CEED problem is typically formulated as a multi-objective optimization problem. As illustrated in Figure I.10, it aims to simultaneously minimize total fuel cost and harmful gas emissions (nitrogen oxides, sulfur oxides) while ensuring optimal output of generated power while satisfying the equality and inequality constraints [16].

$$Min\{G = [F(P_{Gi}), E(P_{Gi})]\} \quad (I.88)$$

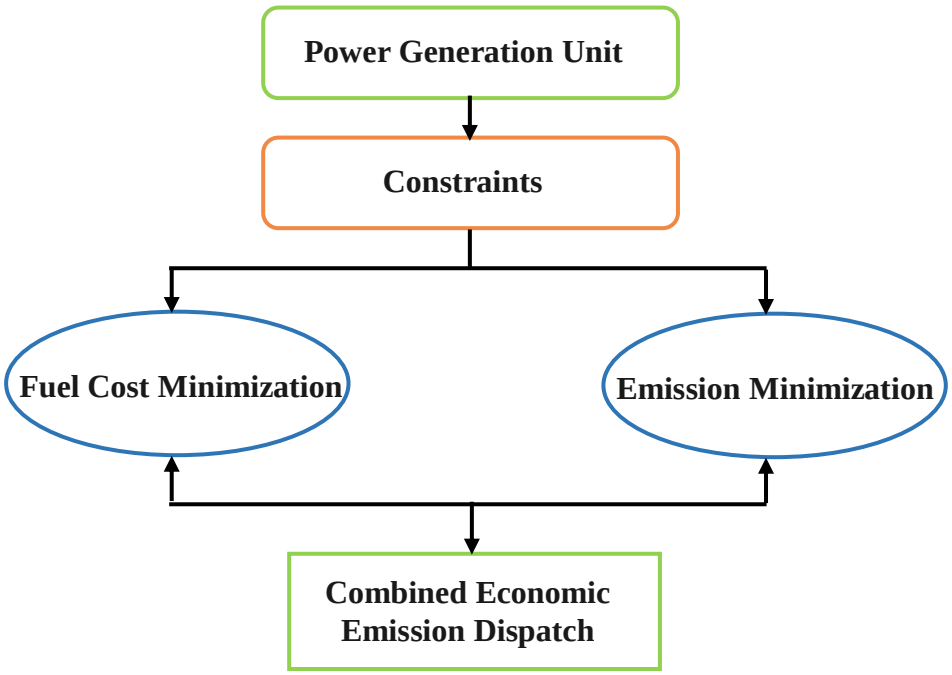

Figure I.10. Presentation of Combined Economic Emission Dispatch (CEED).

I.8 Conclusion

This chapter addresses three primary issues well-known in the power systems literature: power flow (PF), economic dispatch (ED), and optimal power flow (OPF). The power flow problem is defined as calculating how much power should be transmitted to a transmission or distribution network in a given time period while ignoring how that power is produced. While the economic dispatch problem focuses on calculating the power produced by each generator in the power plant within its predetermined constraints, the disadvantage of this problem is that it ignores the limitations imposed by the transmission system devices. Merging these two problems yields the optimal power flow problem, which is an efficient solution to the power generation schedule while accounting for all system constraints.

The OPF is also a significant part of proper planning for any future equipment installation, such as FACTS devices, which will be discussed in the following chapter.

References

[1] J. H. Chow and J. J. Sanchez-Gasca, *Power system modeling, computation, and control*: John Wiley & Sons, 2020.

[2] B.-G. Risi, F. Riganti-Fulginei, and A. Laudani, "Modern techniques for the optimal power flow problem: state of the art," *Energies*, vol. 15, p. 6387, 2022.

[3] M. Ebeed, S. Kamel, and F. Jurado, "Optimal power flow using recent optimization techniques," in *Classical and recent aspects of power system optimization*, ed: Elsevier, 2018, pp. 157-183.

[4] H. MERAH, A. GACEM, D. BENATTOUS, Y. LABBI, and O. P. MALIK, "Solving economic dispatch problem using a new hybrid PSO-ALO Algorithm," in *2020 1st International Conference on Communications, Control Systems and Signal Processing (CCSSP)*, 2020, pp. 487-492.

[5] J. S. Al-Sumait, J. K. Sykulski, and A. K. Al-Othman, "Solution of Different Types of Economic Load Dispatch Problems Using a Pattern Search Method," *Electric Power Components and Systems*, vol. 36, pp. 250-265, 2008.

[6] B. Beavis and I. Dobbs, *Optimisation and stability theory for economic analysis*: Cambridge university press, 1990.

[7] H. Saadat, "Power System Analysis Third Edition ", ed: PSA Publishing LLC, 2011.

[8] A. F. Zobaa, S. A. Aleem, and A. Y. Abdelaziz, *Classical and recent aspects of power system optimization*: Academic Press, 2018.

[9] F. Li, *Optimal Economic Operation of Electric Power Systems Using Genetic Based Algorithms*: Liverpool John Moores University (United Kingdom), 1996.

[10] M. Basu, "Kinetic gas molecule optimization for nonconvex economic dispatch problem," *International Journal of Electrical Power & Energy Systems*, vol. 80, pp. 325-332, 2016.

[11] M. H. Ghani, I. Musirin, S. R. A. Rahim, M. H. Hussain, S. Sivaraju, A. S. Kumar, *et al.*, "Integrated Evolutionary Path-Finder Optimization Technique for Dynamic Economic Dispatch," *Mathematical Statistician and Engineering Applications*, vol. 71, pp. 692–706-692–706, 2022.

[12] A. Soroudi, *Power system optimization modeling in GAMS* vol. 78: Springer, 2017.

[13] A. A. Tagher, "Contribution à l'étude de la répartition optimale de la production d'énergie active et réactive dans un réseau électrique de distribution," ETH Zurich, 1969.

[14] A. F. Zobaa and A. Vaccaro, *Computational intelligence applications in smart grids: enabling methodologies for proactive and self-organizing power systems*: World Scientific, 2014.

[15] S. Zaoui and A. Belmadani, "Solution of combined economic and emission dispatch problems of power systems without penalty," *Applied Artificial Intelligence*, vol. 36, p. 1976092, 2022.

[16] A. Sundaram and P. Erdogmus, "Solution of combined economic emission dispatch problem with valve-point effect using hybrid NSGA II-MOPSO," in *Particle Swarm Optimization with Applications*. vol. 78, ed: IntechOpen, 2017.

CHAPTER II

FACTS CONTROLLERS

II.1 Introduction

As the demand for electrical power increases, so does the strain on a power system. As a result, power system operation becomes more complex, power flow becomes unstable, and losses increase. To increase the capacity of power transported, new manufacturing plants and transmission lines must be built. However, this requires a significant investment as well as a long-term policy with numerous resources. Electrical network specialists face increasing challenges in this new environment.

The rapid advancement of self-commutated power electronic devices has resulted in the development of flexible alternating current transmission system (FACTS) devices. These elements function as impedances whose values change depending on the firing angle of the thyristors. This chapter introduces the FACTS concept and its classification in general. Following that, we will go over the methods used to determine the best location for these FACTS control devices.

II.2 FACTS Controllers

The term FACTs is an abbreviation for (Flexible Alternating Current Transmission System), which is an integrated technology developed in the late 1980s at the Electric Power Research Institute (EPRI) that is based on the integration of devices electronics in the power network in order to effectively control the power flow, reduce losses, and increase the power of the transmission capacity while greatly improving the security of the system [1, 2].

II.2.1 Benefits from FACTS Technology

- Utilization of the current transmission system and eliminating the need to connect new lines.
- Control the power flow more precisely and by demand.
- Provide increased flexibility, even with the addition of a new generator .
- Reduce oscillations in the power system, resulting in better system stability.
- Improve the quality and reliability of the system .
- Environmentally friendly [3].

II.2.2 Types of FACTS devices

FACTS devices are classified into three kinds according on how they are connected to the network: shunts, series, and hybrid compensators (series and shunts). These types can also be divided into two categories according to the electronics devices used. The first category is based on the thyristor, and the second category is based on the GTO thyristor. Figure II.1 illustrates these categories in detail.

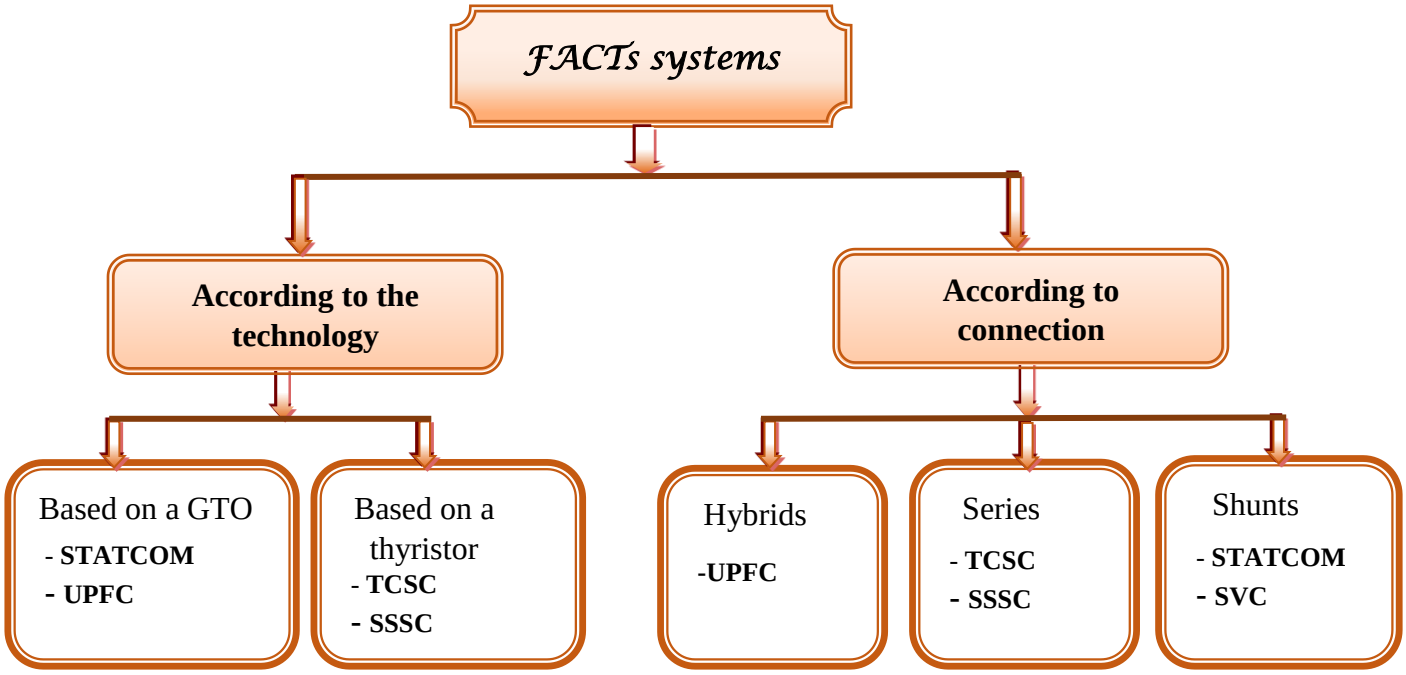

Figure II.1. Classification of FACTS devices.

II.2.2 Shunt Compensators

The main objective of shunt compensation is to increase the transmissible power in the network. The principle consists of supplying or absorbing reactive power so as to modify the natural characteristics of the lines to make them more compatible with the load [4]. We can cite:

II.2.2.1 Static VAR Compensator (SVC)

The SVC is shunt connected to passive elements that include power electronics converters (Figure II.2). This SVC capable of dynamically exchanging reactive power (absorbing by reactor or generating by capacitor) with the network to maintain the bus voltage within the specified limits. Hence, the static protection of the system can be enhanced [5].

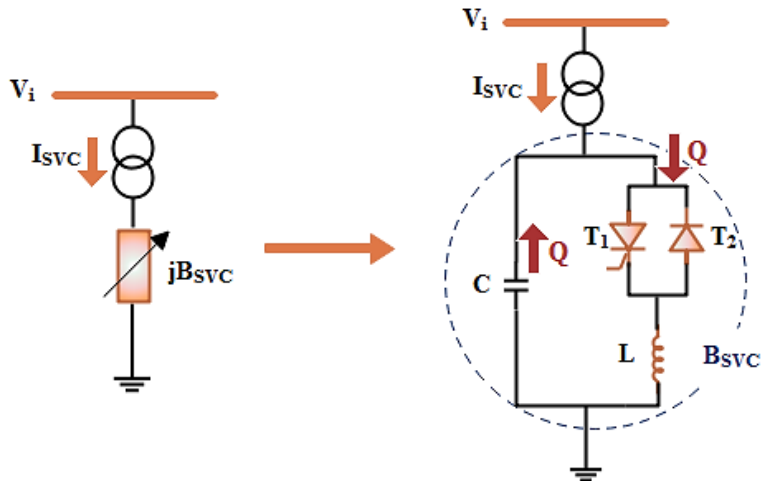

Figure II.2. Simplified model of Static VAR Compensator (SVC).

II.2.2.2. Static Synchronous Compensator (STATCOM)

This type of compensator was developed in the late 1970s but did not become widely used until the 1990s when high-power Gate-Turn-Off (GTO) switches were developed. The first SVC with a voltage source converter, called a Static Synchronous Compensator (STATCOM), went into operation in 1999. The STATCOM controller shown in Figure II.3 serves the same purpose as the SVC, but with greater durability and response speed, earning it the moniker "advanced static var compensator (ASVC)". However, the cost of installing a STATCOM device is higher than the cost of installing an SVC device (owing to higher cost of the GTO thyristors) [6-9].

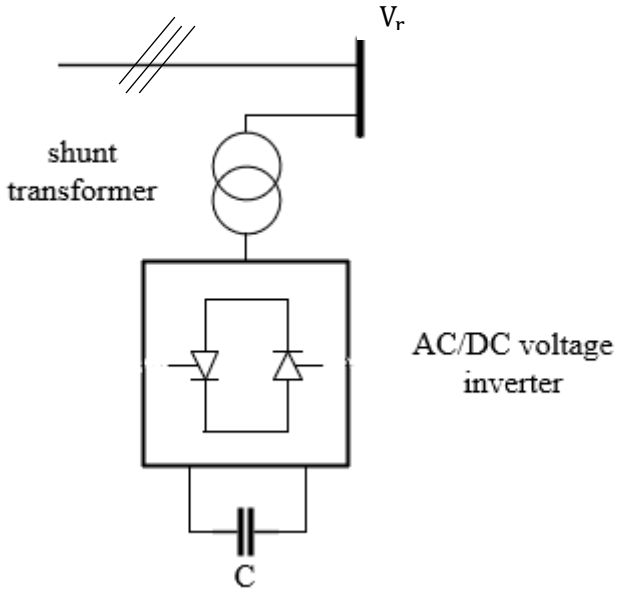

Figure II.3. Static Synchronous Compensator simplified model (STATCOM).

II.2.3 Series Compensators

Series compensation is one of the forms of FACTS that has experienced huge popularity for many years, particularly in long-distance overhead transmission lines, because of its low cost in comparison to the others. It may be represented as a variable impedance linked in series with the power grid, as this sort of connection reduces the possibility of voltage drop and therefore maintains continuous power flow in the transmission lines [6, 10].

II.2.3.1 Static Synchronous Series Compensator (SSSC)

Gyugyi proposed the Static Synchronous Series Compensator (SSSC) in 1989 as an advanced type of controlled Series compensation, just as STATCOM is an advanced SVC. The SSSC functions similarly to STATCOM devices, except that it is connected in series rather than a shunt and thus works to change the equivalent line impedance, allowing us to increase or decrease the power transmitted across the line without changing the lines. It has higher losses when compared to other FACTS systems, which may be a disadvantage, yet it can be an effective FACTS controller to regulate power flow. A schematic representation of the SSSC device is shown in Figure II.4 [6, 11]. A static synchronous series compensator (SSSC) is a type of flexible AC transmission system which consists of a solid-state voltage source inverter coupled with a transformer that is connected in series with a transmission line. This device can inject an almost sinusoidal voltage in series with the line. This injected voltage could be considered as an inductive or capacitive reactance, which is connected in series with the transmission line [12].

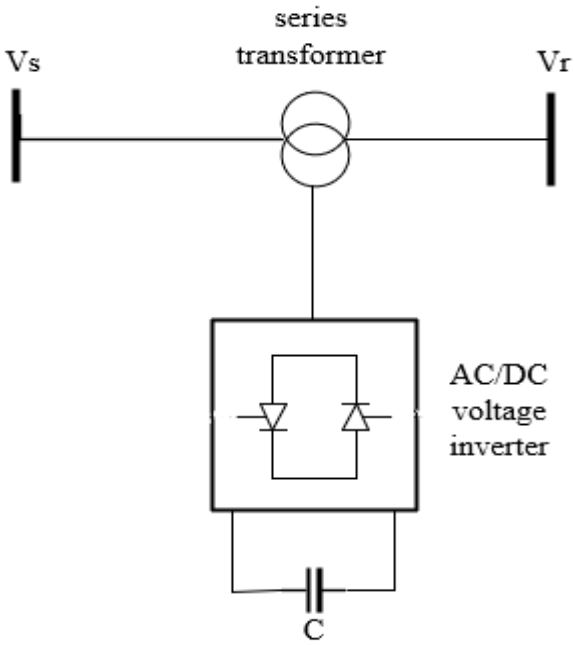

Figure II.4. Static Synchronous Series Compensator (SSSC) model.

II.2.3.2 Thyristor-Controlled Series Capacitor (TCSC)

The TCSC is a conventional static series capacitor that is connected in parallel with a thyristor-controlled reactor (Figure II.5). Vithayathil and colleagues presented it in 1986 as a way for "rapidly adjusting the grid impedance". TCSC helps to keep the safety of the power system in both regular and emergency conditions, and it is utilized in applications that demand sophisticated, quick, and continuous control of the series impedance of an electrical line [1, 6, 11].

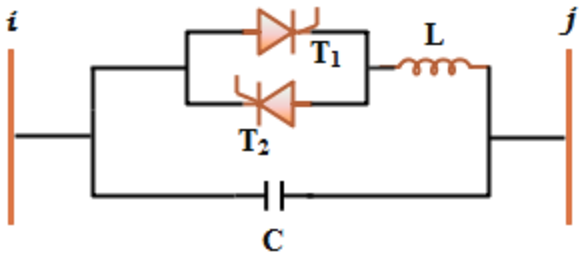

Figure II.5. Simplified model of the TCSC controller.

II.2.4 Combined Series-Shunt Controllers

A combined series-shunt controller is a coordinated mix of the advantages of series and shunt compensation. This combination assures that we can command the three factors (voltage, resistance, and phase shift angle) that govern power transmission on the transmission line.

II.2.4.1 Unified Power Flow Controller (UPFC)

UPFC device is one of the well-known FACTS device which combines two purposes at the same time and can control voltage, resistance and angle at the same time (Figure II.6). Using the UPFC to control power transmission is preferable to increasing the transmission capacity of the system. Basically, UPFC is used to adjust the power transmission between two parallel transmission lines together. This leads to the maximum power transmission capacity in the electrical system. The image below shows a simplified diagram of the UPFC device.

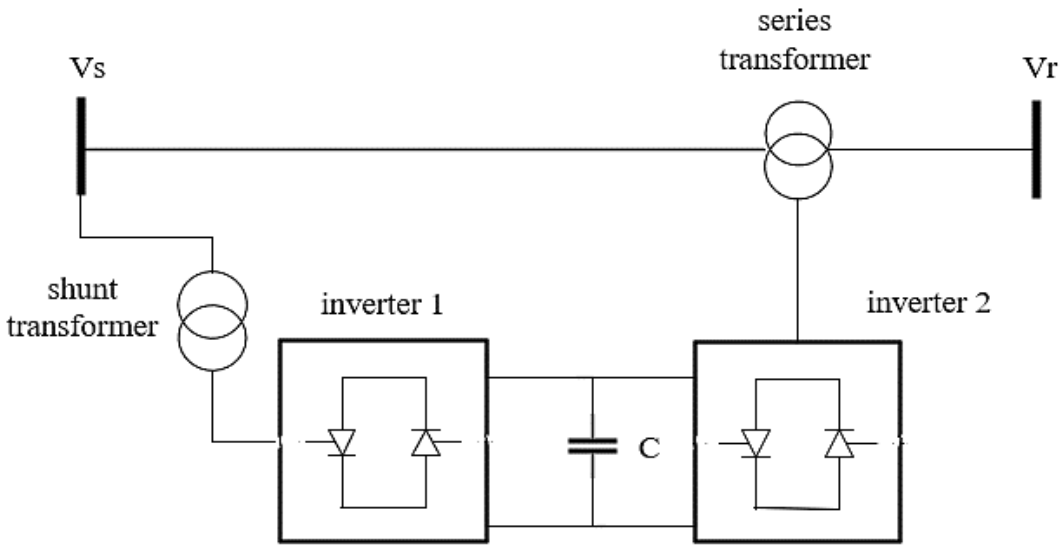

Figure II.6. Unified power flow controller model.

II.3 FACTS Devices Modeling

Several ways for modeling FACTS devices in stationary systems are described, mainly based on the method used to integrate FACTS into the power flow calculation. The three most common models found in the literature are based respectively on the injection of equivalent power, the creation of a fictitious node or even the modification of the admittance matrix.

II.3.1 Modeling types for FACTS devices

There are several approaches to modeling FACTS devices in the power flow domain. These various methods of modeling these devices have been developed for the study of stationary regimes. The three most commonly encountered models in the literature are based on the injection of equivalent power, the creation of a fictitious node, and the modification of the admittance matrix. These three techniques are discussed in the following paragraphs.

II.3.1.1 Power injection at both ends of the line

When a FACTS is added to a network line, the FACT controller affects the active and reactive transport line power.

The principle is to replace the effect of the Facts device on power transits in the line (Figure II.7 (a)) with power injections at both ends (Figure II.7 (b)). These are calculated in such a way that the effect produced is equivalent to the effect produced by the device in question. In node I active and reactive power injections are provided by:

$$P_i^F = P_{ij} - P_{ij}^F \qquad \text{(II.1)}$$

$$Q_i^F = Q_{ij} - Q_{ij}^F \quad \text{(II.2)}$$

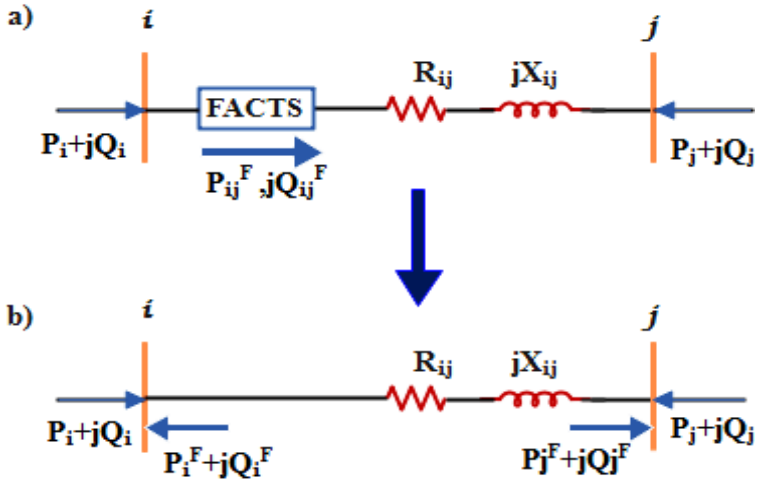

Figure II.7. Power injection modeling: a) line with FACTS controller, b) line with equivalent injections.

P_i^F ,Q_i^F: Equivalent active and reactive power injections at node i.

P_{ij} ,Q_{ij}: Active and reactive power transits in the absence of a FACTS device.

P_{ij}^F ,Q_{ij}^F: Active and reactive power transits with the FACTS in the line.

The active power injections at the PV and PQ nodes are written as follows:

$$P_i + P_i^F = V_i \sum_{k=1}^{n} V_j \left[G_{ij}\, cos(\delta_i - \delta_j) + B_{ij}\, sin(\delta_i - \delta_j)\right] \quad \text{(II.3)}$$

And the reactive powers injected at the PQ nodes are given by the following equation:

$$Q_i + Q_i^F = -V_i \sum_{k=1}^{n} V_j \left[G_{ij}\, cos(\delta_i - \delta_j) - B_{ij}\, sin(\delta_i - \delta_j)\right] \quad \text{(II.4)}$$

With n the number of nodes in the power system.

The injections power, P_i^F and Q_i^F values are calculated after each iteration but are not used in the Jacobian matrix calculation.

II.3.1.2 Creating a fake node

Reference [13] presents a FACTS modeling based on the creation of a fictitious node. Figure II.8 depicts a model of a UPFC device that allows you to control the transits of active and reactive powers.

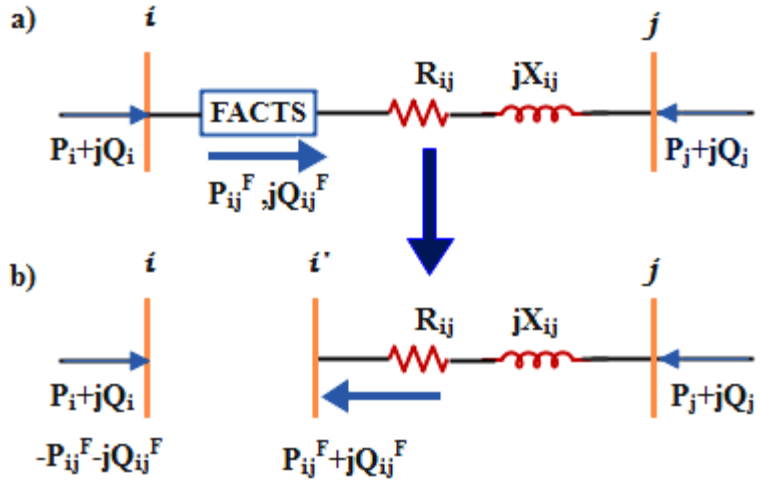

Figure II.8. Modeling with a fictitious node: a) line with FACTS controller, b) equivalent representation.

A fictitious node i' is temporarily created into which the controlled power or powers are injected. To maintain the power balance, the power injected into node i' is subtracted from node i. The new node is accounted for in the power distribution calculation by changing the structure of the Jacobian matrix.

II.3.1.3 Modifications to the nodal admittance matrix

The FACTS are considered as elements that directly modify the nodal admittance matrix of the network. They are placed in the line according to the representation of the Figure II.9 Depending on the type of FACTS modeled, the device can be placed in the middle or at one end of the line [13].

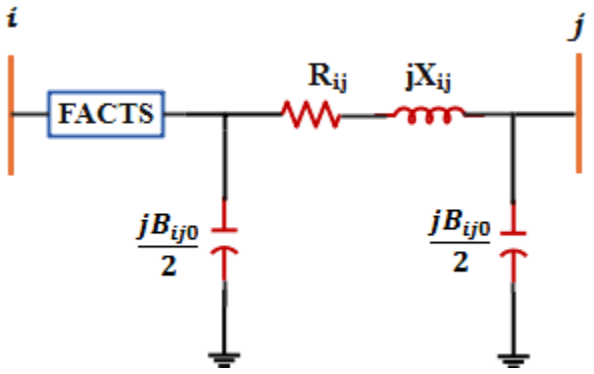

Figure II.9. FACTS device integration into a line.

The parameters of an equivalent line are determined and substituted for those of the line without FACTS in the nodal admittance matrix. This is modified as follows:

$$Y_{mod} = \begin{bmatrix} Y'_{ii} & Y'_{ij} \\ Y'_{ji} & Y'_{jj} \end{bmatrix} = \underbrace{\begin{bmatrix} Y_{ii} & Y_{ij} \\ Y_{ji} & Y_{jj} \end{bmatrix}}_{\text{Ligne}} + \underbrace{\begin{bmatrix} Y^F_{ii} & Y^F_{ij} \\ Y^F_{ji} & Y^F_{jj} \end{bmatrix}}_{\text{FACT}} \quad \text{(II.5)}$$

Only a portion of the Y matrix coefficients are modified depending on the type of FACTS and its position in the line.

II.3.2 SVC modeling

The static reactive power compensator is modeled by a variable shunt admittance and is used to govern the reactive power compensation of a system, where B_{SVC} denotes the shunt equivalent susceptance of the SVC restricted to a minimum and maximum value of B_{SVC}. Figure II.10 depicts the equivalent circuit for the SVC controller in a power system [14].

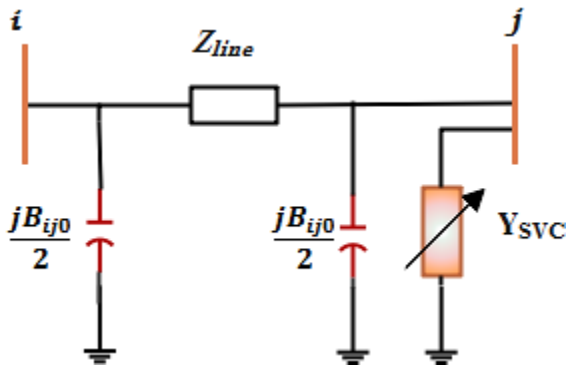

Figure II.10. The basic model of an SVC device in a power system.

The current I_{SVC} and reactive power Q_{SVC} of static var compensator SVC exchanged with the bus (k) can be expressed in Eqs. (II.6) and (II.7):

$$I_{SVC} = jB_{SVC}.V_k \quad \text{(II.6)}$$

$$Q_{SVC} = B_{SVC}.V_K^2 \quad \text{(II.7)}$$

Where V_k is the bus voltage magnitude to which the SVC is connected, and B_{SVC} is expressed as:

$$B_{SVC} = B_C - B_{TCR} = \frac{1}{X_C X_L}\left(X_L - \frac{X_C}{\pi}[2(\pi - \alpha) + sin(2\alpha)]\right) \quad \text{(II.8)}$$

$$X_L = \omega L \quad \text{(II.9)}$$

$$X_C = \frac{1}{\omega L} \tag{II.10}$$

The negative sign shows that the SVC gives reactive power to the system when capacitive, but consumes when inductive.

II.3.3 TCSC modeling

Series compensators are represented by varying impedances connected in series with the line. Figure II.11 depicts a detailed model of a TCSC device in a power system.

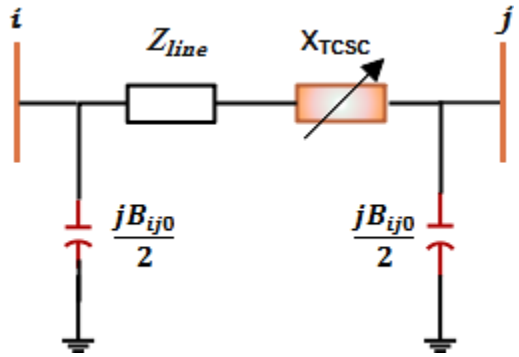

Figure II.11. The basic model of a TCSC device in a power system.

The TCSC model is comprised of two parallel branches, one with capacitance and the other with inductance controlled by a thyristor. The equivalent reactance of TCSC is given as follows:

$$X_{TCSC}(\alpha) = j\frac{X_C X_L}{\frac{X_C}{\pi}(2(\pi-\alpha)+sin(2\alpha))-X_L} \tag{II.11}$$

When a TCSC system is integrated into a power line, the total reaction is the algebraic sum of the TCSC reactor and the real reactance of the line, as indicated in Eq. (II.12).

$$X_{ij} = X_{line} + X_{TCSC} \tag{II.12}$$

To prevent overcompensation in the line, the value of reactance X_{TCSC} is dependent on the value of the line reactance X_{line}, which is given as follows:

$$-0.8X_{line} \leq X_{TCSC} \leq 0.2X_{line} \tag{II.13}$$

The line admittance matrix is adjusted as follows:

$$Y_{mod} = \begin{bmatrix} Y'_{ii} & Y'_{ij} \\ Y'_{ji} & Y'_{jj} \end{bmatrix} = \begin{bmatrix} Y'_{ij} + \frac{Y_{ij0}}{2} & -Y'_{ij} \\ -Y'_{ji} & Y'_{ij} + \frac{Y_{ij0}}{2} \end{bmatrix} \tag{II.14}$$

With:

$$Y'_{ij} = \frac{1}{r_{ij}+j(x_{ij}+X_{TCSC})} \quad \text{(II.15)}$$

II.4 The optimal location and sizing of FACTS devices

Voltage sags are one of the main significant issues in the electrical power system. As well as excessive power flow in some branches. These problems are mainly caused by the unbalance between power generation and load demand, the lack of reactive power supply or unexpected interruptions in transmission lines. All these factors may eventually lead to a complete blackout. To address these issues, flexible AC transmission system (FACTS) devices can be installed in the power system to ensure increased power flow capability and flexible voltage control. These FACTs devices can supply the system with the reactive power it requires. However, integrating these devices into the power system is a difficult problem. Maximum effectiveness is achieved through proper sizing and placement of FACTs controllers.

Many studies on FACTS controllers have been conducted in order to improve power system performance by locating them optimally [5]. The Multi-Objective Multi-Verse Optimizer technique was used in [15] to find the best location and size for the FACTS controller while simultaneously improving three objective functions: active power loss, voltage deviations, and FACTS controller cost. The SVC, and TCSC were all classified as FACTS devices. The proposed method was tested on the IEEE 57 bus test system, and the results revealed that the MOMVO technique was capable of improving system performance. The authors of the references [16, 17] discovered the best locations for three different FACTS controller types, namely TCSC, SVC, and UPFC, to improve the security of the electrical network. These three types are optimally integrated into the IEEE 30 bus system to address the problem of power losses using the differential evolution (DE) algorithm [18]. However, the proposed method did not account for security constraints. Furthermore, there have been no comparisons with other optimization methods to validate this approach. Reference [19] proposed a Whale Optimization Algorithm (WOA) for optimal placement and sizing of various types of FACTS controllers to minimize operating costs, including the price of FACTS devices and active power loss. However, once the reactive power loading is changed, the results may be incorrect.

A novel hybrid method incorporating CS and ALO is proposed in [5] for improving voltage profile, mitigating overload, and reducing power loss in worst-case line outage scenarios. The proposed hybrid CS-ALO is used to solve the problem of sizing and sitting of Static VAR Compensator (SVC) devices in the IEEE 57 bus test system. However, incorporating a type of

serial controller into this study, such as TCSC, can help to highlight the overload issue. The problem of sizing and sitting SVC devices is used in many works of literature by various optimization methods to enhance the performance and security of the power system [5]. Multi-objective cuckoo search algorithm (MOCS) [20], improved harmony search (IHS) [21], and Cuckoo Search (CS) [22] have been introduced for the optimum positioning of SVC devices to enhance investment costs, real and reactive power losses. To enhance security and voltage stability, the optimal location of SVC is reported in [23-26]. The authors of reference [27] attempted to use the autonomous groups PSO method to solve the active power loss minimization problem with SVC devices. The IEEE 14 and 30 bus systems were used to evaluate the effectiveness of the proposed method. Despite the fact that the proposed method outperformed the competing algorithms, the multi-objective optimization problem was not taken into account in this study.

The authors of reference [28] discussed another type of series FACTs controller, the Thyristor-Controlled Series Compensator (TCSC), which is integrated into an IEEE 30 bus system to improve line congestion and reduce total power loss by employing the multi-Objective Genetic Algorithm (MOGA). The results show that the proposed algorithm outperforms other methods in terms of convergence speed, but it is also prone to falling into the local solution. Optimal TCSC placement and sizing were determined using evolutionary optimization techniques in order to reduce transmission loss and installation costs, as well as improve the voltage profile in reference [29]. However, the author did not address how to choose the number of TCSC for their placement. The authors of [26] conducted another study to improve the voltage profile in electrical networks by optimal placement of TCSC devices using the Chaotic Immune Symbiotic Organism Search (CISOS) optimization algorithm. However, the proposed algorithm was not applied to a large system.

Different mathematical approaches have been widely used to determine the optimal position of TCSC controllers in power systems in order to reduce losses and enhance voltage profile [30, 31], mitigate congestion [32-34], and maximize loadability [35, 36].

It is noted that extensive research has been done in previous studies on determining the best location of FACTS devices in electrical networks. The following characteristics distinguish each of these works:

- The models used for the FACTS devices;
- The optimization methods utilised;
- The size of the networks utilized in the simulations.

II.6 Conclusion

Integrating FACTS devices into the electrical grid is critical to its ability to resolve issues such as power losses, overload, instability, and congestion. We provided general information about FACTS systems in this chapter, including their types and benefits, as well as how to model them in the power system. TCSC and SVC, two of the most common types of FACTS in the literature, were also modelled. The chapter concludes with an in-depth look at FACTS controllers and their various applications in power systems for determining the best location.

Reference

[1] A. M. M. A. R. Ahmed, "Optimal Power Flow With Facts Devices," INDIAN INSTITUTE OF TECHNOLOGY, ROORKEE, 2004.

[2] A. M. Othman, "Enhancing the performance of flexible AC transmission systems (FACTS) by computational intelligence," 2011.

[3] R. K. Bindal, "A Review of Benefits of FACTS Devices in Power system," *International Journal of Engineering and Advanced Technology (IJEAT),* vol. 3, pp. 105-108, 2014.

[4] C. Saliha, "Optimisation des Puissances Réactives en tenant compte des Méthodes PHeuristiques d'un Système Electrique Complexe-Application au Réseau Algérien," Université Mohamed Boudiaf des Sciences et de la Technologie d'Oran, 2009.

[5] H. Merah, A. Gacem, D. Ben Attous, A. Lashab, F. Jurado, and M. A. Sameh, "Sizing and sitting of static var compensator (svc) using hybrid optimization of combined cuckoo search (cs) and antlion optimization (alo) algorithms," *Energies,* vol. 15, p. 4852, 2022.

[6] B. R. Andersen and S. L. Nilsson, *Flexible AC Transmission Systems: FACTS*: Springer, 2020.

[7] E. Barrios-Martínez and C. Ángeles-Camacho, "Technical comparison of FACTS controllers in parallel connection," *Journal of applied research and technology,* vol. 15, pp. 36-44, 2017.

[8] A. GACEM, "Commande Robuste d'un Dispositif FACTS par les Méthodes Métaheuristiques pour la Stabilité de Tension d'un Réseau Electrique," Université Mohamed Khider-Biskra, 2019.

[9] R. Mihalic, M. Eremia, and B. Blazic, "Static Synchronous Compensator–Statcom," *Advanced Solutions in Power Systems: HVDC, FACTS, and Artificial Intelligence: HVDC, FACTS, and Artificial Intelligence,* pp. 459-525, 2016.

[10] M. Eremia, C.-C. Liu, and A.-A. Edris, *Advanced solutions in power systems: HVDC, FACTS, and Artificial Intelligence*: John Wiley & Sons, 2016.

[11] N. G. Hingorani and L. Gyugyi, *Understanding FACTS: concepts and technology of flexible AC transmission systems*: Wiley-IEEE Press, 2000.

[12] K. K. Sen, "SSSC-static synchronous series compensator: theory, modeling, and application," *IEEE Transactions on power delivery,* vol. 13, pp. 241-246, 1998.

[13] S. Gerbex, "Métaheuristiques appliquées au placement optimal de dispositifs FACTS dans un réseau électrique," EPFL2003.

[14] S. Mouassa, "Optimisation de l'écoulement de puissance par une méthode métaheuristique (technique des abeilles) en présence d'une source renouvelable (éolienne) et des dispositifs FACTS," 2018.

[15] A. Shehata, A. Refaat, and N. Korovkin, "Optimal allocation of FACTS devices based on multi-objective multi-verse optimizer algorithm for multi-objective power system optimization problems," in *2020 International Multi-Conference on Industrial Engineering and Modern Technologies (FarEastCon)*, 2020, pp. 1-7.

[16] A. Amarendra, L. R. Srinivas, and R. S. Rao, "Security enhancement in power system using FACTS devices and atom search optimization algorithm," *EAI Endorsed Transactions on Energy Web*, vol. 8, pp. e9-e9, 2021.

[17] P. Venkata, K. S. Sarat, and A. Jayalaxmi, "Comparison of Hybrid DifferentialEvolution Algorithm with GeneticAlgorithm Based Power System SecurityAnalysis Using FACTS," 2015.

[18] M. K. Zarkani, A. S. Tukkee, and M. J. Alali, "Optimal placement of facts devices to reduce power system losses using evolutionary algorithm," *Indones. J. Electr. Eng. Comput. Sci*, vol. 21, pp. 1271-1278, 2021.

[19] M. Nadeem, K. Imran, A. Khattak, A. Ulasyar, A. Pal, M. Z. Zeb, *et al.*, "Optimal placement, sizing and coordination of FACTS devices in transmission network using whale optimization algorithm," *Energies*, vol. 13, p. 753, 2020.

[20] T. R. Nartu, M. S. Matta, S. Koratana, and R. K. Bodda, "A fuzzified Pareto multiobjective cuckoo search algorithm for power losses minimization incorporating SVC," *Soft Computing*, vol. 23, pp. 10811-10820, 2019.

[21] R. Sirjani and A. Mohamed, "Improved harmony search algorithm for optimal placement and sizing of static var compensators in power systems," in *2011 First International Conference on Informatics and Computational Intelligence*, 2011, pp. 295-300.

[22] K. P. Nguyen, D. N. Vo, and G. Fujita, "Hybrid cuckoo search algorithm for optimal placement and sizing of static var compensator," in *Handbook of Research on Modern Optimization Algorithms and Applications in Engineering and Economics*, ed: IGI Global, 2016, pp. 288-326.

[23] S. Dixit, L. Srivastava, and G. Agnihotri, "Minimization of power loss and voltage deviation by SVC placement using GA," *International Journal of Control and Automation*, vol. 7, pp. 95-108, 2014.

[24] S. Udgir, S. Varshney, and L. Srivastava, "Optimal placement and sizing of SVC for voltage security enhancement," *International Journal of Computer Applications*, vol. 32, pp. 44-51, 2011.

[25] J. Vanishree and V. Ramesh, "Optimization of size and cost of static var compensator using dragonfly algorithm for voltage profile improvement in power transmission systems," *Int. J. Renew. Energy Res*, vol. 8, pp. 56-66, 2018.

[26] M. Zamani, I. Musirin, S. Suliman, and T. Bouktir, "Chaotic immune symbiotic organisms search for SVC installation in voltage security control," *Indones. J. Electr. Eng. Comput. Sci*, vol. 16, pp. 623-630, 2019.

[27] A. A. Shehata, A. Refaat, M. K. Ahmed, and N. V. Korovkin, "Optimal placement and sizing of FACTS devices based on Autonomous Groups Particle Swarm Optimization technique," *Archives of Electrical Engineering*, vol. 70, pp. 161-172, 2021.

[28] T. T. Nguyen and F. Mohammadi, "Optimal placement of TCSC for congestion management and power loss reduction using multi-objective genetic algorithm," *Sustainability*, vol. 12, p. 2813, 2020.

[29] R. Agrawal, S. Bharadwaj, and D. Kothari, "Population based evolutionary optimization techniques for optimal allocation and sizing of Thyristor Controlled Series Capacitor," *Journal of electrical systems and information technology*, vol. 5, pp. 484-501, 2018.

[30] M. S. Kumar and P. Renuga, "Bacterial foraging algorithm based enhancement of voltage profile and minimization of losses using thyristor controlled series capacitor (TCSC)," *International Journal of Computer Applications*, vol. 7, pp. 21-27, 2010.

[31] M. Shafik, G. Rashed, R. A. El-Sehiemy, and H. Chen, "Optimal sizing and sitting of TCSC devices for multi-objective operation of power systems using adaptive seeker optimization algorithm," in *2018 IEEE region ten symposium (tensymp)*, 2018, pp. 231-236.

[32] A. A. J. Basha, M. Anitha, and E. Elanchezhian, "Optimal placement of TCSC for congestion management in deregulated power system using firefly algorithm," *International Journal of Process Systems Engineering*, vol. 5, pp. 4-29, 2019.

[33] N. R. K. CH and K. C. Sekhar, "Optimal Placement of TCSC Based on Sensitivity Analysis for Congestion Management," *International Journal of Electrical & Computer Engineering (2088-8708)*, vol. 6, 2016.

[34] M. Sarwar and A. S. Siddiqui, "A novel approach for optimal allocation of series FACTS device for transmission line congestion management," *Engineering Reports*, vol. 3, p. e12342, 2021.

[35] A. Abdelaziz, M. El-Sharkawy, and M. Attia, "Optimal location of thyristor-controlled series compensators in power systems for increasing loadability by genetic algorithm," *Electric Power Components and Systems*, vol. 39, pp. 1373-1387, 2011.

[36] E. M. Malatji, B. Twala, and N. Mbuli, "Optimal placement model of TCSC in power system network considering the budget available," in *2017 International Electrical Engineering Congress (iEECON)*, 2017, pp. 1-5.

CHAPTER III

RENEWABLE ENERGY

III.1 Introduction

The rapid rise in energy consumption, combined with the high costs associated with traditional thermal generators, has thrown the world into a complex situation involving greenhouse gas emissions and economic instability. As a result, the attraction of renewable energy sources has grown significantly, owing to falling costs of installing and operating renewable energy systems, as well as increased global concern about environmental issues. The incorporation of RES provides numerous benefits, including economic, societal, and environmental dimensions, all of which contribute to the achievement of sustainability. Solar photovoltaics (SPV) and wind turbines (WT) are currently the two most prominently integrated RES within electricity networks [1, 2]. This chapter provides a comprehensive overview of wind and solar power, as well as information on global consumption trends. Following that is a succinct examination of the operational principles underlying wind and solar energy systems. The chapter then introduces stochastic modelling of power output from wind turbines and solar panels, which is essential for including them in the power flow model to be improved. At its core, this chapter discusses the formulation of the Optimal Power Flow (OPF) problem, highlighting the importance of its resolution through the incorporation of solar and wind power sources.

III.2 Renewable energy

Growing power consumption is one of the most pressing issues confronting the power market, but traditional energy sources are incapable of keeping up. To meet demand, renewable energy sources are combined with existing energy infrastructure. Wind and solar energy are the primary sources of energy used in this context.

As a result of the continued use of fossil fuels, fossil fuel reserves have shrunk, having a severe impact on the ecosystem, depleting the biosphere, and causing global warming [3].

Renewable energy, also known as green energy or clean energy, is energy derived from renewable natural resources or processes such as wind, sunlight, rain, geothermal heat, and tides [4, 5].

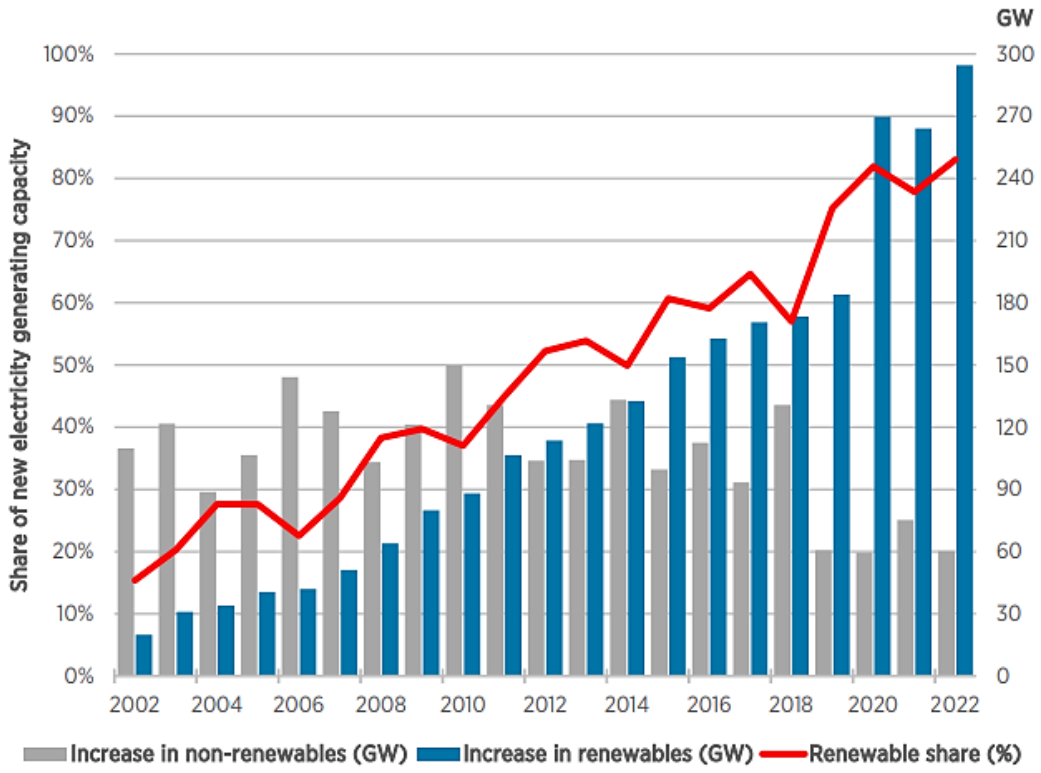

Figure III.1. The proportion of renewable energy sources in the annual electricity capacity expansion [6].

In 2022, renewable generating capacity expansion increased compared to 2021 and stayed well above the long-term trend. As in previous years, most of this expansion occurred in China and, to a lesser extent, the United States. However, a broad range of other countries also increased their expansion of renewable capacity in 2022 compared to 2021. The share of renewables in total capacity expansion reached 83% in 2022, compared to the Figure III.1 of 78% in 2021. The renewable share of total generation capacity also rose by almost two percentage points from 38.3% in 2021 to 40.2% in 2022 [6].

III.2.1 Wind energy

Wind energy is undoubtedly the clean energy par excellence, and its principle of operation is simple, since it captures the kinetic energy of the wind using a generator, and this energy can be exploited to produce mechanical energy and this technology is known as wind turbines or turbines, which can be used to convert mechanical energy into electrical energy [3, 7].

III.2.2 Solar energy

Solar energy is energy that relies on the conversion of sunlight into electricity, either directly using photovoltaic (PV) technology using energy electronics, or indirectly using concentrated

solar power technology (CSP) in which mirrors and lenses are used to concentrate the largest area of sunlight, which uses mirrors and lenses to focus sunlight into a small area. The concentrated sunlight converts water into steam, which is then used to generate power via steam turbines.

In recent years, solar energy has attracted the attention of many researchers, due to its ability to be used in various fields, such as house heating, water heating, industrial activities, etc [5, 8].

III.2.3 Hydropower

This energy is considered among the oldest types of renewable energies that humans used in ancient times in several uses such as water mills, textile factories, home elevators, etc. Where this energy is among the renewable energies that do not release gases polluting the environment [9].

The widespread method of generating electricity in hydroelectric stations is the use of water reservoirs or what is known as dams, where the kinetic energy of water is converted into mechanical energy using water turbines, the latter being connected to electric generators, and in the end, power generation, and thus electricity can be generated whenever we need it [7, 10].

III.2.4 Bioenergy

It is the energy of its total dependence on organic matter which generally comes from plants or animals (wood, algae, agricultural crop waste, and animal remains... etc.), which can be used as a source energy or heat production by burning it directly, and the steam produced the same day by the operation of the steam turbines and then from the production of electrical energy, we therefore extract three main forms of biomass sources, which are thermal, mechanical and electrical.

This combustion generates greenhouse gases, and yet the energy remains a renewable energy due to the ability of trees to absorb them naturally [7, 9].

III.2.5 Geothermal energy

It is a type of renewable energy that has been used since ancient times, and it is derived from heat deep within the earth. This energy was formed through the decay of radioactive minerals many years ago, and more the greater the penetration into the earth, the higher the temperature

and the pressure. This energy can be used for bathing, heating, cooking and heating or cooling buildings...etc.

III.2.6 Ocean energy

There are two types of energy produced by the ocean: thermal energy from sunlight and mechanical energy from tides and waves. In the first type, the sun's heat heats the surface ocean water, which is then used to generate electricity via steam turbines. Although the sun's rays affect the entire ocean, winds and gravity are the primary causes of waves and tides. As a result, tidal and wave energy are variable, as opposed to ocean thermal energy, which is relatively constant [9].

III.3 Wind Power Systems

Wind energy is recognized as one of the most promising renewable energy sources, and it may be an innovative solution to the current energy crisis and the problems related to global warming [11]. Wind energy is the second largest renewable energy source after hydropower, and it is one of the most quickly developing energy sources. One of the key advantages of using wind as an energy source is the speedy installation of supporting infrastructure, such as wind turbines and power plants. Wind farms with a pair or several hundreds of turbines can be built fast based on specific requirements [12].

Wind energy has clearly established itself as an economically competitive type of electricity generation on a national and global scale, according to the World Wind Energy Council's 2023 Report. New global installed capacity for wind electricity generation was 77.6 GW by the end of 2022. This brings total installed capacity to 906 GW, representing a 9% yearly increase over 2021. The majority of this increase has occurred in China, with less impact in the United States, followed by Brazil, Germany, and Sweden. These countries supplied 71% of the global total for wind energy generation that year [13].

III.3.1 System Components

A wind power system is made up of one or more wind turbines that produce energy at the same time. Each turbine contains the following fundamental components:

- **Tower:** This structure supports the turbine and raises it to a greater height where wind speeds are more consistent and higher. Taller towers provide turbines with more powerful and steady winds, increasing overall energy production.

- **Yaw system:** This system automatically aligns the turbine with the wind direction for the best power capture.
- **Blades:** Wind turbine blades capture the kinetic energy of the wind and convert it into rotational motion, which is utilized to produce energy.
- **Pitch system:** it regulates blade angle in response to wind velocity.
- **Brake:** A safety system which stops or slows the turbine's rotation during maintenance , emergencies, or high wind conditions to prevent damage and ensure safe operation.
- **Low and high-speed shafts:** In wind power, the low-speed shaft transmits energy from the rotor to the gearbox, and the high-speed shaft transmits energy from the gearbox to the generator.
- **Gearbox:** It connects the low-speed and high-speed shafts, raising the speed of the turbine from 30 to 60 rpm to 1200 to 1800 rpm, which most generators require to generate power effectively.
- **Generator:** A device that converts mechanical energy from revolving blades and shafts into electrical energy, generating electricity that can be fed into the power grid or consumed locally.
- **Control system:** The control system in a wind turbine supervises operations, maximizes energy capture, guarantees safety, and regulates power output.
- **Anemometers:** It measure wind speed and strength, allowing the wind turbine to adjust propeller angles and performance to maximize power generation efficiency while preserving turbine integrity in various conditions.

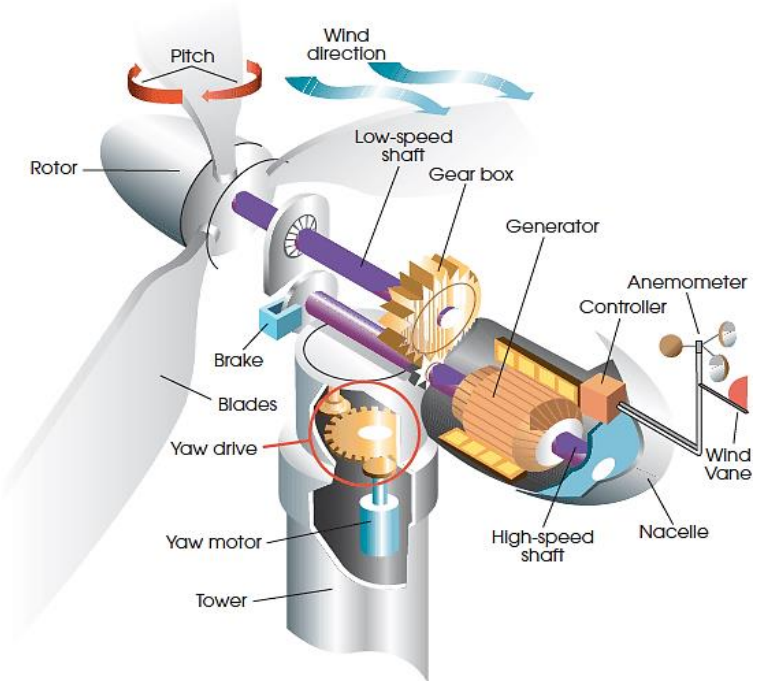

Figure III.2. Overview of Wind Turbine Elements.

III.3.2 Wind power generation

Wind turbines generate electricity by utilizing the available kinetic energy in the wind. This is accomplished via a system of revolving blades connected to a rotating shaft and an electric generator. As the wind blows through the blades, it creates an air thrust that causes the blades to revolve around the shaft. This generator converts rotating motion into usable electrical energy [14].

In order to achieve optimal performance and effective wind energy utilization, the system must include a controller. This device regulates the rotational speed of the blades and, in an emergency, can stop them. This is typically accomplished by employing sophisticated control systems that detect wind speed and direction and adjust the angle of the blades accordingly. This helps to keep turbine performance stable and safe in a variety of wind and weather conditions [15].

The mechanical power (P_a) captured by wind turbines can be expressed mathematically as follows:

Where:

$$P_a = \frac{1}{2} \times \rho \times A \times v^3 \quad \text{(III.1)}$$

P_a denotes the amount of kinetic energy received by the turbine (power unit).

ρ is the air density (mass/volume unit).

A denotes the area of the blade portion that is exposed to air (in the unit area).

v is the velocity unit of the wind passing through the blades.

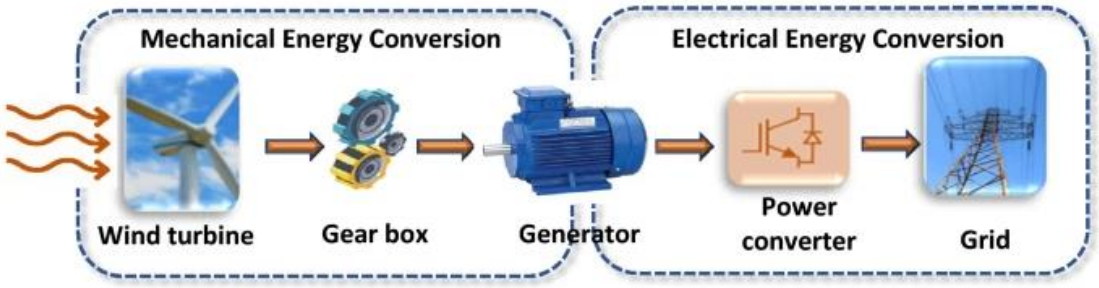

Figure III.3. Schematic representation of a wind turbine system**.**

III.3.3 Wind power modeling

One of the primary variables used in Eq. (III.1) to determine the potential for power generation at potential sites is wind speed. This speed varies constantly due to factors such as meteorological conditions, terrain, and site elevation above ground. Wind speed varies over short time intervals ranging from minutes to hours, days to seasons, and even throughout the year. A probability distribution function can be used to quantify these changes in wind speed over time. This function is frequently used to calculate the probability of various wind speeds and their distribution over time. By analyzing these probabilities, it is possible to estimate the amount of energy that a wind turbine can generate and predict its efficiency in a specific area [16, 17].

The probability density function (PDF) of the Weibull distribution for wind speed is given by Eq. (III.2):

$$f_v(v) = \frac{k}{c} * \left(\frac{v}{c}\right)^{k-1} * e^{-1*\left(\frac{v}{c}\right)^k}, v > 0 \quad \text{(III.2)}$$

Where v is the wind speed and k is the distribution's shape parameter. The value of k determines whether the distribution is skewed or symmetric.c is the scale parameter, which represents the characteristic wind speed of the location.

Weibull distribution average is described as:

$$M_{wbl} = c * \Gamma(1 + k^{-1}) \quad \text{(III.3)}$$

The gamma function (x) can be represented as follows:

$$\Gamma(x) = \int_0^\infty e^{-t} t^{x-1} dt \quad \text{(III.4)}$$

III.3.4 The Electrical Output of the Wind Turbine

The power curve shown in Figure III.4 is a useful tool for demonstrating how wind speed affects the electrical output of a wind turbine. It should be noted that this curve may vary depending on the specific characteristics of each turbine. This curve is created by analyzing data from anemometers located near the turbine. The following equation depicts the relationship between wind speed and predicted productivity [18]:

$$P_w(v) = \begin{cases} 0, & \text{for } v < v_{in} \text{ and } v > v_{out} \\ P_{wr}\left(\frac{v - v_{in}}{v_r - v_{in}}\right), & \text{for } v_{in} \leq v \leq v_r \\ P_{wr}, & \text{for } v_r < v \leq v_{out} \end{cases} \quad \text{(III.5)}$$

Where P_{wr} is the rated energy produced by the wind generator and v_{in} is the starting wind speed for power generation. Furthermore, v_{out} represents the wind speed at which the wind turbine is unplugged. Finally, v_r is the wind speed required for the generator to deliver its maximum mechanical power output.

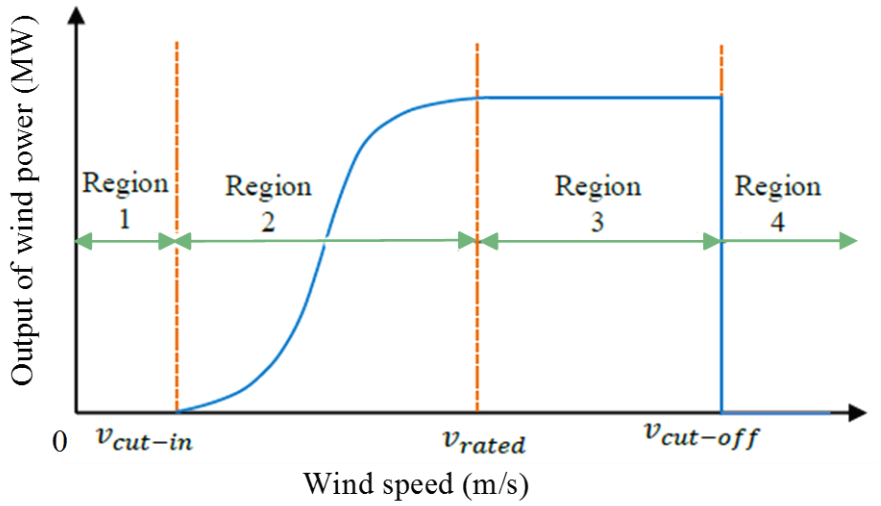

Figure III.4. Curve of Wind Power Output.

III.3.5 Probabilities of Wind Power for Various Wind Speeds

According to Eq. (III.5), the variable power output of wind generators is discretized during given wind speed intervals. When the wind speed (v) falls below or exceeds the cut-in speed (v_{in}), the output power is 0. The output power, on the other hand, reaches its rated value when the wind speed is between the rated wind speed (v_r) and the cut-out speed (v_{out}). The probabilities affecting wind output power within these discrete ranges are calculated as follows [19]:

$$F_w(P_w)\{P_w = 0\} = 1 - \exp\left(-\left(\frac{v_{in}}{c}\right)^k\right) + exp\left(-\left(\frac{v_{out}}{c}\right)^k\right) \quad \text{(III.6)}$$

$$F_w(P_w)\{P_w = P_{wr}\} = \exp\left(-\left(\frac{v_r}{c}\right)^k\right) - exp\left(-\left(\frac{v_{out}}{c}\right)^k\right) \quad \text{(III.7)}$$

Unlike the previously mentioned discrete intervals, the power output of a wind turbine (WT) exhibits a continuous behavior between the cut-in speed and the rated wind speed. As a result, we can express the probability associated with this interval as follows [20]:

$$F_w(P_w) = \frac{k(v_r - v_{in})}{c^k \times P_{wr}}\left[v_{in} + \frac{P_w}{P_{wr}}(v_r - v_{in})\right]^{k-1} \times exp\left[-\left(\frac{v_{in} + \frac{P_w}{P_{wr}}(v_r - v_{in})}{c}\right)^k\right] \quad \text{(III.8)}$$

III.4 Solar power system

A solar power system is a technology that absorbs and converts sunlight into electrical energy. It gets its power from the sun, which is renewable and abundant. These technologies are crucial for lowering reliance on fossil fuels while minimizing the environmental impact of energy consumption. Solar power systems are divided into two main categories: photovoltaic (PV) systems and concentrated solar power (CSP) systems. CSP, like traditional thermal power generation, operates by turning thermal energy, usually in the form of steam, into electricity. PV solar panels, on the other hand, use the "Photovoltaic effect" to convert sunlight directly into direct current (DC). This direct current (DC) then gets converted to alternating current (AC) by inverters and other components, allowing it to connect to the power grid.

Although CSP offers advantages in grid integration, its technology and cost limit large-scale growth. PV benefits from lower costs and favorable energy market circumstances, making it more appealing [21].

The solar industry is rapidly expanding and achieved a major milestone in 2022 by surpassing the terawatt (TW) threshold for new solar capacity installations worldwide. This represents a remarkable 45% increase in solar power capacity compared to the previous year. China continues to dominate the global market, with extraordinary growth rates resulting in a whopping 94.7 GW of solar installations in 2022. followed by the United States (21.9 GW), India (17.4 GW), Brazil (10.9 GW), and Spain (8.47 GW).

Based on the encouraging developments seen in the first few months of 2023, it appears like there is potential for significant growth this year. According to forecasts, an additional 341 GW of solar capacity might be added to the grid by year's end, representing a 43% increase [22].

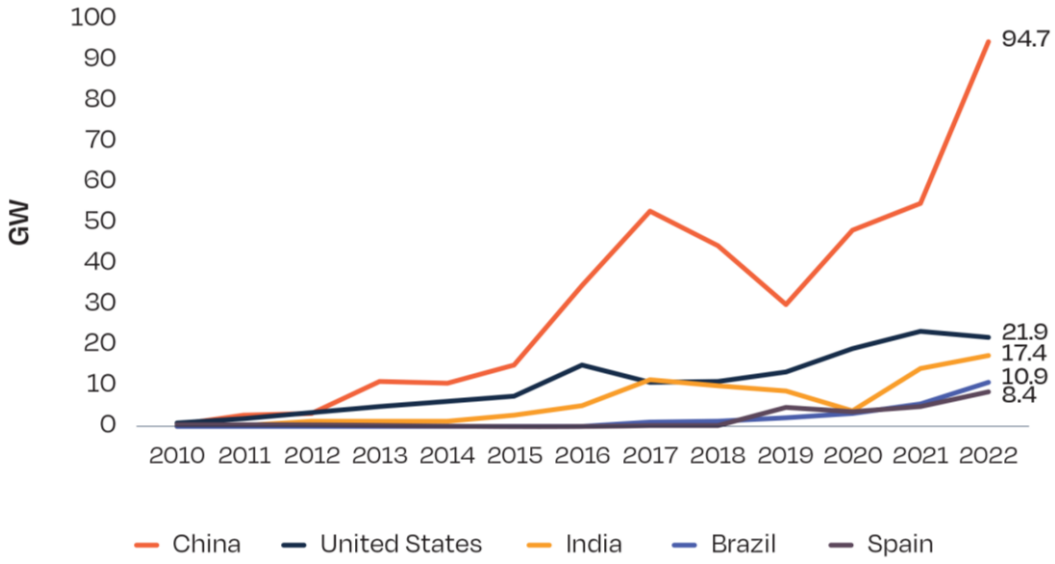

Figure III.5. The Five Dominant Solar PV Markets from 2010 to 2022.

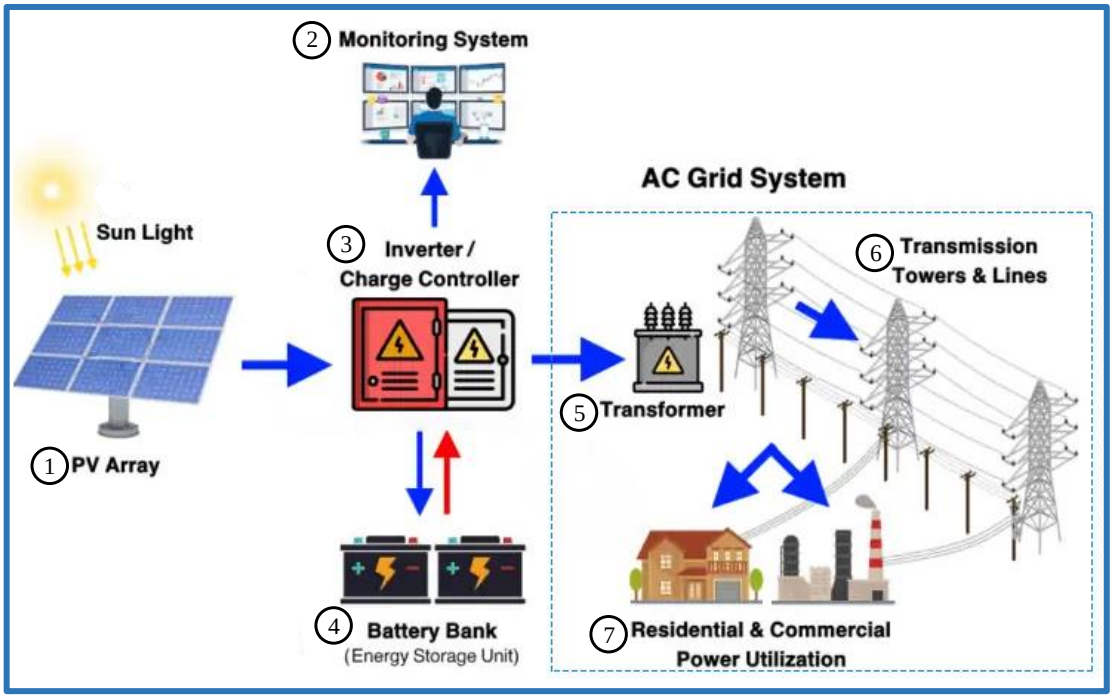

Figure III.6. The key components of a solar photovoltaic (PV) system.

III.4.1 System Components

In Figure III.6, the key elements of a solar photovoltaic (PV) power system are illustrated, including:

- **Solar Panels (Photovoltaic Modules):** These are the key components that convert sunlight into direct current (DC) electricity using photovoltaic cells. A solar module

is constructed by the sequential arrangement of several solar cells, as shown in Figure III.7. These modules are then joined to produce a string. These strings are subsequently connected in parallel, resulting in the creation of an array. This structured assembly meets rising energy demands, from small-scale applications with kilowatt outputs to big utility-scale projects with megawatts and even gigawatts [23].

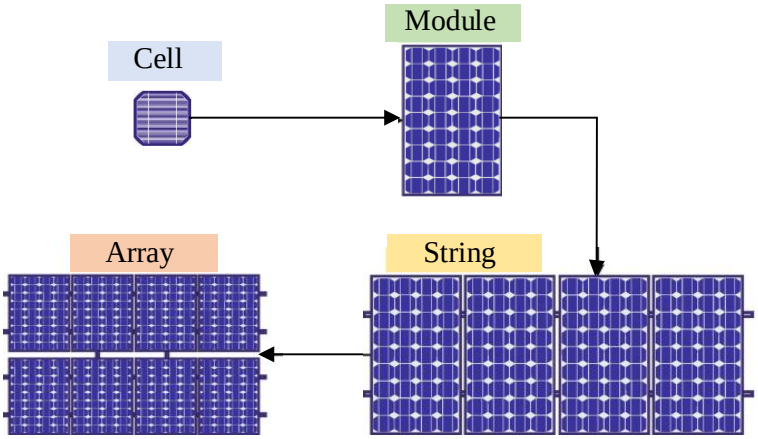

Figure III.7. Conversion of a Single PV Cell into a Photovoltaic (PV) String.

- **Monitoring System:** This system checks the functioning of the solar PV system, including energy output and potential problems.
- **Inverter:** A device that converts direct current (DC) electricity produced by solar panels into alternating current (AC) electricity appropriate for household and grid use. Inverters also help to achieve optimal output from PV modules by utilizing MPPT techniques.
- **Batteries:** They play a significant part in storing extra energy generated by solar panels during sunny days. This stored energy is thus ready for use during low sunlight or high demand periods, ensuring a constant and consistent power supply, and is employed in both off-grid and hybrid systems.
- **Transformers:** They are responsible for managing the voltage levels of the electricity generated by solar panels. They increase the voltage for effective long-distance transmission over power lines and decrease the voltage before it enters homes and businesses for safe and practical use. This ensures that the electricity generated by solar power systems may be successfully integrated into the larger electrical grid and used by consumers [24].

III.4.2 Solar power generation

Photovoltaic (PV) systems harness the power of solar panels made of semiconductor materials, also known as PV cells. The most prevalent of these materials is silicon, which comes in monocrystalline, polycrystalline, and amorphous forms. When these panels are exposed to sunlight, they allow energy to be emitted in the form of photons. When photons interact with semiconductor material, they excite electrons, resulting in the flow of electric current (Figure III.8). Inverters convert the generated direct current (DC) power to alternating current (AC). The electricity produced can be utilized to operate common household equipment inside buildings or fed back into the power grid. These cells convert sunlight to electrical energy with a typical efficiency of 15% to 20%. The highest power that a solar cell can produce under specified testing conditions is measured in watts or kilowatt peak [23, 25].

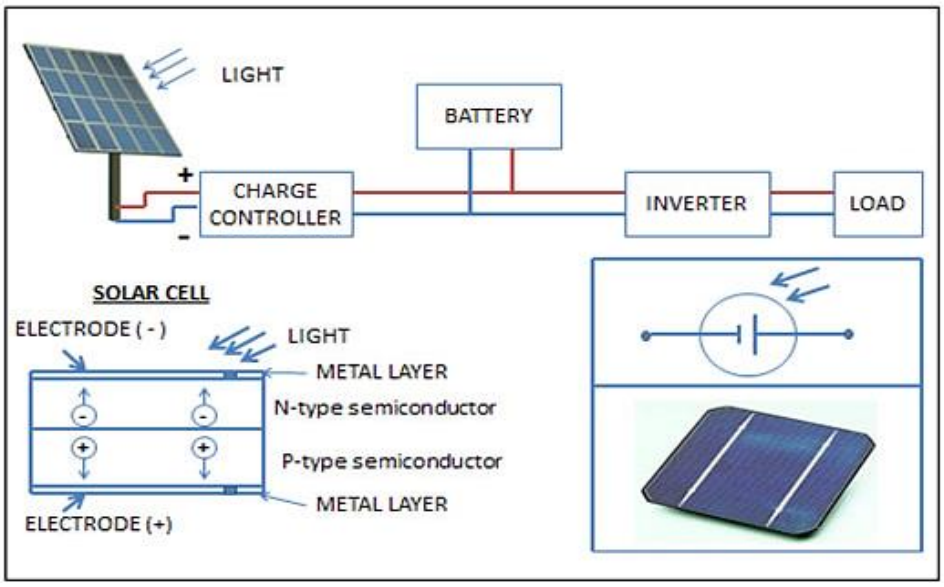

Figure III.8. The Working Principle of a Solar Panel.

III.4.3 Solar power modeling

Weather factors such as cloud cover and sun irradiation affect solar power generation. This causes electricity generation to fluctuate and be unpredictable. The variance in solar irradiance, denoted by G, has a role in this. To address this issue, we provide a probabilistic method for predicting solar irradiance that is based on the lognormal probability distribution function $f_G(G)$, as shown in Eq. (III.9).

$$f_G(G) = \frac{1}{G\sigma\sqrt{2\pi}} \exp\left\{\frac{-(\ln G - \mu)^2}{2\sigma^2}\right\} \text{ for } G > 0 \qquad \text{(III.9)}$$

Where μ and σ indicate the mean and standard deviation of the lognormal probability distribution function.

lognormal distribution average is described as:

$$M_{lgn} = exp\left(\mu + \frac{\sigma^2}{2}\right) \quad \text{(III.10)}$$

III.4.4 Realized Output Power of PV Systems

The primary goal of solar power generation systems is to catch sunlight and transform it into usable electricity. This approach comprises calculating solar irradiation and using it as a parameter to determine the output power of solar systems. The following equation depicts the link between sun irradiance and output power for these systems.

$$P_s(G) = \begin{cases} P_{sr}\left(\frac{G^2}{G_{std}R_c}\right) & \text{for } 0 < G < R_c \\ P_{sr}\left(\frac{G}{G_{std}}\right) & \text{for } G \geq R_c \end{cases} \quad \text{(III.11)}$$

G denotes the intensity of solar power incident on the surface of a PV module and is measured in watts per square meter (W/m2), P_{sr} is the rated output power of a solar PV unit, G_{std} denotes the irradiance under normal conditions (STC) with a consistent value of 800 W/m2. Finally, R_c denotes a particular fixed irradiance point of 120 W/m2.

III.5 OPF formulation considering stochastic wind and solar power

This section outlines the problem formulation of the Optimal Power Flow (OPF), wherein wind, solar, and thermal generators are treated as pivotal elements within the power generation framework. The primary objective is to curtail generation costs while adhering to the limitations imposed by the system. Achieving optimal power scheduling with Renewable Energy Resources (RERs) necessitates the adept management of uncertainties that arise from the intermittent nature of solar and wind power generation. The cumulative generation output from thermal generators and RERs must satisfy the overall load demand. The subsequent segment delves into the specifics of calculating individual generation costs, as well as addressing both equality and inequality constraints.

III.5.1 The operational cost of fuel

To sustain the operation of thermal generators, fossil fuels are imperative, as their output power correlates directly with fuel consumption. This interdependence between fuel costs ($/h) and output power (MW) of the thermal generators can be articulated as follows:

$$C_T(P_{Gi}) = \sum_{i=1}^{NG} (a_i + b_i P_{Gi} + c_i P_{Gi}^2) \quad \text{(III.12)}$$

Where C_T denotes the fuel cost of the generated power, Ng denotes the total number of conventional thermal generators, P_{Gi} is the actual power generated by unit i, and a_i, b_i, and c_i indicate the cost coefficients associated with the respective i-th conventional thermal generator.

The cost function of thermal generators powered by multi-valve steam turbines is highly variable. As a result, including valve point effects into a more exact and thorough cost function for these generators is required. These effects, which take the form of a sinusoidal function, must be included as an intrinsic component in the fundamental cost structure of thermal generators. As a result, the cost function equation is altered to account for the valve point effect:

$$C_T(P_{Gi}) = \sum_{i=1}^{NG} (a_i + b_i P_{Gi} + c_i P_{Gi}^2) + \left| d_i \times sin\left(e_i\left(P_{TG}^{min} - P_{Gi}\right)\right)\right| \quad \text{(III.13)}$$

Where d_i and e_i stand for the valve point cost coefficients associated with unit i, while P_{TG}^{min} indicates the lowest actual power output produced by the i-th conventional generator when it is actively operating.

III.5.2 Direct Expenses for Wind and Solar Photovoltaic power

Wind and solar farms are often privately owned. As a result, the grid operator or ISO bears the cost of planned electricity procurements from these private operators, classifying this as a direct cost. The direct cost associated with the j-th wind power station in terms of planned power is calculated as follows:

$$C_{w,j}\left(P_{ws,j}\right) = g_j P_{ws,j} \quad \text{(III.14)}$$

Where g_j is the scheduled cost coefficient for the j-th wind farm and $P_{ws,j}$ is the planned wind power generated by the j-th wind farm.

Similarly, a direct expense ascribed to the k-th solar photovoltaic (SPV) sources generating $P_{ss,j}$ planned power can be stated as:

$$C_{s,k}(P_{ss,k}) = h_k P_{ss,k} \quad \text{(III.15)}$$

Where h_j is the direct cost coefficient associated with the solar photovoltaic (SPV) generator [26].

III.5.3 Underestimation of Wind and Solar Power Costs

The following scenario occurs when the wind power plant's output exceeds the projected power output value. This is known as an underestimate of output power. As a result, if surplus electricity cannot be absorbed by reducing the output of traditional generators, it is wasted. In such cases, the Independent System Operator (ISO) is liable for the penalty cost associated with the excess power. This cost can be calculated for the wind power generator indexed as 'j' using the following formula [27]:

$$\begin{aligned} C_{Pw,j}(P_{wav,j} - P_{ws,j}) &= K_{Pw,j}(P_{wav,j} - P_{ws,j}) \\ &= K_{Pw,j} \int_{P_{ws,j}}^{P_{wr,j}} (p_{w,j} - P_{ws,j}) f_w(p_{w,j}) dp_{w,j} \end{aligned} \quad \text{(III.16)}$$

Where $K_{Pw,j}$ is the penalty cost coefficient and $P_{wr,j}$, $P_{wav,j}$ and $P_{ws,j}$ are the rated, available, schedule power associated with the j-th wind power station, respectively, $f_w(p_{w,j})$ is the PDF representing the wind power produced by the j-th power plant.

Solar energy, like wind energy, has erratic and intermittent output. The strategy used to address underestimation of solar output power should largely be the same as that used to address underestimation of wind output power.

The penalty cost for the solar PV plant is outlined as follows [19]:

$$\begin{aligned} C_{Ps,k}(P_{sav,k} - P_{ss,k}) &= K_{Ps,k}(P_{sav,k} - P_{ss,k}) \\ &= K_{Ps,k} * f_s(P_{sav,k} > P_{ss,k}) * [E(P_{sav,k} > P_{ss,k}) - P_{ss,k}] \end{aligned} \quad \text{(III.17)}$$

Where $K_{Ps,k}$ denotes the penalty cost constant connected with the kth solar PV plant. $P_{sav,k}$ and $P_{ss,k}$ are the available, schedule power associated with the k-th solar power station, respectively, $f_s(P_{sav,k} > P_{ss,k})$ denotes the probability of the k-th solar power plant producing more power than PSs, and $E(P_{sav,k} > P_{ss,k})$denotes the predicted surplus power output.

III.5.4 Overestimation of Wind and Solar Power Costs

Wind turbines may fail to produce the scheduled power in some circumstances, resulting in periods when actual output falls short of projections. This is known as the overestimation of output power. To address this problem, system operators must assign spinning reserves from traditional generators. These reserves are a precautionary measure intended to offset any overestimation of renewable energy source output, ensuring consumers have a continuous power supply. The costs of maintaining this reserve capacity are known as reserve generation costs, which can be elucidated as follows:

$$C_{Rw,j}(P_{ws,j} - P_{wav,j}) = K_{Rw,j}(P_{ws,j} - P_{wav,j}) = K_{Rw,j}\int_0^{P_{ws,j}} (P_{ws,j} - p_{w,j}) f_w(p_{w,j}) dp_{w,j} \quad \text{(III.18)}$$

Where $K_{Rw,j}$ K is the reserve cost coefficient particular to the wind power plant. Furthermore, $P_{wav,j}$ represents the actual power generated by the same plant [4] .

Solar energy, like wind energy, has erratic and intermittent output. The strategy used to address overestimation of solar output power should largely be the same as that used to address overestimation of wind output power. The following equation provides the formula for calculating the reserve cost of a solar photovoltaic (PV) plant:

$$C_{Rs,k}(P_{ss,k} - P_{sav,k}) = K_{Rs,k}(P_{ss,k} - P_{sav,k}) = K_{Rs,k} * f_s(P_{sav,k} < P_{ss,k}) * [P_{ss,k} - E(P_{sav,k} < P_{ss,k})] \quad \text{(III.19)}$$

Where $C_{Rs,k}$ denotes the cost incurred as a result of a decrease in solar power output and $K_{Rs,k}$ denotes the reserve cost coefficient particular to the solar power plant. Furthermore, $f_s(P_{sav,k} < P_{ss,k})$ represents the probability of a solar power generation shortfall, whereas $E(P_{sav,k} < P_{ss,k})$ represents the predicted solar PV power production falling below $P_{ss,k}$ [4].

The cost of wind electricity generated by a wind farm and solar power supplied by PV panels are displayed as follows:

$$C_{wind} = \sum_{j=1}^{N_{WG}} [C_{w,j}(P_{ws,j}) + C_{pw,j}(P_{wav,j} - P_{ws,j}) + C_{Rw,j}(P_{ws,j} - P_{wav,j})] \quad \text{(III.20)}$$

$$C_{Solar} = \sum_{k=1}^{N_{SG}} [C_{s,k}(P_{ss,k}) + C_{ps,k}(P_{sav,k} - P_{ss,k}) + C_{Rs,k}(P_{ss,k} - P_{sav,k})] \quad \text{(III.21)}$$

III.5.5 Carbon tax

In response to the global warming issue, governments around the world have put enormous pressure on the energy industry to reduce carbon emissions. This has resulted in the establishment of the carbon tax (C_{Tax}) imposed on each unit of greenhouse gas emissions, intending to encourage investment in environmentally friendly energy sources such as wind and solar power. The cost of emissions is symbolized by the symbols C_{emi} (dollars/hour) and is defined as follows [2]:

$$C_{emi} = C_{Tax}E \tag{III.22}$$

III.5.6 Objective function

The primary goal of this section is to reduce the overall cost of generating power in order to meet the energy demands of the system. This necessitates optimizing the scheduling of thermal, wind, and solar units while ensuring that they operate within their capabilities. The objective function is defined by Eq. (III.23), which considers the costs of fuel, wind, and solar power.

$$F_1 = C_T(P_{TG}) + \sum_{j=1}^{N_{wG}} \left[C_{w,j}(P_{ws,j}) + C_{Rw,j}(P_{ws,j} - P_{wav,j}) + C_{Pw,j}(P_{wav,j} - P_{ws,j})\right] + \sum_{k=1}^{N_{sG}} \left[C_{s,k}(P_{ss,k}) + C_{Rs,k}(P_{ss,k} - P_{sav,k}) + C_{Ps,k}(P_{sav,k} - P_{ss,k})\right] \tag{III.23}$$

III.5.7 Constraints

The overall objective of OPF is contingent on the system adhering to a set of equality and inequality constraints.

III.5.7.1 Equality constraints

Equality constraints include fundamental load flow equations that strive to achieve power balance for both active and reactive power generated within the system. This condition requires that these powers equal the total demand and system losses. The formulation of these equality restrictions is shown below [19]:

$$P_{Gi} - P_{Di} - V_i \sum_{j=1}^{NB} V_j\left(G_{ij}cos\,\theta_{ij} + B_{ij}sin\,\theta_{ij}\right) = 0 \tag{III.24}$$

$$Q_{Gi} - Q_{Di} - V_i \sum_{j=1}^{NB} V_j\left(G_{ij}sin\,\theta_{ij} - B_{ij}cos\,\theta_{ij}\right) = 0 \tag{III.25}$$

III.5.7.2 Inequality constraints

The inequality constraints that illustrate the restrictions of power system operation while integrating solar and wind generation are as follows:

a. Constraints pertaining to generators

$$P_{TGi}^{min} \leq P_{TGi} \leq P_{TGi}^{max}, i = 1, \dots\dots, N_{TG} \quad \text{(III.26)}$$

$$P_{\text{ws,j}}^{min} \leq P_{\text{ws},j} \leq P_{\text{ws,j}}^{max}, j = 1, \dots\dots, N_{WG} \quad \text{(III.27)}$$

$$P_{\text{ss,k}}^{min} \leq P_{ss,k} \leq P_{\text{ss,k}}^{max}, k = 1, \dots\dots, N_{SG} \quad \text{(III.28)}$$

$$Q_{TGi}^{min} \leq Q_{TGi} \leq Q_{TGi}^{max}, i = 1, \dots\dots, N_{TG} \quad \text{(III.29)}$$

$$Q_{\text{ws,j}}^{min} \leq Q_{ws,j} \leq Q_{\text{ws,j}}^{max}, j = 1, \dots\dots, N_{Wc} \quad \text{(III.30)}$$

$$Q_{ss,\text{k}}^{min} \leq Q_{ss,k} \leq Q_{ss,\text{k}}^{max}, k = 1, \dots\dots, N_{SG} \quad \text{(III.31)}$$

$$V_{Gi}^{min} \leq V_{Gi} \leq V_{Gi}^{max}, i = 1, \dots\dots, NG \quad \text{(III.32)}$$

b. Safety constraints

$$V_{Li}^{min} \leq V_{\text{Li}} \leq V_{Li}^{max}, p = 1, \dots\dots, N_{PQ} \quad \text{(III.33)}$$

$$S_{li} \leq S_{li}^{max}, q = 1, \dots\dots, NL \quad \text{(III.34)}$$

III.6 Conclusion

This chapter describes a comprehensive strategy for dealing with optimal power flow (OPF) complexity when stochastic elements from wind and solar energy are present. We begin by introducing several well-known renewable energy sources that can help promote sustainable energy. Then, wind and solar energy systems were highlighted, along with their numerous components and energy-producing processes. As a result, a detailed discussion of the modeling techniques used to deal with unexpected fluctuations in the production of these systems is presented. On that basis, the formulation of the OPF problem is provided, considering the effects of wind and sun random variables. Several probability density functions are used to overcome the uncertainties associated with renewables. The cost of generation, which includes all sources, was discussed, as well as the variation in generation cost with changes in cost factors (reserve cost and penalty cost), with an emphasis on the critical role of carbon taxation in incentivizing the optimal use of clean, particularly renewable energy sources. Finally, an emphasis is placed on maintaining power system restrictions in order to ensure the safe operation of the power system within prescribed limits.

References

[1] K. Nusair, F. Alasali, A. Hayajneh, and W. Holderbaum, "Optimal placement of FACTS devices and power-flow solutions for a power network system integrated with stochastic renewable energy resources using new metaheuristic optimization techniques," *International Journal of Energy Research*, vol. 45, pp. 18786-18809, 2021.

[2] M. Riaz, A. Hanif, S. J. Hussain, M. I. Memon, M. U. Ali, and A. Zafar, "An optimization-based strategy for solving optimal power flow problems in a power system integrated with stochastic solar and wind power energy," *Applied Sciences*, vol. 11, p. 6883, 2021.

[3] H. K. C. Prateek Shrivastava, *Optimal Integration of Renewable Energy for Micro-Grid*, 2022.

[4] T. H. B. Huy, T. P. Nguyen, N. M. Nor, I. Elamvazuthi, T. Ibrahim, and D. N. Vo, "Performance improvement of multiobjective optimal power flow-based renewable energy sources using intelligent algorithm," *IEEE Access*, vol. 10, pp. 48379-48404, 2022.

[5] A. J. Wood, B. F. Wollenberg, and G. B. Sheblé, *Power generation, operation, and control*: John Wiley & Sons, 2013.

[6] IRENA. (20 March 2023). *Renewable capacity highlights*. Available: https://www.irena.org/Data/Statistical-publications/Notes-and-Methodology

[7] R. Kouadri, "Contribution to the optimization of renewable energies integration in electrical network considering FACTS-HVDC devices," 2021.

[8] I. Sarbu, M. Mirza, and D. Muntean, "Integration of Renewable Energy Sources into Low-Temperature District Heating Systems: A Review," *Energies*, vol. 15, p. 6523, 2022.

[9] J. G. Speight, *Encyclopedia of renewable energy*. MA, USA: Wiley-Scrivener: Beverly, 2022.

[10] N. Nwulu and S. L. Gbadamosi, *Optimal Operation and Control of Power Systems Using an Algebraic Modelling Language*: Springer Nature, 2021.

[11] S. Feleke, R. Satish, B. Pydi, D. Anteneh, A. Y. Abdelaziz, and A. El-Shahat, "Damping of Frequency and Power System Oscillations with DFIG Wind Turbine and DE Optimization," *Sustainability*, vol. 15, p. 4751, 2023.

[12] G. Nikitas, S. Bhattacharya, and N. Vimalan, "Wind energy," in *Future Energy*, ed: Elsevier, 2020, pp. 331-355.

[13] G. W. E. Council–GWEC, "Global wind report 2023," ed: Brussels: Global Wind Energy Council. Retrieved in, 2023.

[14] M. B. A. Bashir, "Principle parameters and environmental impacts that affect the performance of wind turbine: an overview," *Arabian Journal for Science and Engineering*, vol. 47, pp. 7891-7909, 2022.

[15] M. G. Molina and P. E. Mercado, "Modelling and control design of pitch-controlled variable speed wind turbines," in *Wind turbines*, ed: IntechOpen, 2011.

[16] H. Chen, Y. Birkelund, S. N. Anfinsen, R. Staupe-Delgado, and F. Yuan, "Assessing probabilistic modelling for wind speed from numerical weather prediction model and observation in the Arctic," *Scientific Reports,* vol. 11, p. 7613, 2021.

[17] M. R. Patel and O. Beik, *Wind and solar power systems: design, analysis, and operation*: CRC press, 2021.

[18] V. Sohoni, S. Gupta, and R. Nema, "A critical review on wind turbine power curve modelling techniques and their applications in wind based energy systems," *Journal of Energy,* vol. 2016, 2016.

[19] M. Farhat, S. Kamel, A. M. Atallah, and B. Khan, "Optimal Power Flow Solution Based on Jellyfish Search Optimization Considering Uncertainty of Renewable Energy Sources," *IEEE Access,* vol. 9, pp. 100911-100933, 2021.

[20] M. H. Hassan, S. K. Elsayed, S. Kamel, C. Rahmann, and I. B. M. Taha, "Developing chaotic Bonobo optimizer for optimal power flow analysis considering stochastic renewable energy resources," *International Journal of Energy Research,* vol. 46, pp. 11291-11325, 2022.

[21] K. Nwaigwe, P. Mutabilwa, and E. Dintwa, "An overview of solar power (PV systems) integration into electricity grids," *Materials Science for Energy Technologies,* vol. 2, pp. 629-633, 2019.

[22] S. Europe, "Global market outlook for solar power 2023-2027," *Solar Power Europe: Brussels, Belgium,* 2023.

[23] B. N. C. V. Chakravarthi, L. Hari Prasad, R. L. Chavakula, and V. Vijetha Inti, "Solar Energy Conversion Techniques and Practical Approaches to Design Solar PV Power Station," in *Sustainable and Clean Energy Production Technologies*, ed: Springer, 2022, pp. 179-201.

[24] Y. Abou Jieb, E. Hossain, Y. Abou Jieb, and E. Hossain, "Solar System Components," *Photovoltaic Systems: Fundamentals and Applications,* pp. 95-192, 2022.

[25] O. B. a. G. G. Massimiliano Lo Faro, *Hybrid Technologies for Power Generation*. London Elsevier Science, 2022.

[26] N. A. Nguyen, D. N. Vo, T. T. Nguyen, T. L. Duong, and T. Hong, "An Improved Equilibrium Optimizer Algorithm for Solving Optimal Power Flow Problem with Penetration of Wind and Solar Energy," *International Transactions on Electrical Energy Systems,* vol. 2022, pp. 1-21, 2022.

[27] M. A. Ali, S. Kamel, M. H. Hassan, E. M. Ahmed, and M. Alanazi, "Optimal power flow solution of power systems with renewable energy sources using white sharks algorithm," *Sustainability,* vol. 14, p. 6049, 2022.

CHAPTER IV

METAHEURISTIC OPTIMIZATION METHODS

IV.1 Introduction

Optimization issues are among the problems that researchers confront today. An optimization problem is one in which we can discern one or more objective functions, allowing us to distinguish between a good and a bad solution. Metaheuristic algorithms are one of the most important types of optimizations that have received significant attention from researchers due to their outstanding contribution to solving difficult problems and finding near-optimal solutions, unlike traditional algorithms, we find that these methods have several tangible applications, whether in industry, engineering or others.

The fundamental concepts of optimization will be covered in the first part of this chapter, followed by discussions of the various optimization problem types, issues with multi-objective optimization, and techniques for gauging proficiency in the second section. The cuckoo search algorithm, the ant lion algorithm, and other metaheuristic algorithms will be listed in the chapter's final part along with a brand-new multi-objective algorithm that is based on the contemporary spider wasp algorithm.

IV.2 Definition of optimization

Optimization has been used in a variety of fields, including engineering, business, industrial activities, and science. The optimization process is defined as the process of determining the best or optimal value (maximum or minimum value depending on the type of problem at hand) for the target function f while meeting predetermined conditions (constraints) [1, 2].

IV.3 General formulation of an optimization problem

The optimization problems are divided into sections according to the control variables, the objective function, the constraints, and so on. The single or multi-objective function criterion will be the focus of this work.

IV.3.1 Formulation of a single-objective optimization problem

Mathematically, the problem of minimization of a single-objective function can be defined as follows:

$$\begin{cases} Min: \{f_1(x,u)\} \\ g_i(x,u) = 0; \quad i = 1,2,3,\dots,m \\ h_j(x,u) \leq 0; \quad j = 1,2,3,\dots,p \end{cases} \tag{IV.1}$$

Where f is the objective function to be reduced, also known as the cost function, and m and p are the numbers of equality and inequality constraints of the optimization problem, respectively. s denotes the search space in which the variables of the objective function f can be found [1].

IV.3.1.1 Local and global minima

Local and global minima are fundamental concepts in optimization theory, and they are frequently used to characterize the best solutions to a given problem. These optimums can be applied to a wide range of mathematical, engineering, and scientific problems. Here is a definition for both terms, as well as their equations:

a. Local minimum

This refers to the solution with the best objective function in its neighborhood. Mathematically, a local minimum occurs when the function value at a specific place is less than the values of surrounding points within a defined range. In the context of a one-dimensional optimization issue, a feasible decision variable x^* is regarded as a local minimum in a minimization problem if there is a very small positive number ε such that $f(x^*) \leq f(x)$ for any x in the range $(x^* - \varepsilon, x^* + \varepsilon)$. As a result, the local minimum is occasionally denoted as:

$$f(x^*) = \min_{x \in (x^* - \varepsilon,\, x^* + \varepsilon)} f(x) \qquad \text{(IV.2)}$$

b. Global minimum

This is the lowest point in the function, i.e. the point at which the function achieves its lowest value across its entire domain. Finding the global optimum is the ultimate goal in most optimization tasks, though it may be more difficult than finding the local optimum. In a one-dimensional optimization issue with a decision variable x and an objective function $f(x)$, the value x^* denotes a global minimum in a minimization problem if $f(x^*) \leq f(x)$ for any x in the space of f.

Figure IV.1 emphasizes the distinction between global and local minima by demonstrating how an objective function can have multiple local minima while only having one global minimum.

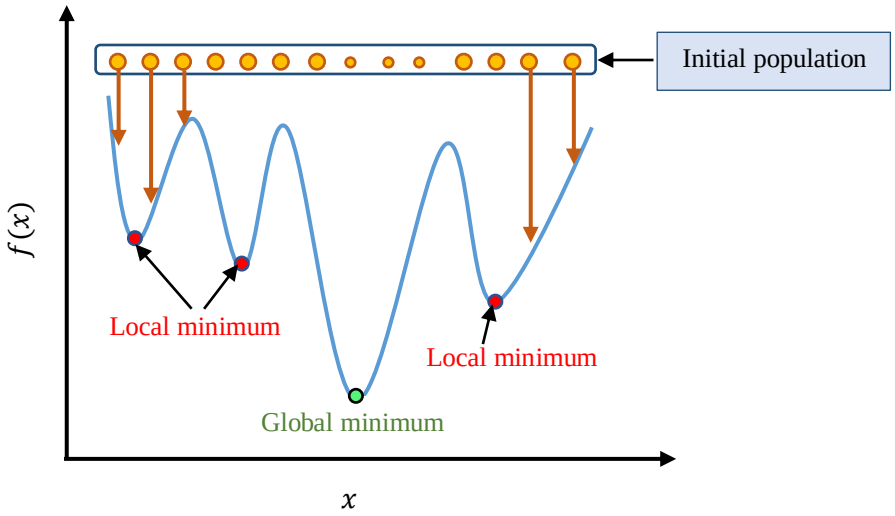

Figure IV.1. A diagram of the global and local minima of an objective function.

IV.3.2 Formulation of the multi-objective optimization problem

As the name implies, multi-objective optimization considers multiple objectives at the same time while maintaining equality and inequality constraints. It can be expressed as a minimization problem as follows:

$$\begin{cases} Min: \{f_1(x,u), f_2(x,u), \dots, f_n(x,u)\} \\ Subject\ to: \quad g_i(x,u) = 0; \quad i = 1,2,3,\dots,m \\ \qquad\qquad h_j(x,u) \leq 0; \quad j = 1,2,3,\dots,p \end{cases} \tag{IV.3}$$

n: represents the number of objective functions to be reduced.

x: is a vector containing the feasible variables in the search space, also known as the solution.

IV.3.2.1 Pareto optimum

The Pareto concept is defined as a group of non-dominant solutions known as the Pareto front. These solutions cannot dominate each other in the same group. When one objective function of a solution increases, another decreases. This is referred to as the non- dominant solution. While the dominant solution is the objective function whose increase is unrelated to the effect on another objective function.

Mathematically, we can say that the vector $\vec{x} = (x_1, x_2, \dots, x_k)$ dominates the vector $\vec{y} = (y_1, y_2, \dots, y_k)$ (signified as $\vec{x} \prec \vec{y}$) in the search space if it meets the following conditions:

$$\forall i \in \{1,2,\dots,k\}: f_i(\vec{x}) \leq f_i(\vec{y}) \wedge \exists i \in \{1,2,\dots,k\}: f_i(\vec{x}) < f_i(\vec{y}) \tag{IV.4}$$

IV.3.2.2 Metrics for Convergence and Diversity

In multi-objective algorithms, the quality of the resulting solution is evaluated using measures, whether in terms of closeness or the distribution of solutions in the search space. In this chapter, we will discuss four measures, which are defined as follows [3].

a. Generational Distance (GD)

The generational distance index was introduced for the first time in the reference [4]. This measure is simple to compute because it is based on the distance between each element in the generated Pareto front and each component Pareto ideal front. This indicator is expressed mathematically as follows:

$$GD = \frac{\sqrt{\sum_{i=1}^{n} d_i^2}}{n} \qquad \text{(IV.5)}$$

Where $d_i = \min_j \left\| F(x_i) - \mathrm{PF}(x_j) \right\|$ represents the distance connecting the obtained non-dominant solution and the nearest true Pareto best solution in the reference set as shown in Figure IV.2 (a), and n denotes the overall number of non-dominated solutions [5, 6].

b. Inversion Generational Distance (IGD)

Veldhuizen and Lamont developed another metric, Inversion Generational Distance (IGD), which is defined mathematically as follows [7]:

$$IGD = \frac{\sqrt{\sum_{i=1}^{n} (d_i')^2}}{N} \qquad \text{(IV.6)}$$

Where N is the number of solutions in the Pareto front, and d_i is the distance between each element of the reference Pareto front and the elements of the generated Pareto front; that is, it does not neglect any part of the real Pareto group as shown in Figure IV.2 (b), which is the difference between it and the GD metric. Because the IGD measure ensures solution convergence and distribution, it is one of the most often used measures in evaluating the performance of multi-objective algorithms [5, 8]

c. Spread (Δ)

The spread metric was initially proposed by [9]. for two-objective problems and later extended by [10]. to handle multi-objective problems. This metric quantifies the proximity of solutions to each other within the solution set. A lower value of the spread metric indicates a

more uniform distribution of non-dominant solutions along the Pareto front. The mathematical expression of this indicator is expressed as follows:

$$\Delta = \frac{\sum_{i=1}^{m} \mathrm{d}(e_i, N_D) + \sum_{X \in PF} |d(X, N_D) - \bar{d}|}{\sum_{i=1}^{m} \mathrm{d}(e_i, N_D) + |\mathrm{PF}| \times \bar{d}} \quad \forall\, e_i \in PF \tag{IV.7}$$

$$d(X,\, N_D) = \min_{Y \in N_D, Y \neq X} \|F(X) - F(Y)\|^2 \tag{IV.8}$$

$$\bar{d} = \frac{1}{|PF|} \sum_{X \in PF} d(X,\, N_D) \tag{IV.9}$$

Where F symbolizes the set of m objectives, N_D represents the set of non-dominated solutions in the approximate front, and PF refers the set of known Pareto optimal solutions for the problem. Furthermore, $e_i (i = 1,2, \dots, m)$ denotes the extreme solutions (beginning and finishing points) in the Pareto front as shown in Figure IV.2(c).

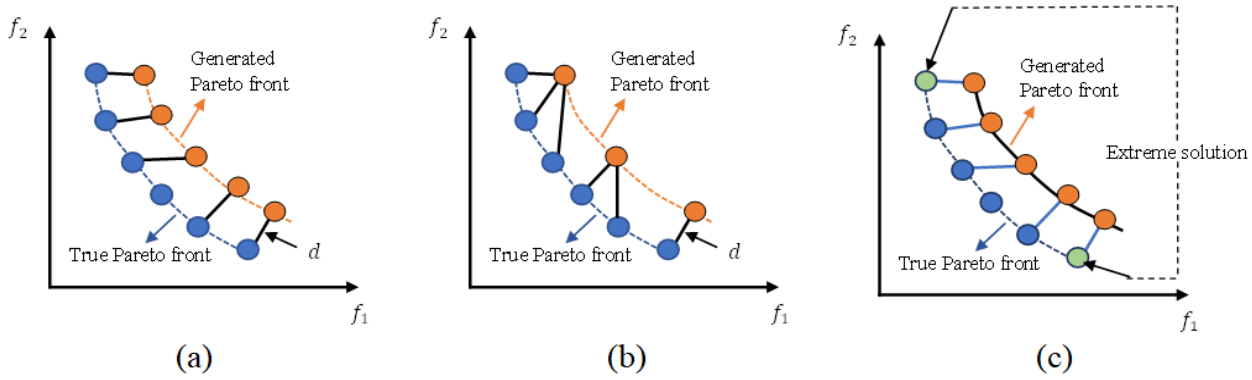

Figure IV.2. Schematic illustration of the (a) Generational distance (GD), (b) Inverse generational distance (IGD), and (c) Spread measure.

IV.3.2.3 Comprise solution

In a multi-objective problem, we find several non-dominant solutions represented by Pareto ideal solutions. To compare the results, we must choose the best compromise solution (BCS) that balances the various objectives to some extent. Many researchers used fuzzy set theory to solve this proposition, and this method is applied to all objective functions, resulting in a fuzzy membership function, which is represented as follows [6, 11]:

$$\mu_i = \begin{cases} 1 & F_i \geq F_i^{max} \\ \frac{F_i^{max} - F_i}{F_i^{max} - F_i^{min}} & F_i^{min} < F_i < F_i^{max} \\ 0 & F_i \leq F_i^{min} \end{cases} \tag{IV.10}$$

Where F_i^{max} and F_i^{min} are the highest and lowest values of the ith objective function. Eq. (IV.10) reflects degrees of satisfaction for each objective function of a given solution, i.e. with $\mu_i = 1$ as fully satisfactory and $\mu_i = 0$ as unsatisfactory, the membership function is represented as follows:

$$\mu^k = \frac{\sum_{i=1}^{N_{\text{obj}}} \mu_i^k}{\sum_{k=1}^{M} \sum_{i=1}^{N_{obj}} \mu_i^k} \qquad \text{(IV.11)}$$

Where M is the number of non-dominant solutions in the Pareto front and N_{obj} is the number of objective functions. Finally, the best compromise solution (BCS) can be considered as the highest value of the membership function μ^k [12].

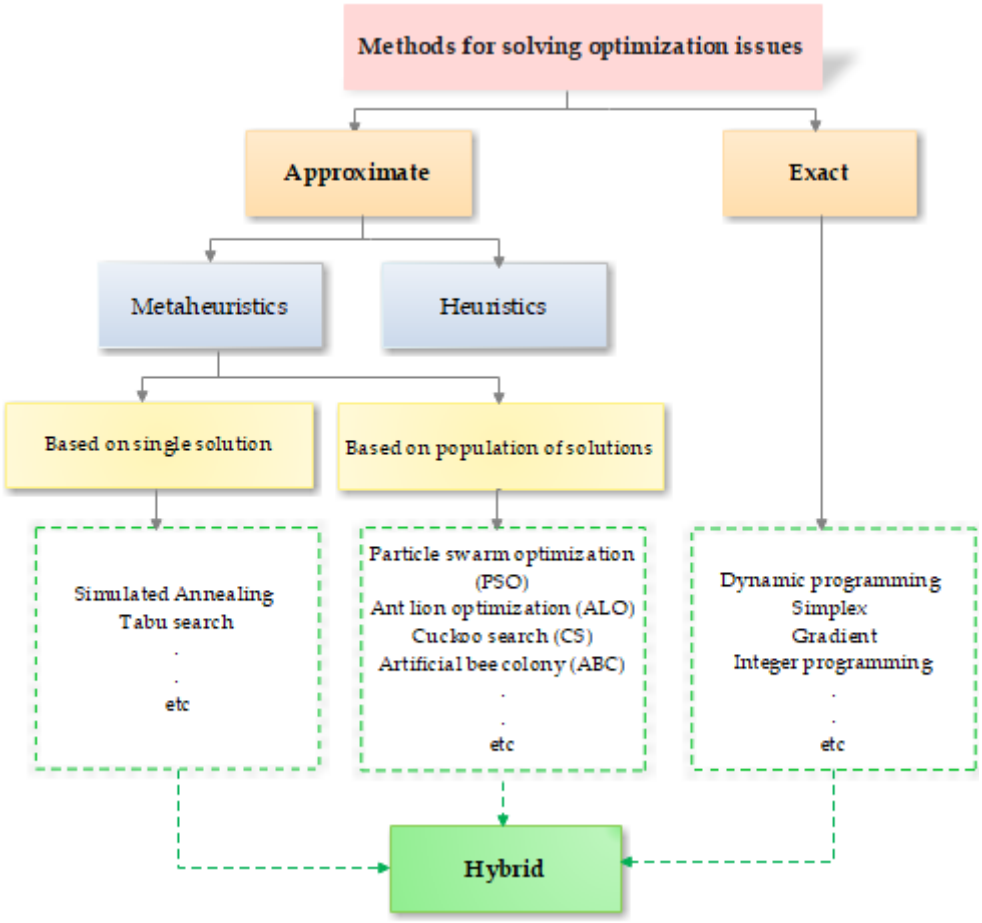

Figure IV.3. classification of techniques for solving optimization problems.

IV.4 Methods for solving optimization problems

IV.4.1 Exact methods

Exact algorithms rely primarily on integration and differentiation to find an accurate solution in a specific time. These algorithms have proven to be effective in various optimization problems, but as the complexity of the problems increases, it becomes difficult, and these algorithms may fail to find an ideal solution or take a long time. Here, it is necessary to address the so-called approximate algorithms, some of which are listed below [13, 14].

IV.4.2 Approximate methods

Approximation methods appeared for the first time in the late 1960s and early 1970s. These algorithms are also known as not-quite-exact methods or heuristics with a guarantee because, unlike exact methods, they allow us to provide a high-quality solution in the shortest possible computational time. Where the closer the result obtained to the optimal solution, the better the method [15, 16].

IV.5 Heuristic methods

In the 1960s, heuristics emerged as a popular problem-solving concept. The term "heuristics" is derived from the Greek word "heurisken," which means "to seek convincing answers rather than imposing them." According to the Cambridge Dictionary, heuristics is a problem-solving method and approach that allows individuals to make discoveries and learn from their own experiences. Heuristic approaches are problem-solving methodologies that use available knowledge to provide promising solutions in a short period of time. Heuristics appear to be viable strategies for dealing with computationally complex problems, particularly when the goal is to find an optimal solution quickly. When data accuracy is in doubt, relying on estimated data can lead to subpar results. Heuristic algorithms are known for their ease of implementation and swift execution, but it's important to acknowledge their potential to become trapped in local optima or miss superior solutions [17].

IV.6 Metaheuristic methods

Metaheuristic techniques were developed to overcome the limitations of exact methods by striking a balance between finding better quality solutions and reducing computing time. These algorithms have been discussed since the 1980s by researcher Glover. The word metaheuristic

consists of two words, meta (meaning “a higher level”) and heuristic (meaning “search”). Thus, the term metaheuristic means finding a higher or better level of search. These algorithms are often random and are inspired by natural behaviors such as animal behavior, genetics, physical processes, etc [18, 19].

IV.6.1 General operation of metaheuristics

Any metaheuristic algorithm is based on three fundamental concepts that ensure the algorithm finds the best solutions by diversifying and intensifying the search and storing the best solutions:

- Exploration is the ability of the algorithm to scan all search areas due to randomness, increasing the likelihood of diversifying solutions and avoiding local areas.
- Exploitation is the use of the information gathered during the research to improve the quality of the solution [20].
- Memory is the storage of the best solutions obtained by the algorithm in each iteration.

IV.6.2 Classification of Metaheuristic Methods

The metaheuristic features are further classified into two different types. First thing is based on single solution; other category is population solution that is multiple solutions. Let us discuss about those factors now [21].

IV.6.2.1 Unique solution-based metaheuristics

Single Solution Algorithm: also known as the Local Algorithm or the Trajectory-Based Algorithm, the initial solution begins with a transition from one solution to another better than it in the form of a trajectory and in a stepwise manner, and this process continues until the condition of completion in the algorithm is met or an optimal solution is found; however, while this algorithm has proven its effectiveness in multiple research fields, it suffers hey suffer from a decrease in the diversity and quality of solutions. Among the well-known one-solution algorithms in research are hill-climbing [22] search, tabu search (TS), and simulated annealing (SA)... etc [23, 24].

IV.6.2.2 Population-based metaheuristics of solutions

Population-based algorithms use a set of solutions (or the population) at each iteration until they reach the global optimal solution, which is considered a solution to the problem to be solved. Focusing on a set of solutions rather than a single solution allows us to better explore the search space and find high-quality solutions, so this type of algorithm has piqued the interest of researchers. Among the algorithms developed in recent years are driving Training-Based Optimization (DTBO) [25], chef-based optimization algorithm (CBOA) [26], Slime mould algorithm [27], marine predators algorithm [28], Aquila Optimizer (AO) [29], and others.

a. Particle Swarm Optimization (PSO)

Particle swarm optimization, originally developed by Kennedy and Eberhart, is based on the social behavior of swarms. A PSO method conducts search using a group of particles. While the research process, every particle is speeded up towards the particles with previous best site and the global best site. A new speed $V_{jk}(t+1)$ for every particle is calculated in an iteration based on its current speed $V_{jk}(t)$ and the distances from its previous best site $X_{pbest,jk}$ and the global best site $X_{gbest,k}$. The new speed is then utilized to calculate the next site of the particle in the search space. Velocity of each particle are often modified by the subsequent equation:

$$V_{jk}(t+1) = w(t) \cdot V_{jk}(t) + C_1 \cdot r_1\left(X_{pbest,jk} - X_{jk}(t)\right) + C_2 \cdot r_2\left(X_{gbest,k} - X_{jk}(t)\right) \quad \text{(IV.12)}$$

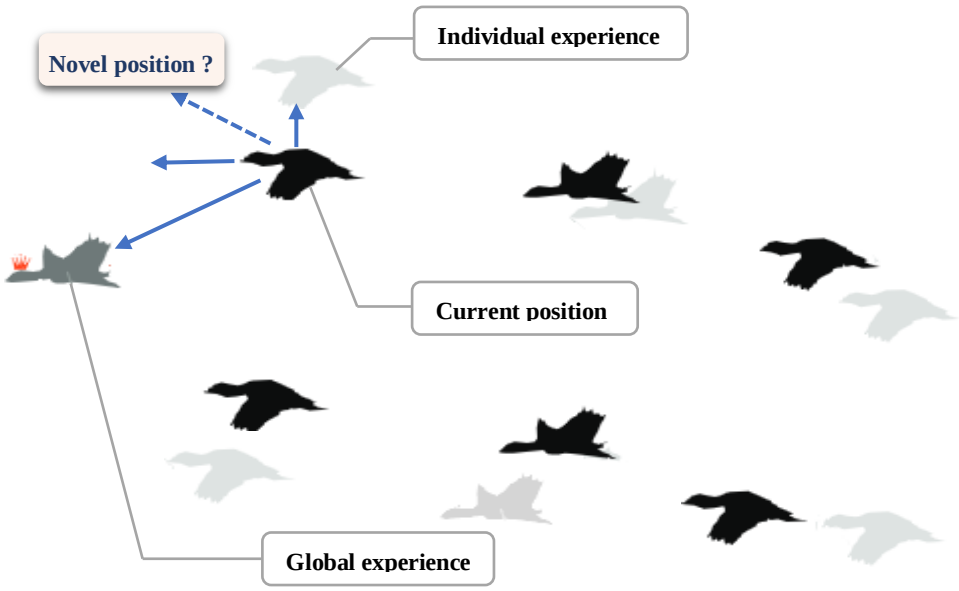

Figure IV.4. Illustration of updated particle positions in PSO.

The current position $X_{jk}(t+1)$ (searching point in the solution area) can be changed by the following equation:

$$X_{jk}(t) = X_{jk}(t+1) + V_{jk}(t) \quad (IV.13)$$

Where r_1 and r_2 represent random numbers between [0, 1], C_1 and C_1 are cognitive and social acceleration constants, respectively, and $w(t)$ the inertia weight factor can be computed by the next equation:

$$w(t) = w_{min} - \frac{(w_{max} - w_{min})}{MAXiter}.t \quad (IV.14)$$

Where $MAXiter$ and t are maximum number of iterations and the current number of iterations, respectively [30].

The fundamental particle motion diagram is depicted in Figure IV.4. The pseudocode of particle swarm optimization (PSO) is also described in Table IV.1.

Table IV.1. Pseudo code of Particle swarm optimization (PSO).

	Algorithm of PSO
1	***Initialize optimization***
2	*Generate random particles* X_i.
3	*Initialize the position and velocity of each particle.*
4	*Calculate the fitness value of each position.*
5	*Calculate* X_{pbest}, X_{gbest}
6	***Perform optimization***
7	***While*** $t <= MAXiter$ *or (stop criterion)*
8	***For*** *every particle*
9	*Update particle's velocity* V_i *using Eq (IV.12).*
10	*Update particle's position* X_i *using Eq (IV.13).*
11	*Calculate the fitness value* F_i *of each new particle* X_i.
12	*Update* X_{pbest} , X_{gbest}.
13	***End for***
14	***End While***
15	*Post process results and visualization;*
16	***End perform optimization***

b. Cuckoo search algorithm (CS)

Yang and Deb created the CS algorithm by combining the parasitic breeding behavior of certain cuckoo species with the Lévy flight behavior of some birds and fruit flies. In nature, most cuckoo species rest their eggs in the nests of other birds (host birds) and extract native bird eggs to increase their chances of hatching their eggs. If the host bird finds out the replacement of its eggs, it either throws eggs or leaves its nest and builds a new one (Figure

IV.5). Each egg in the nest is essentially a potential solution in CS, and every cuckoo egg corresponds to a new solution. The candidate solutions (eggs in the nests) are replaced by possible solutions (cuckoos' eggs) that may be better than them, and the aim of repeating this process is to improve the quality of the solutions produced by the CS algorithm.

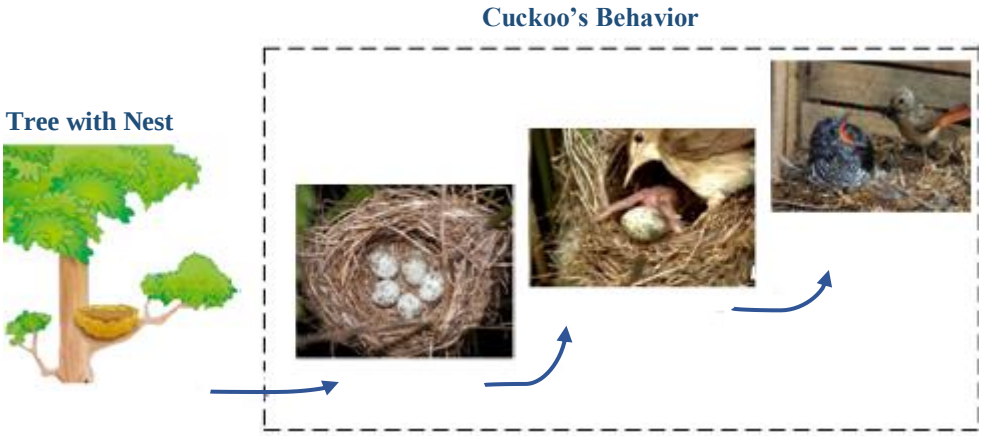

Figure IV.5. Cuckoo breeding conduct in nature.

A CS technique performs a search using the population of eggs. During the search process, the Lévy flight operator is used to calculate a new solution X_i^{t+1} (cuckoo's egg) as follows:

$$X_i^{t+1} = X_i^t + \alpha \oplus lévy(s,\lambda) \qquad \text{(IV.15)}$$

Where

$$Lévy(s,\lambda) = \frac{\lambda\Gamma(\lambda)\sin(\pi\lambda/2)}{\pi}\frac{1}{s^{1+\lambda}} \quad s >> s_0 > 0 \qquad \text{(IV.16)}$$

In Eqs. (IV.15) and (IV.16), $\alpha > 0$ represents a scaling factor of the step size s and the symbol $\oplus$ is the input-wise product, and Γ is the gamma function [31]. The pseudo-code of CS is described in Table IV.2.

Table IV.2. Pseudo code of Cuckoo search algorithm (CS).

	Algorithm of CS
1	***Initialize optimization***
2	*Generate initial population of n host nests* X_i.
3	*Set t=0*
4	***Perform optimization***
5	***While*** *t<= MAXiter or (stop criterion)*
6	*Get a cuckoo randomly by Lévy flights*
7	*Evaluate its quality fitness* F_i
8	*Choose a nest among n (say, j) randomly*
9	***If*** $F_j < F_i$
10	*Replace i by the new solution j.*
11	***End if***
12	*A fraction (pa) of worse nests are abandoned and new ones*
13	*Keep the best solutions or nests with quality solutions;*
14	*Rank the solutions and find the current best;*
15	***End While***
16	*Post process results and visualization;*
17	***End perform optimization***

c. Ant lion optimization algorithm (ALO)

Antlion optimizer ALO is a new metaheuristic algorithm developed by Mirjalili depending on the principle of the hunting mechanism of antlion in nature. The ALO approach simulates the interaction of antlions and ants in the pit, where ants travel stochastically to forage in the search space, and antlions chase the ants using the pits.

The mathematical model of the antlion optimization (ALO) algorithm can be described here after:

$$X(t) = [0, cumsum(2r(t_1) - 1), cumsum(2r(t_2) - 1), \dots, cumsum(2r(t_n) - 1)] \quad (IV.17)$$

Here the cumulative sum determined by $cumsum$, t indicates the random step, n is the maximum number of iterations, and $r(t)$ is a stochastic function specified as in the following:

$$r(t) = \begin{cases} 1 & if\ rand > 0.5 \\ 0 & if\ rand \leq 0.5 \end{cases} \quad (IV.18)$$

$rand$ is a number generated at random between 0 and 1.

In order to maintain the random walks of ants within the search space according to lower and upper boundary change during the search process, they are normalized using the following expression:

$$X_i = \frac{(X_i - a_i) \times (d_i - c_i)}{(b_i - a_i)} + c_i \quad \text{(IV.19)}$$

Where a_i and b_i represent the lower and upper boundary of X_i, c_i and d_i indicate the lower and upper boundary around the selected antlion in the i^{th} dimension respectively.

The lower and upper boundary around the selected antlion to build traps can be calculated using:

$$\begin{cases} c = c' + Antlion \\ d = d' + Antlion \end{cases} \quad \text{(IV.20)}$$

Where c' and d' denote the lower and upper of changing limit at the current iteration in process.

Updating each ant's position is done by a random walk around antlion. The latter is pre-selected by the roulette wheel and the elite. It can be defined as follows:

$$Ant = \frac{R_A + R_E}{2} \quad \text{(IV.21)}$$

Where Ant is a novel position, R_A is the random walk around the antlion chosen by the Roulette wheel, R_E is the random walk around the elite.

In ALO algorithm, ants catch prey when ants are fitter (dives inside soft sand) than its attached antlion. To increase its chances of capturing a new victim, an antlion is required to update its position to the latest location of the hunted ant. The process is modelled as follows:

$$Antlion_j^t = Ant_i^t \ \ if \ \ f(Ant_i^t) < f(Antlion_i^t) \quad \text{(IV.22)}$$

Where $Antlion_j^t$ indicates the position of the selected j^{th} antlion at t^{th} iteration while Ant_i^t presents the position of i^{th}ant at t^{th} iteration [31]. Figure IV.6 depicts how antlions capture ants in nature.

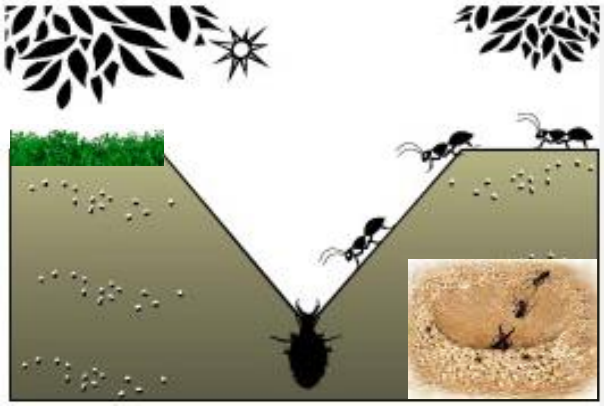

Figure IV.6. Hunting behavior of an antlion in the nature.

The pseudo-code of antlion optimization (ALO) is described in Table IV.3.

Table IV.3. Pseudo code of antlion optimization (ALO).

	Algorithm of ALO
1	***Initialize optimization***
2	*Initialize the first population of ants and antlions randomly.*
3	*Calculate the fitness of ants and antlions.*
4	*Find the best antlions and assume it as the elite (determined optimum).*
5	***Perform optimization***
6	***While** the end criterion is not satisfied.*
7	***For** every ant*
8	*Select an antlion using Roulette wheel.*
9	*Create a random walk and normalize it using Eqs (IV.17) and (IV.19).*
10	*Update the position of ant using Eq (IV.21).*
11	***End for***
12	*Calculate the fitness of all antsF.*
13	***If*** $F_{ant} < F_{antlion}$
14	*Replace an antlion with its corresponding ant.*
13	***End if***
14	*Update elite if an antlion becomes fitter than the elite.*
15	***End While***
16	*Post process results and visualization.*
17	***End perform optimization***

d. Multi-objective Spider wasp optimizer (MOSWO)

This section begins by introducing the SWO algorithm, followed by the introduction of its multi-objective version.

1. Spider wasp optimizer

Spider Wasp Optimizer (SWO) is a novel metaheuristic algorithm introduced by Abdel-Basset et al. in [32] that draws inspiration from the hunting, nesting, and mating

behaviors of female spider wasps (Figure IV.7(a)) (Abdel-Basset et al., 2023). SWO has demonstrated promising performance in solving various benchmark optimization problems. The algorithm consists of three main steps:

1) Initialization
2) Hunting and nesting behavior
3) Mating behavior

(a) (b)

Figure IV.7. (a) Female spider wasp (b) Female spider wasp drags a paralyzed spider towards her uncovered burrow.

The above three main steps can be mathematically described as follows.

1) Initialization

SWO begins by initializing the population randomly using Eq. (IV.23):

$$X_i^t = L + r \times (H - L), \qquad i = 1,2,\ldots, N_{pop}. \tag{IV.23}$$

Where t represents the number of iterations. H and L represent the upper and lower boundaries, respectively, for a problem with D dimensions. r is a random vector generated within the interval [0, 1]. In SWO, each spider-wasp (female) represents a solution in the search space.

2) Hunting and nesting behavior

This behavior can be divided into two stages: the first stage is the search for prey (exploration), and the second stage is the nesting stage (exploitation).

- **Searching stage (exploration)**

After the initial population of N_{pop} female spider-wasps are initialized, each individual begins the exploration stage, where they search for a suitable spider or prey to feed their larvae. This stage involves randomly exploring the search space. The exploration behavior of the female wasps is simulated using Eq. (IV.22), which updates their current position at each generation t with a constant motion, mimicking their exploratory behavior.

$$X_i^{t+1} = X_i^t + \mu_1 * (X_a^t - X_b^t) \quad \text{(IV.24)}$$

Where a and b represent two indices selected at random from the population. μ_1 is a parameter calculated utilizing Eq. (IV.25):

$$\mu_1 = |rn| * r_1 \quad \text{(IV.25)}$$

Where r_1 is a random number created within the interval [0, 1], and rn is another random number created utilizing the normal distribution. The indices a and b are employed to determine the exploration direction, while the parameter $\mu_1$is employed to calculate the constant motion along the current direction.

To account for the behavior of female wasps searching for a dropped spider, an additional equation is introduced in the algorithm. This equation allows the algorithm to explore the surrounding regions of the dropped spider with a smaller step size compared to the previous equation (Eq. (IV.26)). The update in this equation is based on the position of a randomly selected female wasp in the population, which represents the position of the dropped spider. The equation is as follows:

$$X_i^{t+1} = X_c^t + \mu_2 * \left(L + r_2 * (H - L)\right) \quad \text{(IV.26)}$$

$$\mu_2 = B * \cos(2\pi l) \quad \text{(IV.27)}$$

$$B = \frac{1}{1+e^l} \quad \text{(IV.28)}$$

Where c is an index chosen randomly from the population, and l is a random value created within the range of 1 to -2. The parameter μ_2 is proposed to determine direction of search. To determine whether to use Eq. (IV.24) or Eq. (IV.26) for generating the next position of the female wasp, a random selection process is employed. The preference between the two equations is determined randomly using Eq. (IV.29):

$$X_i^{t+1} = \begin{cases} Eq.(IV.22) & r_3 < r_4, \\ Eq.(IV.24) & Else, \end{cases} \quad \text{(IV.29)}$$

Where r_3 and r_4 are two random values within the interval [0, 1].

After locating the prey, the spider wasp engages in attacking them within the hub of the web. However, the prey often drops to the ground in an attempt to escape. The spider wasp follows the dropped spiders, paralyzes them, and drags them to pre-prepared nests (as shown in Figure IV.7(b)). In some cases, the spider loses track of the spiders that drop from the hub, resulting in the wasp simultaneously attempting to catch the spider while also evading it. These behaviors simulate two distinct scenarios: the first scenario represents the wasp actively hunting and pursuing the spiders, where Eq. (IV.30) is used to update the wasp's position and follow the prey. The second scenario simulates the wasp evading the spiders by introducing a distance factor that increases as the iteration progresses. This allows the prey to potentially hide in distant regions away from the wasp.

In the first scenario, a mathematical model is proposed to simulate two cases: (1) when the prey is faster than the wasp (C > 0.5), and (2) when the wasp is faster than the prey (C < 0.5). Here, C represents a distance control factor that determines the speed of the wasp. Initially, the speed of the wasp is set to two and gradually decreases linearly to zero. When the wasp's speed is lower than 0.5, the changes in its position become very small, hindering its ability to reach the prey. This simulates the scenario where the spider is successfully evading the pursuing wasp, resulting in an increasing distance between them.

$$X_i^{t+1} = X_i^t + C * |2 * r_5 * X_a^t - X_i^t| \quad \text{(IV.30)}$$

$$C = \left(2 - 2 * \left(\frac{t}{T_{max}}\right)\right) * r_6 \quad \text{(IV.31)}$$

Where t and T_{max} represent the current and maximum evaluations, respectively. r_5 and r_6 represent of randomly generated values within the interval [0, 1].

The distance between the female wasp and the spider gradually increases as the spider flees, transitioning the stage from initial exploitation to exploration. This behavior is modeled using Eq. (IV.32):

$$X_i^{t+1} = X_i^t * vc \quad \text{(IV.32)}$$

Where vc is a vector generated between k and -k using the normal distribution. The value of k is defined using Eq. (IV.33):

$$k = 1 - 1 * \left(\frac{t}{T_{max}}\right) \quad \text{(IV.33)}$$

The tradeoff between the two scenarios is randomly determined using Eq. (IV.34):

$$X_i^{t+1} = \begin{cases} Eq.(IV.28) & r_3 < r_4 \\ Eq.(IV.30) & Else \end{cases} \quad \text{(IV.34)}$$

Finally, the transition between the searching stage and the following mechanism is controlled using Eq. (IV.35):

$$X_i^{t+1} = \begin{cases} Eq.(IV.27) & p < k \\ Eq.(IV.32) & Else \end{cases} \quad \text{(IV.35)}$$

where p is a random value between 0 and 1.

- ***Nesting stage (exploitation)***

At this stage, the female wasps retrieve the paralyzed spider and transport it to a pre-prepared nest, where they proceed to lay eggs on its abdomen. This process can be mathematically represented using Eq. (IV.36):

$$X_i^{t+1} = X^* + cos(2\pi l) * (X^* - X_i^t) \quad \text{(IV.36)}$$

where X^* is the best individual so far. To construct the nest, the position of a randomly selected female spider from the population is used as a reference. The nest is built within this position by incorporating an additional step size to ensure that two nests are not created in the same location. This process can be expressed mathematically using Eq. (IV.37):

$$X_i^{t+1} = X_a^t + r_3 * |\gamma| * (X_a^t - X_i^t) + (1 - r_3) * U * (X_b^t - X_c^t) \quad \text{(IV.37)}$$

where r_3 is a random value within the interval [0, 1]; γ is a number created using the levy flight; U is a binary vector defined using Eq. (IV.38):

$$U = \begin{cases} 1 & r_6 > r_7 \\ 0 & Else \end{cases} \quad \text{(IV.38)}$$

where r_6 and r_7 are two random values between 0 and 1. The preference between Eq. (IV.36) and Eq. (IV.37) is determined randomly using Eq. (IV.39):

$$X_i^{t+1} = \begin{cases} Eq.(IV.34) & r_3 < r_4 \\ Eq.(IV.35) & Else \end{cases} \quad \text{(IV.39)}$$

Finally, the trade-off among hunting behavior (exploration) and nesting behaviors (exploitation) are achieved using Eq. (IV.40):

$$X_i^{t+1} = \begin{cases} Eq.(IV.33) & i < N * k \\ Eq.(IV.37) & Else \end{cases} \quad \text{(IV.40)}$$

3) Mating behavior

In SWO, the mating behavior of spider wasps is incorporated. These wasps possess the ability to determine the gender of their offspring. In the context of SWO, each spider wasp represents a potential solution in the current iteration, and the spider wasp eggs symbolize newly generated solutions in that generation. The new solutions spider wasp eggs are determined using Eq. (IV.41):

$$X_i^{t+1} = Crossover(X_i^t, X_m^t, CR) \quad \text{(IV.41)}$$

The mating behavior in SWO involves the use of the uniform crossover operator, denoted as "Crossover," which is applied between two solutions: the male spider wasp X_m^t and the female spider wasp X_i^t. The crossover rate (CR) determines the probability of performing this crossover operation. The male spider wasp is generated uniquely in the algorithm using Eq. (IV.42):

$$X_m^{t+1} = X_i^t + \boldsymbol{e}^l * |\beta| * v_1 + (1 - e^l) * |\beta_1| * v_2 \quad \text{(IV.42)}$$

$$v_1 = \begin{cases} x_a - x_i & f(x_a) < f(x_i) \\ x_i - x_a & Else \end{cases} \quad \text{(IV.43)}$$

$$v_2 = \begin{cases} x_b - x_c & f(x_b) < f(x_c) \\ x_c - x_b & Else \end{cases} \quad \text{(IV.44)}$$

where β and β_1 are two numbers randomly created using to the normal distribution, e is the exponential constant, and a, b, and c are indices of three solutions randomly selected from the population, such that $a \neq i \neq b \neq c$. The tradeoff between hunting and mating behaviors in SWO is determined by a predefined factor called the tradeoff rate (TR).

In the SWO algorithm, population reduction and memory-saving mechanisms are utilized to enhance convergence speed and preserve the best-spider positions. The population reduction equation (Eq. (IV.45)) reduces diversity and accelerates convergence towards near-optimal solutions. Memory-saving is implemented by comparing each wasp's current solution with its

corresponding solution from the previous generation. If the new solution is more fit, it replaces the previous one.

$$N_{pop} = N_{min} + (N_{pop} - N_{min}) \times \left(\frac{T_{max}-t}{T_{max}}\right) \quad \text{(IV.45)}$$

where the parameter N_{min} in the SWO algorithm represents the minimum population size required to prevent getting trapped in local minima during various stages of the optimization process. In the original SWO, the CR, TR, and N_{min} is set to 0.2, 0.3, and 20, respectively. The pseudo-code for the SWO is descried in Table IV.4.

Table IV.4. Pseudo code of spider wasp optimizer (SWO).

Algorithm of SWO
Input: N_{pop}, N_{min}, *CR, TR,* T_{max}
Output: *The best solution found*
1. *Initialize* N_{pop} female spider-wasps, $X_i(i = 1,2, \dots\dots, N_{pop})$, using Eq. (IV.23)
2. Evaluate each X_i and finding the one with the best fitness.
3. $t = 1$; //the current function evaluation
4. **while** $(t < T_{max})$
5. r_1: generating a random value within the interval [0, 1].
6. if $r_1 < TR$) */*Hunting and Nesting behaviors*/*
7. **for** *i=1:* N_{pop}
8. Update the position of spider-wasp using Eq. (IV.40).
9. *Compute f(* X_i)
10. *t=t+1;*
11. **End for**
12. **Else** */*Mating Behavior*/*
13. **for** *i=1:* N_{pop}
14. Update the position of spider-wasp using Eq. (IV.41).
15. *t=t+1;*
16. **End for**
17. **End if**
18. Applying ***Memory Saving***
19. Updating N_{pop} using Eq. (IV.45)
20. **End while**

2. Multi-objective Spider wasp optimizer (MOSWO)

This study extends the Single-Objective Spider Wasp Optimizer (SWO) to address multi-objective optimization problems through the introduction of the Multi-Objective Spider Wasp Optimizer (MOSWO). MOSWO incorporates three fundamental mechanisms that closely resemble those of the Multi-Objective Particle Swarm Optimization (MOPSO) proposed by Coello and Lechuga [33]. These three mechanisms are described as follows:

1) Archive: The Archive in MOSWO serves as a repository for storing all non-dominated Pareto optimal solutions obtained during the optimization process. An Archive Controller plays a crucial role in managing the addition of solutions to the archive, especially when the archive becomes full. Additionally, the archive has a capacity limit (let suppose $Arch\_size$), meaning it can only accommodate a certain number of solutions. During each iteration of the training process, the non-dominated solutions obtained thus far are compared with the existing archive to determine which solutions should be included.

2) Grid mechanism: The grid mechanism implemented in MOSWO is a powerful technique for improving the diversity of non-dominated solutions in the archive. When the archive reaches its capacity, the grid technique is employed to reorganize the segmentation of the objective space. This reorganization aims to identify the most densely populated region within the grid and remove a solution from that area. The newly generated solution is then placed in the least crowded segment, enhancing the diversity of the final approximated Pareto optimal front.

As the number of potential solutions within each hypercube of the grid expands, the likelihood of removing a solution also increases. When the archive is full, priority is given to the most crowded segments, and a solution is randomly selected from one of these segments for removal, creating space for the new solution. It's worth noting that when a solution is placed outside the hypercubes, a special case arises. In this case, all segments are expanded to accommodate the latest solutions, potentially causing changes in the segments of alternative solutions as well.

3) Leader selection: In MOSWO, comparing solutions in a multi-objective search space is not straightforward due to Pareto optimality. To overcome this challenge, the Leader Selection Mechanism is employed as the final component. This mechanism involves selecting leaders from the search candidates to guide them towards

promising regions of the search space, aiming to obtain solutions that are close to the global optimum.

As mentioned earlier, the archive in MOSWO consists of the best non-dominated solutions. The leader selection mechanism focuses on identifying the least crowded regions of the search space and presenting the best solutions from those regions as non-dominated answers. The selection process for each hypercube is performed using a roulette-wheel approach with the following probability distribution:

$$P_{selection} = \frac{C}{ns_i} \tag{IV.46}$$

Where $C > 1$ is a constant, and ns_i is the number of solutions in the ith hypercube.

From Eq. (IV.46), it can be observed that less crowded hypercubes have a higher probability of being selected, implying that they are more likely to contain desirable solutions. Once the appropriate hypercube is chosen, a random selection process called roulette-wheel selection is utilized to designate an individual as the leader. The Pseudo-code of the MOSWO is presented in in Table IV.5.

Table IV.5. Pseudo code of Multi-objective Spider wasp optimizer (MOSWO).

Algorithm of the proposed MOSWO
Input: N_{pop}, N_{min}, *CR, TR*, T_{max}, $Arch\_size$
Output: $Return\ Archive$
21. *Initialize* the population *pop* with N_{pop} female spider-wasps, $X_i(i = 1,2, \dots \dots, N_{pop})$, using Eq. (IV.23)
22. Run grid mechanism to prepare the archive to the first iteration.
23. **while** $(t < T_{max})$
24. r_1: generating a random value within the interval [0, 1].
25. **IF** $r_1 < TR$) */*Hunting and Nesting behaviors*/*
26. Select a global best individual X^* the archive.
27. **for** *i=1:* N_{pop}
28. Update the position of spider-wasp using Eq. (IV.40).
29. *Compute f(* X_i)
30. **End for**
31. **Else** */*Mating Behavior*/*
32. **for** *i=1:* N_{pop}
33. Update the position of spider-wasp using Eq. (IV.40).
34. **End for**
35. **End If**

36. Evaluate each individual in {Archive ∪ *pop*}
37. Update the archive.
38. **IF** ($T_{max} > |pop|$)
39. ***use*** the grid mechanism to delete the current archives
40. ***add*** the new answer to the archive
41. **End If**
42. $t = t+1$
43 Applying ***Memory Saving***
44 Updating N_{pop} using Eq. (45)
45. **End while**

IV.7 Hybrid methods

The hybrid algorithm is the result of combining two or more optimization methods (exact and approximate), where knowing the strengths of each algorithm and combining them into one algorithm allows us to balance exploration and exploitation and thus obtain more efficient and accurate solutions than using a single optimization algorithm.

The following is a synopsis of two new algorithms that have been used to solve real-world problems.

IV.7.1 Hybrid PSO-ALO algorithm

The novel hybrid PSO-ALO technique proposed here, consists of the strong collaboration of PSO and ALO, without changing the general mechanism of the search process. In every iteration the population is split into two parts and it is developed with the two techniques, respectively. The two parts are then recombined in the updated population that is again split randomly into another two parts in the following iteration for another run of particle swarm optimization operators or ant lion optimization [30].

IV.7.2 Hybrid cuckoo search and antlion optimization (CS-ALO)

The previous studies in the literature indicated that both ALO and CS algorithms have a good performance in achieving the global optimal solution compared to many optimization algorithms. However, some difficulties may appear when suitable solutions for some complex and multimodal optimization issues could not be found. Based on the cuckoo search algorithm (CS) and the antlion optimizer (ALO), a novel CS-ALO hybrid algorithm is proposed based on the opposite advantages and disadvantages of both algorithms by adding a loop to the CS

algorithm where new super-elite solutions are generated based on the mechanisms of the ALO algorithm. The main idea of this hybrid method is to increase the exploitation capacity by applying an adaptive limit shrinking mechanism of the antlion algorithm, thus ensuring a good balance between exploring the research space and exploiting the best existing solutions [31].

IV.8 Conclusion

In this chapter, we presented general concepts about optimization and the formulation of single-objective and multi-objective optimization problems, next we discussed the various types of optimization methods: exact methods, and approximate methods, and more focus was placed on population-based metaheuristic algorithms because they contribute to a good balance between the quality of the solution and the reduction of the computational time. This has lately prompted researchers to combine these methods to achieve the best possible performance, and later, some types of metaheuristic algorithms inspired by nature were reviewed in order to employ them in the following chapter to solve mono-objective and multi-objective problems.

References

[1] M. Chawla and M. Duhan, "Levy flights in metaheuristics optimization algorithms–a review," *Applied Artificial Intelligence,* vol. 32, pp. 802-821, 2018.

[2] C. Venkateswarlu and S. E. Jujjavarapu, *Stochastic global optimization methods and applications to chemical, biochemical, pharmaceutical and environmental processes*: Elsevier, 2019.

[3] F. S. Lobato and V. Steffen Jr, *Multi-objective optimization problems: concepts and self-adaptive parameters with mathematical and engineering applications*: Springer, 2017.

[4] D. A. Van Veldhuizen and G. B. Lamont, "Multiobjective evolutionary algorithm research: A history and analysis," Citeseer1998.

[5] J. K. Mandal, S. Mukhopadhyay, and P. Dutta, "Multi–Objective Optimization," *Springer, Singapore,* 2018.

[6] V. Sakthivel, M. Suman, and P. Sathya, "Combined economic and emission power dispatch problems through multi-objective squirrel search algorithm," *Applied Soft Computing,* vol. 100, p. 106950, 2021.

[7] D. A. Van Veldhuizen, *Multiobjective evolutionary algorithms: classifications, analyses, and new innovations*: Air Force Institute of Technology, 1999.

[8] H. Ishibuchi, H. Masuda, Y. Tanigaki, and Y. Nojima, "Modified distance calculation in generational distance and inverted generational distance," in *Evolutionary Multi-Criterion*

Optimization: 8th International Conference, EMO 2015, Guimarães, Portugal, March 29--April 1, 2015. Proceedings, Part II 8, 2015, pp. 110-125.

[9] K. Deb, A. Pratap, S. Agarwal, and T. Meyarivan, "A fast and elitist multiobjective genetic algorithm: NSGA-II," *IEEE transactions on evolutionary computation*, vol. 6, pp. 182-197, 2002.

[10] A. Zhou, Y. Jin, Q. Zhang, B. Sendhoff, and E. Tsang, "Combining model-based and genetics-based offspring generation for multi-objective optimization using a convergence criterion," in *2006 IEEE international conference on evolutionary computation*, 2006, pp. 892-899.

[11] R. T. A. King, H. C. Rughooputh, and K. Deb, "Best Compromise Solutions for Stochastic Multi-Objective Environmental/Economic Dispatch of Power Systems using Evolutionary Chance-Constrained Nonlinear Programming and Latin Hybercube Sampling," *University of Mauritius Research Journal*, vol. 15, pp. 491-512, 2009.

[12] J. P. Roselyn, D. Devaraj, and S. S. Dash, "Multi-objective differential evolution for voltage security constrained optimal power flow in deregulated power systems," *International Journal of Emerging Electric Power Systems*, vol. 14, pp. 591-607, 2013.

[13] W. A. Khan, N. N. Hamadneh, S. L. Tilahun, and J. Ngnotchouye, "A review and comparative study of firefly algorithm and its modified versions," *Optimization Algorithms-Methods and Applications*, vol. 45, pp. 281-313, 2016.

[14] K. Kumar, D. Zindani, and J. P. Davim, *Optimizing Engineering Problems through Heuristic Techniques*: CRC Press, 2019.

[15] C. P. Gomes and R. Williams, "Approximation algorithms," in *Search Methodologies: Introductory Tutorials in Optimization and Decision Support Techniques*, ed: Springer, 2005, pp. 557-585.

[16] A. Prakasam and N. Savarimuthu, "Metaheuristic algorithms and probabilistic behaviour: a comprehensive analysis of Ant Colony Optimization and its variants," *Artificial Intelligence Review*, vol. 45, pp. 97-130, 2016.

[17] A. M. Al-Shaery, M. O. Khozium, N. S. Farooqi, S. S. Alshehri, and M. A. M. Al-Kawa, "Problem solving in crowd management using heuristic approach," *IEEE Access*, vol. 10, pp. 25422-25434, 2022.

[18] S. E. De León-Aldaco, H. Calleja, and J. A. Alquicira, "Metaheuristic optimization methods applied to power converters: A review," *IEEE Transactions on Power Electronics*, vol. 30, pp. 6791-6803, 2015.

[19] G. Lindfield and J. Penny, *Numerical methods: using MATLAB*: Academic Press, 2018.

[20] X.-S. Yang, *Nature-inspired optimization algorithms*: Academic Press, 2020.

[21] T. Sengodan, M. Murugappan, and S. Misra, *Advances in Electrical and Computer Technologies: Select Proceedings of ICAECT 2020*: Springer, 2022.

[22] H. Joe and J. Juan, "Power System Modeling, Computation, and Control," *JohnWiley & Sons Ltd*, 2020.

[23] I. Boussaïd, J. Lepagnot, and P. Siarry, "A survey on optimization metaheuristics," *Information sciences*, vol. 237, pp. 82-117, 2013.

[24] N. S. Jaddi and S. Abdullah, "Global search in single-solution-based metaheuristics," *Data Technologies and Applications*, vol. 54, pp. 275-296, 2020.

[25] M. Dehghani, E. Trojovská, and P. Trojovský, "A new human-based metaheuristic algorithm for solving optimization problems on the base of simulation of driving training process," *Scientific reports*, vol. 12, p. 9924, 2022.

[26] E. Trojovska and M. Dehghani, "A new human-based metahurestic optimization method based on mimicking cooking training," *Sci Rep*, vol. 12, p. 14861, Sep 1 2022.

[27] S. Li, H. Chen, M. Wang, A. A. Heidari, and S. Mirjalili, "Slime mould algorithm: A new method for stochastic optimization," *Future Generation Computer Systems*, vol. 111, pp. 300-323, 2020.

[28] A. Faramarzi, M. Heidarinejad, S. Mirjalili, and A. H. Gandomi, "Marine Predators Algorithm: A nature-inspired metaheuristic," *Expert systems with applications*, vol. 152, p. 113377, 2020.

[29] L. Abualigah, D. Yousri, M. Abd Elaziz, A. A. Ewees, M. A. A. Al-qaness, and A. H. Gandomi, "Aquila Optimizer: A novel meta-heuristic optimization algorithm," *Computers & Industrial Engineering*, vol. 157, p. 107250, 2021.

[30] H. MERAH, A. GACEM, D. BENATTOUS, Y. LABBI, and O. P. MALIK, "Solving economic dispatch problem using a new hybrid PSO-ALO Algorithm," in *2020 1st International Conference on Communications, Control Systems and Signal Processing (CCSSP)*, 2020, pp. 487-492.

[31] H. Merah, A. Gacem, D. Ben Attous, A. Lashab, F. Jurado, and M. A. Sameh, "Sizing and sitting of static var compensator (svc) using hybrid optimization of combined cuckoo search (cs) and antlion optimization (alo) algorithms," *Energies*, vol. 15, p. 4852, 2022.

[32] M. Abdel-Basset, R. Mohamed, M. Jameel, and M. Abouhawwash, "Spider wasp optimizer: a novel meta-heuristic optimization algorithm," *Artificial Intelligence Review*, vol. 56, pp. 11675-11738, 2023.

[33] Y. Collette and P. Siarry, *Optimisation multiobjectif: Algorithmes*: Editions Eyrolles, 2011.

CHAPTER V

TEST AND APPLICATION

V.1 Introduction

The spider wasp method is introduced in this chapter as a technique for optimizing single power flow problems. Furthermore, a new version of the Spider Wasp Optimizer (SWO) method is proposed to handle the complexities of multi-objective optimization flow issues. The modified approach, known as Multi-objective Spider Wasp Optimization (MOSWO), includes critical components such as an archive, leader selection, and grid processes that efficiently handle numerous optimization goals. MOSWO's performance is thoroughly evaluated on nine mathematical functions, and a comprehensive comparison is performed using three commonly recognized performance measures. This comparative analysis aims to illustrate the effectiveness of the MOSWO algorithm in dealing with multi-objective optimization situations. Furthermore, the suggested algorithm is evaluated on real-world scenarios. First, the proposed technique is used to solve the optimal power flow problem on an IEEE 30-bus system, addressing four separate single-objective functions as well as three multi-objective functions. Second, the OPF (Optimal Power Flow) problem is addressed, taking into account the impact of random renewable energy with and without SVCs devices. To provide a thorough evaluation, the results obtained from implementing the proposed algorithm (both in single and multi-objective problems) are compared to various approaches mentioned in the literature. This comparison analysis is critical for determining the utility of the proposed algorithm in addressing difficult optimization problems.

V.2 Mathematical application

V.2.1 Single objective function

Abdel-Basset et al. present spider wasp optimizer (SWO), a new nature-inspired swarm-based meta-heuristic algorithm for stochastic optimization based on mimicking the hunting, nesting, and mating activities of female spider wasps in nature. It is evaluated using four different test benchmarks: twenty-three standard test functions, CEC2014, CEC2017, and CEC2020 to study its exploration, exploitation, avoidance of local optima, and convergence speed [1].

V.2.2 Multi-objective function

The findings of the MOSWO algorithm are detailed for the first time in this part, as they are validated on multi-objective functions, and the optimal Pareto front is determined. The simulation results are generated using the MATLAB 2013a program, which has the following

features: Intel(R) Core (TM) i3-4005U, 1.70 GHz, PC with 4 GB RAM and a 64-bit operating system.

The effectiveness of the MOSWO technique in solving standard test functions was demonstrated by conducting experiments on nine test functions obtained from [2, 3]. These test functions include ZDT1, ZDT2, ZDT3, ZDT4, ZDT6, SRN, BNH, TNK, and OSY (as shown in Figures V.2 to V.10). To evaluate the performance of the proposed method, a comparison was made against other competing algorithms such as MAOA and MOGOA.

Table V.1 outlines the control settings employed for all algorithms. It is important to note that consistent settings were utilized across all experiments. These settings include a population size of 100, a maximum iteration count of 500, and an archive size of 100. To ensure robustness and reliability of the results, each method was executed ten times for each test function. The statistical outcomes of these experiments are provided in Tables V.2 and V.3, offering a comprehensive analysis of the algorithmic performance and its comparative effectiveness.

Table V.1. The specific parameter settings for each algorithm.

Algorithm	Specific Parameters	Value
MAOA	Mu, alpha, MOP_Min, MOP_Max, $Arch\_size$, N_{pop}, T_{max}	0.1, 5, 0.1, 1 ,100, 100, 500
MOGOA	$cmin$, $cmax$, $Arch\_size$, N_{pop}, T_{max}	0.00004, 1,100, 100, 500
MOSWO	TR, CR, N_{min}, α, β, γ, nGrid, $Arch\_size$, N_{pop}, T_{max}	0.3, 0.2, 20,0.1, 4,2,30, 100, 100, 500

The following metrics are used to assess the performance of the suggested approach in terms of convergence and diversity: Generational Distance (GD), Inversion Generational Distance (IGD), and Spread Metrics (Δ).

Table V.2. Statistical findings of MOO algorithms in terms of IGD, GD, and Δ metrics for unrestricted test functions.

Algorithm→ Function↓	**PFs**	MOSWO		MAOA		MOGOA	
		Ave	**Std**	**Ave**	**Std**	**Ave**	**Std**
ZDT1	IGD	**3.9917e-4**	**3.9142e-5**	5.7589e-4	5.8138e-5	0.0016	0.0010
	GD	**3.1941e-4**	**1.0137e-4**	0.0037	0.0025	0.0023	0.0021
	Spread	**0.6457**	0.0792	0.9877	**0.0767**	1.2542	0.0932
ZDT2	IGD	**4.8402e-4**	7.3948e-5	1.8449e-4	7.0854e-5	0.0050	**2.8542e-7**
	GD	1.0092e-4	9.0095e-6	8.2599e-4	1.8140e-4	**9.1655e-5**	**1.1390e-7**
	Spread	**0.7905**	0.0574	1.1294	0.0667	1.0595	**3.1334e-4**
ZDT3	IGD	**5.7840e-4**	**6.6982e-5**	8.8082e-4	1.2028e-4	0.0087	0.0068
	GD	**6.0109e-4**	**9.1732e-5**	0.0054	0.0031	0.0082	0.0083
	Spread	**0.9452**	0.0557	1.1348	**0.0411**	1.2756	0.0575

	IGD	**6.5028e-4**	**1.1777e-4**	0.0010	1.8653e-4	0.0048	6.5631e-4
ZDT4	GD	**4.4852e-4**	**9.3873e-5**	8.4212e-4	1.0063e-4	0.0015	3.8838e-4
	Spread	**0.6925**	**0.0362**	1.0549	0.0728	1.5530	0.0590
	IGD	**1.2369e-4**	**1.7790e-5**	1.4670e-4	4.0722e-5	2.0287e-4	7.9339e-5
ZDT6	GD	**0.0017**	**0.0051**	0.0707	0.0136	0.0136	0.0220
	Spread	0.8521	0.1196	**0.6152**	**0.0470**	1.0544	0.0877

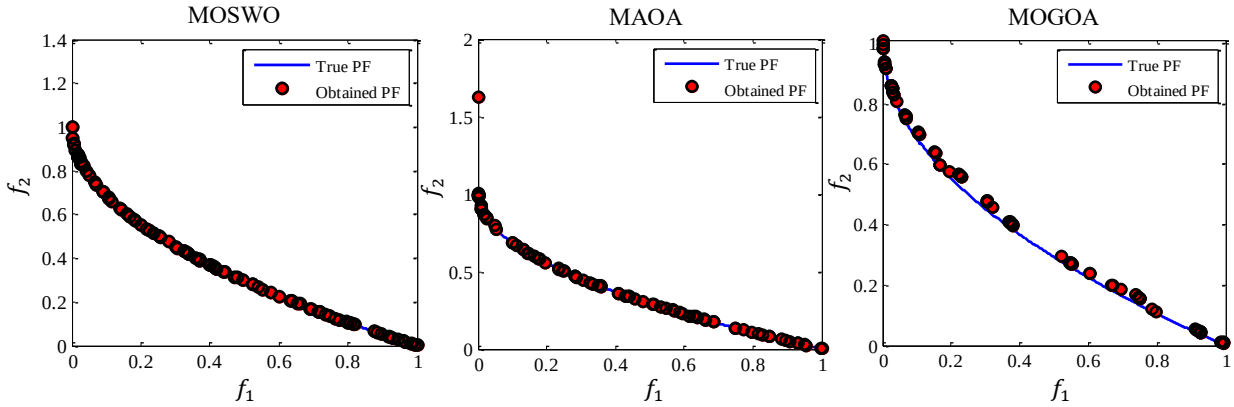

(a) (b) (c)

Figure V.1. Best Pareto optimal front of ZDT1 obtained by the multi-objective algorithms.

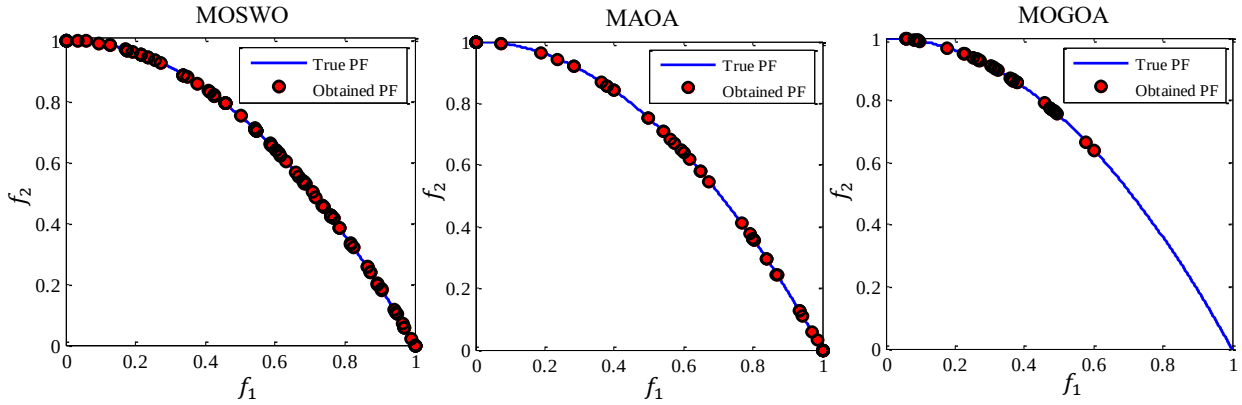

(a) (b) (c)

Figure V.2. Best Pareto optimal front of ZDT2 obtained by the multi-objective algorithms.

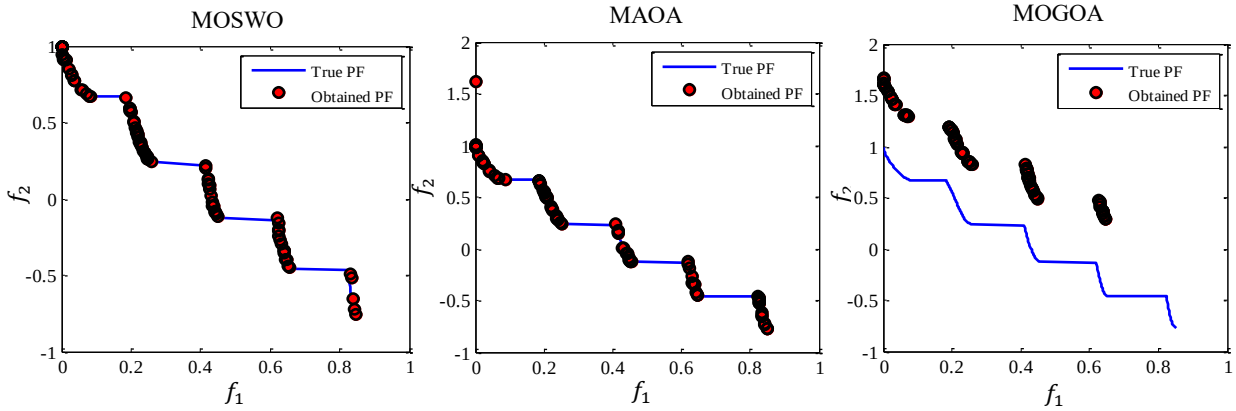

(a) (b) (c)

Figure V.3. Best Pareto optimal front of ZDT3 obtained by the multi-objective algorithms.

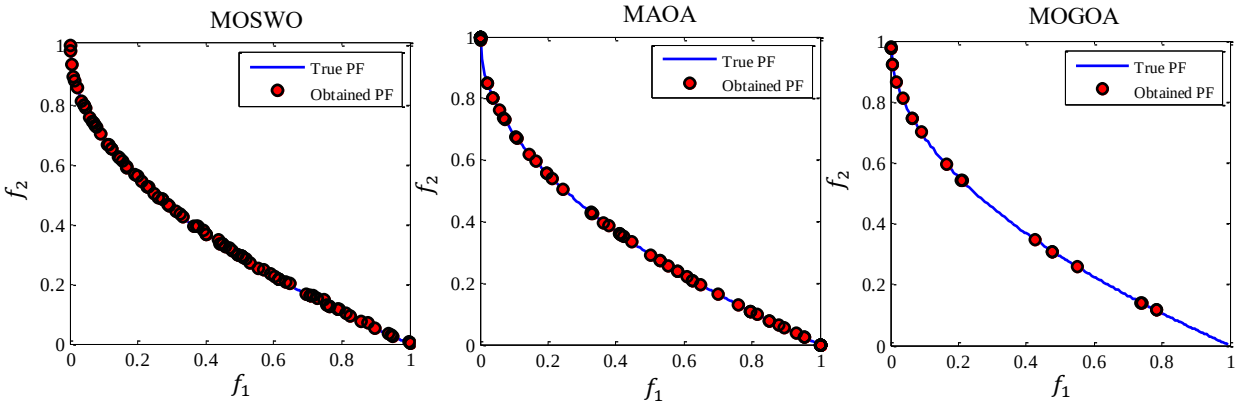

Figure V.4. Best Pareto optimal front of ZDT4 obtained by the multi-objective algorithms.

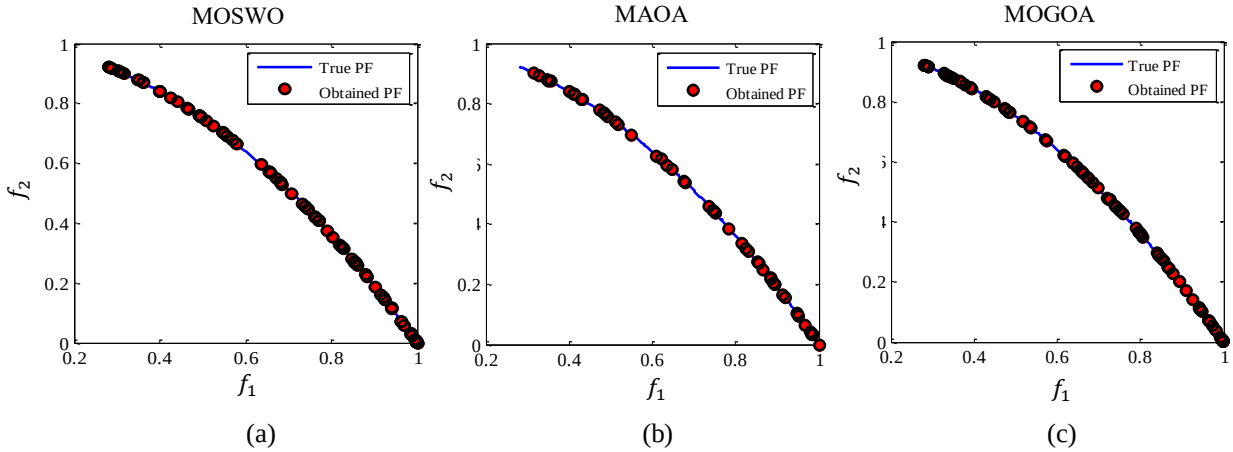

Figure V.5. Best Pareto optimal front of ZDT6 obtained by the multi-objective algorithms.

Table V.3. Statistical findings of MOO algorithms in terms of IGD, GD, and Δ metrics for restricted test functions

Function	PFs	MOSWO		MAOA		MOGOA	
		Ave	**Std**	**Ave**	**Std**	**Ave**	**Std**
SRN	IGD	**1.4293e-4**	**7.6822e-6**	2.3725e-4	6.9049e-5	6.4881e-4	8.0700e-5
	GD	0.0650	0.0148	**1.5912e-4**	**8.7279e-5**	0.0779	0.0547
	Spread	**0.6755**	**0.0354**	1.1003	0.3369	1.6566	0.0408
BNH	IGD	**0.0013**	**1.8142e-4**	0.0045	0.0015	0.0026	2.6789e-4
	GD	**0.0723**	0.0111	0.0961	0.0337	0.1154	**0.0060**
	Spread	0.9125	0.0707	1.5010	0.0560	**0.8677**	**0.0246**
TNK	IGD	**0.0010**	**9.4115e-5**	0.0017	2.6008e-4	0.0140	0.0231
	GD	**0.0010**	**1.6645e-4**	0.0010	2.1300e-4	0.0022	0.0014
	Spread	**0.9266**	**0.0298**	1.2227	0.0454	1.2682	0.1295
OSY	IGD	0.0116	**0.0031**	**0.0094**	0.0088	0.0353	0.0115
	GD	**0.4809**	**0.1624**	1.4668	1.5754	0.5113	0.2984
	Spread	**1.0627**	**0.0629**	1.1294	0.0959	1.1026	0.1113

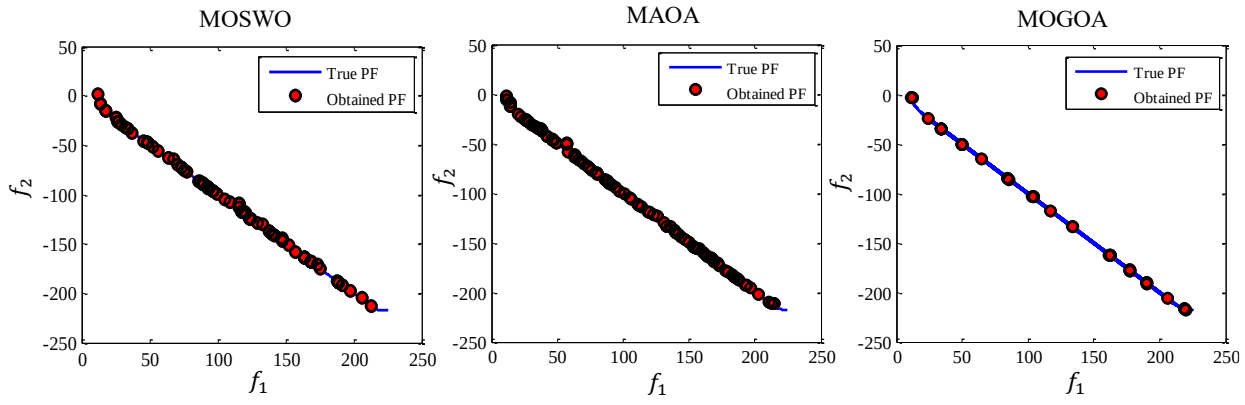

Figure V.6. Best Pareto optimal front of SRN acquired by the MOSWO algorithm.

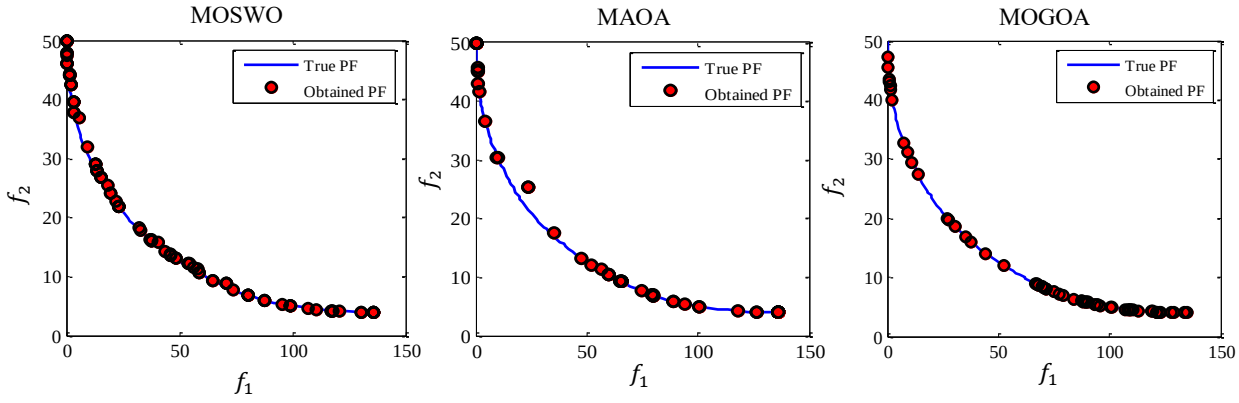

Figure V.7. Best Pareto optimal front of BNH acquired by the MOSWO algorithm.

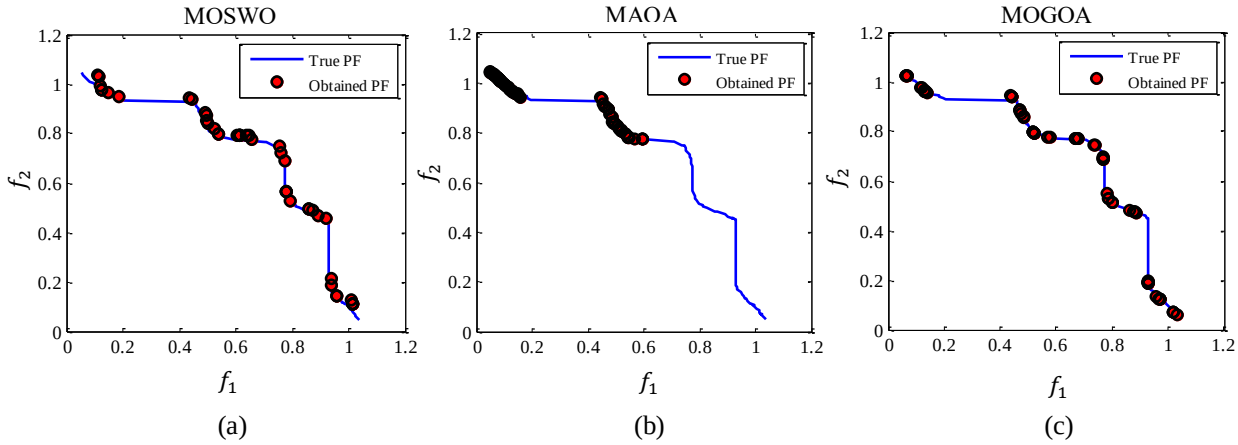

Figure V.8. Best Pareto optimal front of TNK acquired by the MOSWO algorithm.

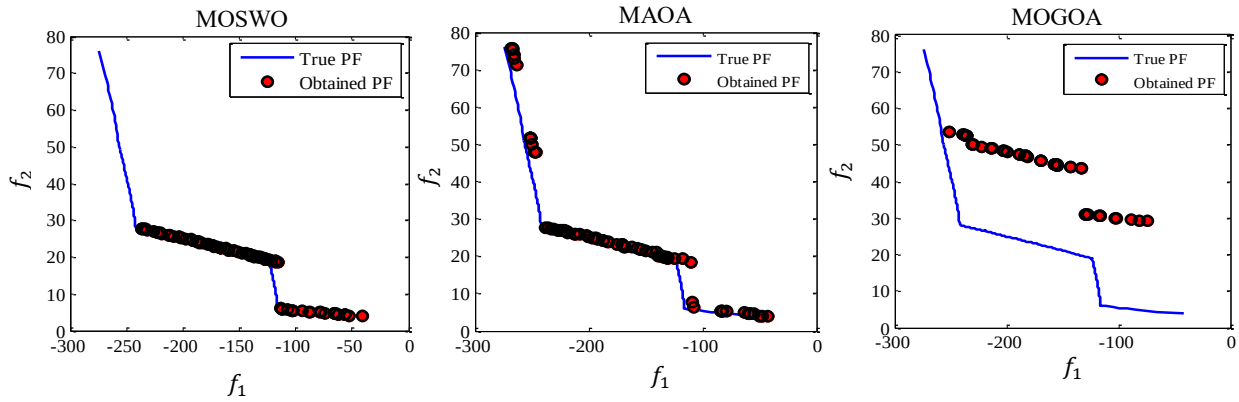

Figure V.9. Best Pareto optimal front of OSY acquired by the MOSWO algorithm.

V.2.2.1 Analyzing the Results

This section presents a comparative analysis of the performance of the suggested MOSWO algorithm with other existing algorithms. The findings obtained from various test functions are categorized into unrestricted test problems (ZDT1-ZDT4 and ZDT6) and restricted test problems (SRN, BNH, TNK, and OSY), as shown in Tables V.2 and V.3. Three performance indicators, namely the IGD, GD, and spread metric, are used to assess the quality of the proposed MOSWO algorithm and other competing methods.

In terms of the IGD indictor, the suggested method demonstrates superior performance on several problems, such as ZDT2, ZDT6, SRN, and TNK, achieving the best results in eight out of nine test cases. The MOAO method closely follows, obtaining the best results in one problem (OSY) among the nine test cases. However, the MOGOA method did not achieve the best findings in any of the test issues. Furthermore, based on the GD metric, the presented approach outperforms other methods in seven out of nine multiplex problems, including ZDT1, ZDT3, ZDT4, ZDT6, BNH, TNK, and OSY. The MAOA method achieves the best results in one problem (SRN), while the MOGOA method performs best in the ZDT2 problem. Finally, with regards to the diffusion scale, the results indicate that the MOSWO algorithm, introduced as a novel approach in this study, excels in generating well-distributed solutions in the majority of cases. Overall, the presented approach outperforms other methods in seven out of nine problems, showcasing its effectiveness and superiority. Additionally, the low standard deviation values demonstrate the consistency of the proposed method in producing reliable results across various instances.

Through these comprehensive evaluations using multiple performance metrics, the study demonstrates the significant advantages of the MOSWO algorithm over existing methods,

emphasizing its potential for solving multi-objective optimization problems effectively and efficiently.

Figures V.1 to V.9 provide a visual representation of the best non-dominated solutions produced by the MOSWO, MAOA, and MOGOA algorithms for across all test problems. Figures V.1 to V.5 specifically presents the results for the ZDT1, ZDT2, ZDT3, ZDT4, and ZDT6 problems respectively. While Figures V.6 to V.9 focuses on the outcomes for the SRN, BNH, TNK, and OSY problems respectively. These figures serve as graphical evidence showcasing the effectiveness of the MOSWO algorithm in generating high-quality solutions.

In both figures, it is evident that the best non-dominated solutions produced by the MOSWO algorithm exhibit excellent convergence towards the true Pareto-optimal front. Furthermore, these solutions are well-distributed across the Pareto front, indicating a harmonious balance between the different objectives. This clearly demonstrates the MOSWO algorithm's ability to effectively explore and exploit the solution space, offering a diverse set of solutions that cover the trade-off space between conflicting objectives.

A comparison of the MOSWO algorithm's results with those of the MAOA and MOGOA algorithms reveals that the proposed approach consistently outperforms or performs on par with the other methods in terms of convergence and the distribution of non-dominated solutions. This visual evidence further strengthens the claim of the MOSWO algorithm's superiority in achieving high-quality solutions for multi-objective optimization problems.

V.3 Application of Real-World Problems

V.3.1 Single and Multi-objective Optimal Power Flow problems

In this study, the MOSWO algorithm was employed to tackle the SOOPF and MOOPF issues. The IEEE 30-bus system was used to prove the efficacy of the proposed approach. Seven case studies were tested on this system, as indicated in Table V.4. The control variables changed to produce the optimal objective function include active power generation without the slack bus, generation bus voltages, transformer tap settings, and shunt capacitors devices coupled to transmission lines.

Table V.4. Summary of studied cases.

Type of OPF	Case	F_1	F_2	F_3	F_4
Single-OPF	1	√			
	2		√		
	3			√	
	4				√
Multi-OPF	5	√	√		
	6	√		√	
	7	√			√

V.3.1.1 Test network

Table V.5 gives the fundamental characteristics of an IEEE 30-bus power system, while the rest data is presented in [4]. Figure V.10 represents the IEEE 30 JB standard network one-line diagram, whereas Table V.6 shows generator cost and emission factors. The fuel cost in the initial case was $902.1311 per hour, emissions were 0.2391 tons per hour, the active power loss was 5.8943 MW, and the voltage deviation was 1.1226 per unit.

Table V.5. The primary characteristics of the system employed in this research.

System Characteristics	IEEE-30 Bus
Buses	30
Branches	41
Generators	9 (Buses:1, 2, 5, 8, 11 and 13)
Generators voltage limits	0.9−1.1[p.u.]
Load voltage limits	0.95−1.05[p.u.]
Limit of tap changer setting	0.9−1.1[p.u.]
Limit of VAR	0−5 [p.u.]
Shunts	9 (Buses:10, 12, 15, 17, 20, 21, 23, 24 and 29)
Transformers	4 (Buses:11,12,15 and 36)
MW demand	283.4 [MW]
Control variables	24

Table V.6. Cost and emission coefficients of generators for the IEEE 30-bus test system.

	Generator Coefficients					
	G_1	G_2	G_5	G_8	G_{11}	G_{13}
	Fuel cost coefficient					
a	0	0	0	0	0	0
b	2	1.75	1	3.25	3	3
c	0.00375	0.0175	0.0625	0.00834	0.025	0.025
	Emission coefficient					
α	4.091	2.543	4.258	5.326	4.258	6.131
β	−5.554	−6.047	−5.094	−3.550	−5.094	−5.555
γ	6.49	5.638	4.586	3.38	4.586	5.151
δ	0.0002	0.0005	0.000001	0.002	0.000001	0.00001
ε	2.857	3.333	8	2	8	6.667

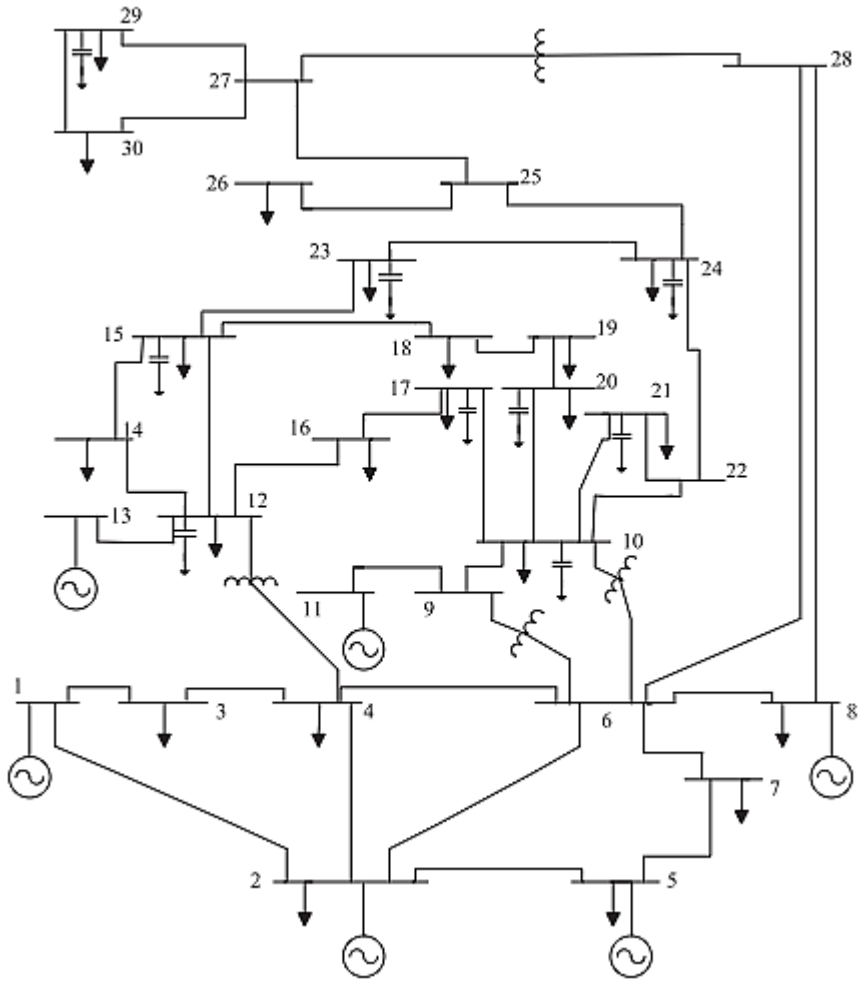

Figure V.10. One-line diagram of an IEEE 30 bus system.

V.3.1.2 Single objective Cases

The four objective functions evaluated to address the OPF problem are fuel cost, generation emissions, active power loss, and voltage deviation. Table V.7 summarizes the findings of this single-objective OPF study, which used the following parameters: $TR = 0.3, CR = 0.2$, and $N_{min} = 30$. As for the parameters of the comparison algorithms, they are as follows:

PSO: C_1=C_2=2, W_{max}=0.9, W_{min} =0.4

CS: pa=0.25;

In addition, there are 250 population sizes and 1000 maximum iterations.

Case 1: Minimization of generation fuel cost

The fuel cost is regarded as the first objective function to be optimized by the suggested SWO algorithm in this section. Table V.7 shows that the fuel cost decreased by 11.35% from the initial value of 902.1311 $/h to the optimal value of 799.72088 $/h.

Case 2: Minimization of emission

With the advent of the challenge of global warming and the growth in environmental pollution, emission research has recently attracted greater interest from researchers. In this case, environmental emissions are regarded as a second objective function that is reduced to a minimum. As shown in Table V.7, the suggested algorithm delivered a good performance in lowering emissions with a reduction rate of 14.38% (from the initial value of 0.2391 tons / h to the minimal value of 0.2047 tons / h).

Case 3: Minimization of active power transmission losses

In this case, active power transmission losses are seen as another singular objective function that can be decreased using the SWO method in Table V.7. This objective function was improved by 48.58% (from an initial value of 5.8943 MW to a minimum value of 3.0305 MW).

Case 4: Enhancement of voltage profile

The final objective function is to reduce voltage deviation. The goal of addressing this function is to ensure that the voltage profile on PQ buses is optimized within its limits. This objective was significantly reduced using the proposed algorithm, with a decrease rate of 92.22% (from the initial value of 1.1226 p.u to the minimum value of 0.0872 p.u).

Table V.7. Best Control Variables Achieved by SWO algorithm for Cases 1-4.

Parameters	Min	Initial	Case 1	Case 2	Case 3	Case 4	Max
Pg1(MW)	50	99.294	177.2862	63.8956	51.4341	82.1806	200
Pg2(MW)	20	80	48.7331	67.6051	79.9999	79.967	80
Pg5(MW)	15	50	21.3517	49.9999	49.9998	37.668	50
Pg8(MW)	10	35	20.9463	34.9999	34.9987	34.8782	35
Pg11(MW)	10	30	11.9080	29.9999	29.9989	29.5854	30
Pg13(MW)	12	40	12.0023	39.9999	39.9981	24.108	40
Vg1(p.u.)	0.95	1.05	1.0605	1.0536	1.0616	1.0060	1.1
Vg2(p.u.)	0.95	1.04	1.0565	1.0480	1.0572	1.0033	1.1
Vg5(p.u.)	0.95	1.01	1.0380	1.0295	1.0376	1.0187	1.1
Vg8(p.u.)	0.95	1.01	1.0443	1.0366	1.0444	0.9990	1.1
Vg11(p.u.)	0.95	1.05	1.0703	1.0627	1.0461	1.0335	1.1

Vg13(p.u.)	0.95	1.05	1.0498	1.0513	1.0504	1.0160	1.1
Qc10(MVAR)	0	0	0.0236	3.2478	3.1805	3.5663	5
Qc12(MVAR)	0	0	4.9410	2.9499	4.8707	4.0838	5
Qc15(MVAR)	0	0	4.0395	4.1442	3.7380	4.9999	5
Qc17(MVAR)	0	0	4.9080	3.9737	4.9842	0.1120	5
Qc20(MVAR)	0	0	4.2085	4.3681	4.1315	4.9933	5
Qc21(MVAR)	0	0	4.9995	4.9992	4.9996	4.9969	5
Qc23(MVAR)	0	0	2.9828	4.0097	3.4774	4.9812	5
Qc24(MVAR)	0	0	4.9993	4.9866	4.9995	4.9878	5
Qc29(MVAR)	0	0	1.9182	1.8560	2.1213	2.9857	5
T11(p.u.)	0.9	1.078	1.0218	0.9868	1.0264	1.0472	1.1
T12(p.u.)	0.9	1.069	0.9347	0.9708	0.9180	0.9	1.1
T15(p.u.)	0.9	1.032	0.9907	0.9807	0.9911	0.9954	1.1
T36(p.u.)	0.9	1.068	0.9746	0.9660	0.9755	0.9684	1.1
Fuel cost ($/h)		902.1311	**799.7208**	944.0604	967.4841	888.8286	-
Emission (t/h)		0.2391	0.3667	**0.2047**	0.20725	0.2229	-
Ploss (MW)		5.8943	8.8279	3.1996	**3.0295**	4.9872	-
VD (p.u.)		1.1226	0.9171	0.8798	0.9088	**0.0872**	-

Table V.8. Comparative Analysis of the Best Results Obtained by SWO and Other Algorithms for Cases 1 to 4.

Case	Algorithm	Fuel cost ($/h)	Emission (t/h)	Ploss (MW)	DV (p.u.)
Case 1	SWO	**799.7208**	0.36671	8.8279	0.9171
	CS	799.7262	0.36767	8.84844	0.91979
	ALO	799.9383	0.3665	8.8875	0.61550
	PSO	800.5484	0.3674	9.0807	0.3627
	CS-GWO [5]	799.9978	-	8.9034	0.9386
	Chaotic Rao-2 [6]	800.1537	-	9.03445	0.8981
	Rao-2 [6]	800.3865	-	9.05358	0.9056
	IBSA [7]	800.3975	0.36567	8.9965	0.9238
	DE [7]	800.3978	0.36622	8.9959	0.9215
	SF-DE [8]	800.4131	0.366652	9.0104	0.9207
	ECHT-DE [8]	800.4148	0.36593	8.999	0.91231
	SP-DE [8]	800.4293	0.36806	9.0583	0.91015
	AGTLBO [9]	800.4811	0.3662	9.0222	0.9109
	ISSA[10]	800.4752	-	9.1044	0.8965
	HHO [11]	801.829	1.263	9.3870	-
Case 2	SWO	944.0604	**0.2047**	3.1966	0.8798
	CS	943.9885	0.20478	3.1976	0.8715
	ALO	944.2305	0.20481	3.2927	0.6392
	PSO	944.1417	0.2048	3.2530	0.64574
	AGTLBO [9]	944.3385	0.2048	3.2233	0.9017
	SSA [12]	943.9201	0.2048	3.0582	1.8335
	DE [7]	1015.4273	0.20482	3.2177	0.9040
	ECHT-DE [8]	944.3782	0.20482	3.2179	0.8924
	IBSA [7]	1015.6857	0.20484	3.2907	0.9057
	HGS [13]	933.703	0.2174	3.3515	0.7971

	SMA[14]	936.1166	0.2175	3.5935	0.4754
	HHO [11]	950.98	0.285	3.57	-
Case 3	SWO	967.4841	0.20725	**3.0295**	0.9088
	CS	967.4758	0.20725	3.0297	0.9002
	ALO	967.5391	0.2073	3.0484	0.9091
	PSO	968.5834	0.2073	3.4858	0.5613
	SP-DE [8]	967.5962	0.20726	3.0844	0.9035
	DE [7]	1027.362	0.20726	3.0828	0.91058
	CS-GWO [5]	967.6026	-	3.0861	0.9222
	AGTLBO [9]	967.6336	0.2073	3.0906	0.9086
	SMA [14]	967.6636	0.20727	3.1005	0.8886
	IBSA [7]	1027.4002	0.20727	3.0951	0.90383
	HHO [11]	966.12	0.296	3.49	-
Case 4	SWO	888.8286	0.2229	4.9872	**0.0872**
	CS	900.1257	0.2324	5.0013	0.0880
	ALO	893.6815	0.2275	5.0920	0.1234
	PSO	897.7503	0.2469	5.7514	0.1098
	SSA [12]	867.0718	0.3179	9.4135	0.0920
	BSOA [9]	809.7582	0.3383	10.4199	0.0934
	IEO [15]	803.6371	-	9.9343	0.0944
	SMA [14]	868.0514	0.2569	6.2099	0.1097
	CS-GWO [5]	803.5477	-	9.903	0.1023
	HFPSO [16]	803.6002	-	9.8538	0.1163
	HGS [13]	889.278	0.2343	5.1253	0.1195

Table V.8 clearly shows that the proposed SWO approach outperforms the other algorithms used in the study, including the Cuckoo Search (CS), Ant Lion Optimizer (ALO), and Particle Swarm Optimization (PSO) algorithms, as well as other recent algorithms documented in the literature. These findings demonstrate the effectiveness of the proposed SWO technique in improving the objective function for the four different individual cases studied. This superiority reflects the approach's adaptability in dealing with a wide range of scenarios and difficulties.

Figure V.11 displays the suggested approach's approximation of an individual objective function for fuel cost, environmental pollutant emissions, active power losses, and voltage deviation regarding the number of repetitions.

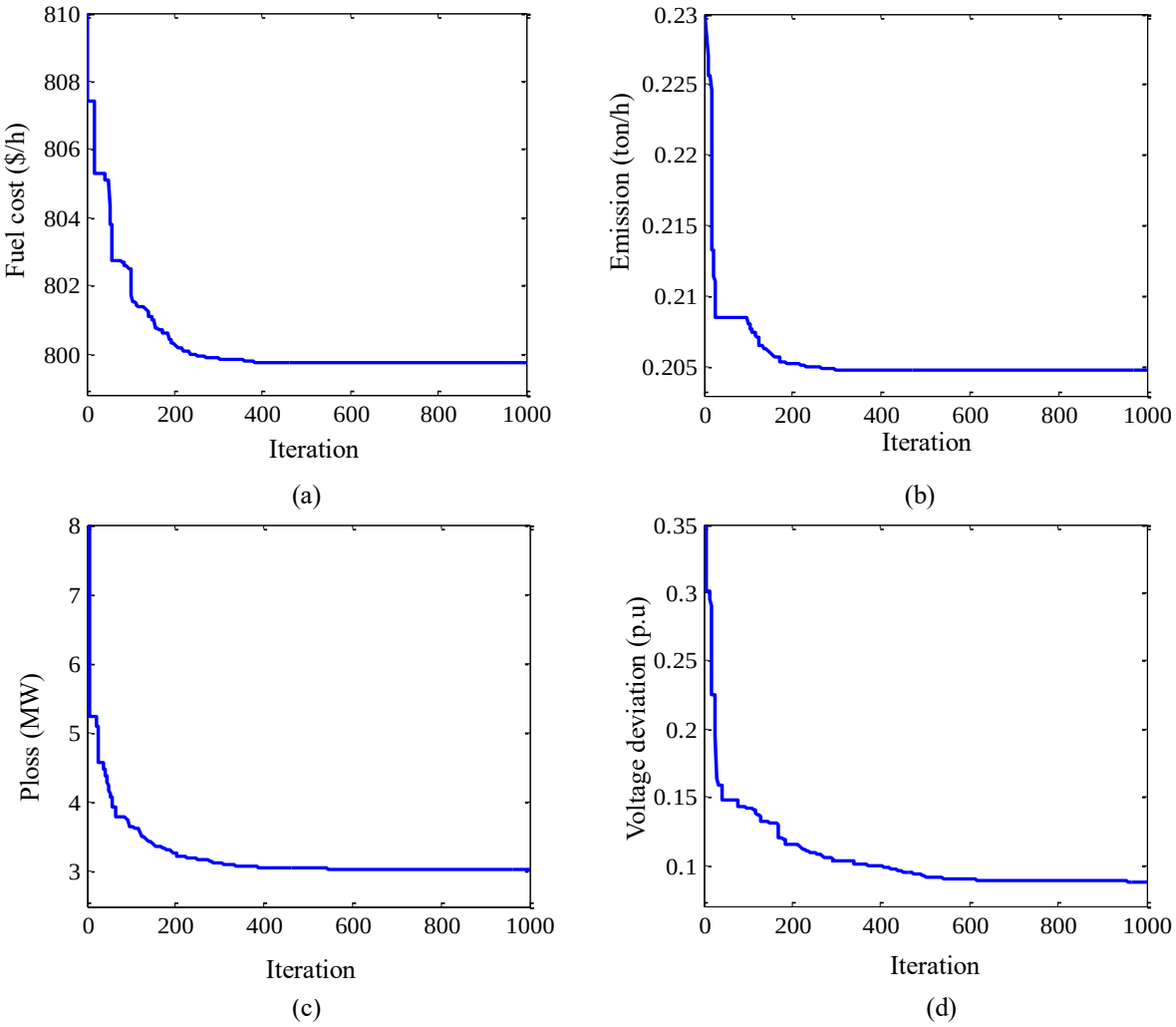

Figure V.11. Convergence curves derived by the SWO approach for cases (1-5) (a) Fuel Cost, (b) Emission, (c) Power Loss, (d) Voltage Regulation.

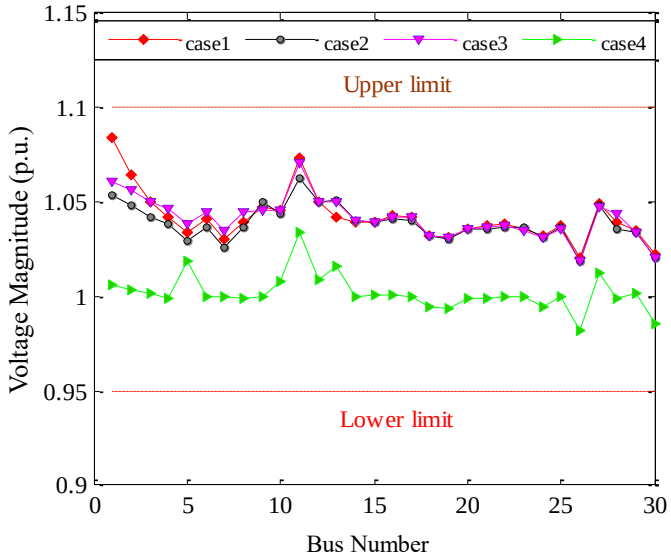

Figure V.12. The optimized voltage profile for all buses from case 1 to case 4.

V.3.1.3 Multi objective Cases

Following the discussion of single-objective issues in the preceding section, three cases were addressed to demonstrate the effectiveness of the proposed algorithm in solving various problems, with a focus on cost because it is the main objective in this study and was mentioned in all MOOPF cases. Table V.9 displays the best compromise solutions discovered for all MOOPF cases.

In this study, the following MOSWO parameters were determined:

$TR = 0.3, CR = 0.2$, $N_{min} = 30$, N_{pop}=250: Population sizes, T_{max}=1300: The maximum number of iterations, α = 0.1: The grid inflation parameter, β = 4: The leader selection pressure parameter, nGrid= 20: The number of grids per dimension, γ =2: Additional (to be removed) archive Member Selection Pressure, $Arch\_size$ =100: The maximum size of the archive.

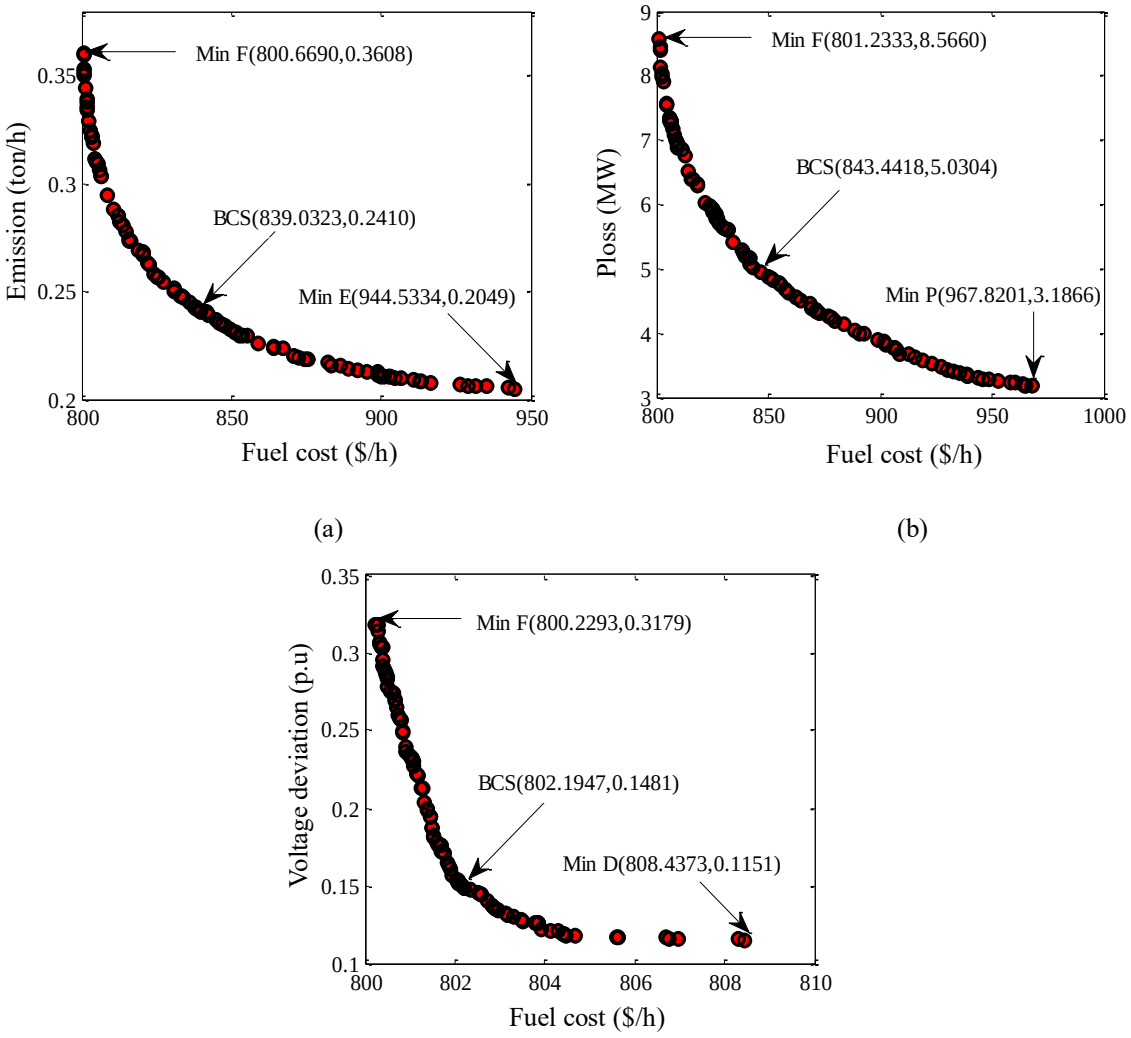

Figure V.13. Pareto-optimal solutions obtained by MOSWO of the three cases. Case 5 (a), Case 6 (b), Case 7 (c).

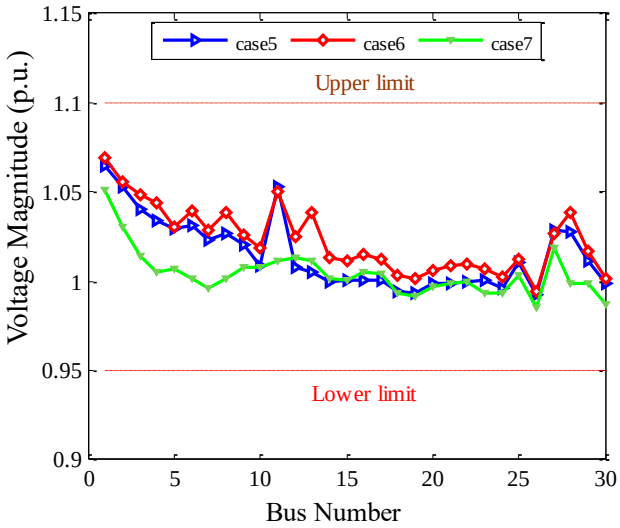

Figure V.14. Voltage levels acquired by MOSWO for the three cases.

Case 5: Minimization of total generation cost and emission

The first case of a multi-objective function is to jointly improve fuel cost and emissions using the MOSWO approach. The best compromise solution was 839.03226 $/h and 0.2400 t/h, respectively, compared with case 1 and case 2 (799.7208 $/h, 0.3667) and (944.0604 $/h, 0.2047 t/h), respectively. We can conclude that the suggested algorithm gave a good distribution between the two objective functions.

Case 6: Minimization of total generation cost and active power losses

Because power balance is critical in network planning, active power loss has an important effect on the economic operation of the power system. To ensure practical system stability, active power losses should be incorporated as an objective to be adjusted with fuel cost at the same time, as the best compromise solution found from the suggested technique was (Cost = 843.4415 $/h and Ploss = 5.0304 MW) when compared to Case 1 and Case 3 (799.7208 $/h, 8.8279 MW) and (967.3771 $/h, 3.0305 MW), respectively. We discover that the MOSWO algorithm can produce an optimal solution that meets two of the required goals.

Case 7: Minimization of total generation cost and voltage magnitude deviation

The last case of the MOOPF is to reduce fuel cost with voltage deviation simultaneously, where the suggested algorithm provided the best compromise solution (cost = 802.1947 $/h and DV = 0.1481 p.u) when compared to Case 1 and Case 4 (799.7208 $/h, 0.9171p.u) and (888.8286 $/h, 0.0872 p.u), respectively.

Table V.9. Optimal Compromise Solutions Achieved using the SWO Method for Multi-Objective OPF

Parameters	Case 5	Case 6	Case 7
Pg1(MW)	112.9868	113.7128	178.3494
Pg2(MW)	55.7273	52.9355	48.3407
Pg5(MW)	29.3430	35.1578	21.7298
Pg8(MW)	34.9585	33.2601	20.2637
Pg11(MW)	30.0000	29.7576	12.0844
Pg13(MW)	25.7673	23.6062	12.1973
Vg1(p.u.)	1.0648	1.0694	1.0514
Vg2(p.u.)	1.0526	1.0553	1.0300
Vg5(p.u.)	1.0293	1.0300	1.0065
Vg8(p.u.)	1.0264	1.0383	1.0013
Vg11(p.u.)	1.0530	1.0503	1.0118
Vg13(p.u.)	1.0052	1.0388	1.0117
Qc10(MVAR)	5.0000	1.8598	2.3178
Qc12(MVAR)	0	1.8562	1.2366
Qc15(MVAR)	5.0000	3.2624	4.3836
Qc17(MVAR)	0.1859	0.8774	4.7790
Qc20(MVAR)	4.5781	2.4037	3.4186
Qc21(MVAR)	1.5333	3.7579	4.7752
Qc23(MVAR)	4.8624	2.4321	0.1317
Qc24(MVAR)	4.2735	3.4202	4.8292
Qc29(MVAR)	1.0034	3.4503	0.0255
T11(p.u.)	1.0169	1.0196	0.9975
T12(p.u.)	1.0068	0.9772	0.9337
T15(p.u.)	1.0050	1.0166	0.9655
T36(p.u.)	0.9660	0.9907	0.9495
Fuel cost ($/h)	**839.0322**	**843.4415**	**802.1947**
Emission (t/h)	**0.2410**	0.2410	0.3693
Ploss (MW)	5.3831	**5.0304**	9.5657
DV (p.u.)	0.2736	0.4240	**0.1481**

Table V.10. Comparison of the best compromise solutions for three Cases.

Case	Algorithms	Fuel cost ($/h)	Emission (t/h)	Ploss (MW)	VD (p.u.)
Case 5	MOSWO	**839.0322**	**0.2410**	5.3831	0.2736
	MOMICA [17]	865.066	0.2221	4.5703	1.0202
	BB-MPSO [17]	865.0985	0.2227	-	-
	MO-IPSO [18]	841.052	0.2585	-	-
	NSGA2 [19]	850.99166	0.2442	-	-
	rNSGA2 [19]	848.1499	0.2464	-	-
	MOEMA [20]	876.89	0.263	7.4078	-
	MOHHO [11]	903.2200	0.3150	4.2900	
Case 6	MOSWO	**843.4415**	0.2410	**5.0304**	0.4240
	MOMICA [17]	848.0544	1.4171	4.5603	0.2343

	PSO–Fuzzy [21]	847.01	-	5.666	-
	MO-IPSO [18]	850.916	-	7.893	-
	SF-DE [8]	859.1458	0.2289	4.5245	0.9273
	MOEMA [20]	852.438	0.2806	7.0084	-
Case 7	MOSWO	**802.1947**	0.36938	9.5657	**0.14819**
	MOALO [22]	803.0611	-	-	0.3787
	PSO [23]	803.41	-	9.78	0.2480
	GA [23]	803.17	-	9.62	0.198
	MOSMA [14]	802.0533	-	-	0.3267
	MOHCS [13]	803.094	0.3678	9.6092	0.1813
	TiGEA-22 [24]	802.1883	-	-	0.156947
	MOEADDAE [24]	802.1935	-	-	0.1594
	MOJaya [25]	803.9	-	9.489	0.16665

Figure V.13 depicts the non-dominant solutions for the multi-objective functions produced using the SWO approach, illustrating that the Pareto solutions are evenly spread throughout the Pareto front.

Table V.9 displays the best compromise solutions (BCS) of the suggested algorithm and their comparison with other algorithms for the three cases of the multi-objective function of fuel cost with generation emissions (case 5), fuel cost with active power transmission losses (case 6), and finally fuel cost with voltage deviation (case 7), where the proposed algorithm appears to be a very competitive solution compared to the rest of the optimization algorithms

Figures V.12 and V.14 depict the voltage profile in the load bus for single and multi-objective functions, with the voltage always falling within the prescribed range.

V.3.2 Optimizing Power Flow with integrating Renewable Energy Sources

The standard IEEE 30-bus test system was modified by substituting renewable energy sources for three thermal power generators. As shown in Figure V.15, two wind farms have been installed on buses 5 and 11, and a solar PV unit on bus 13.

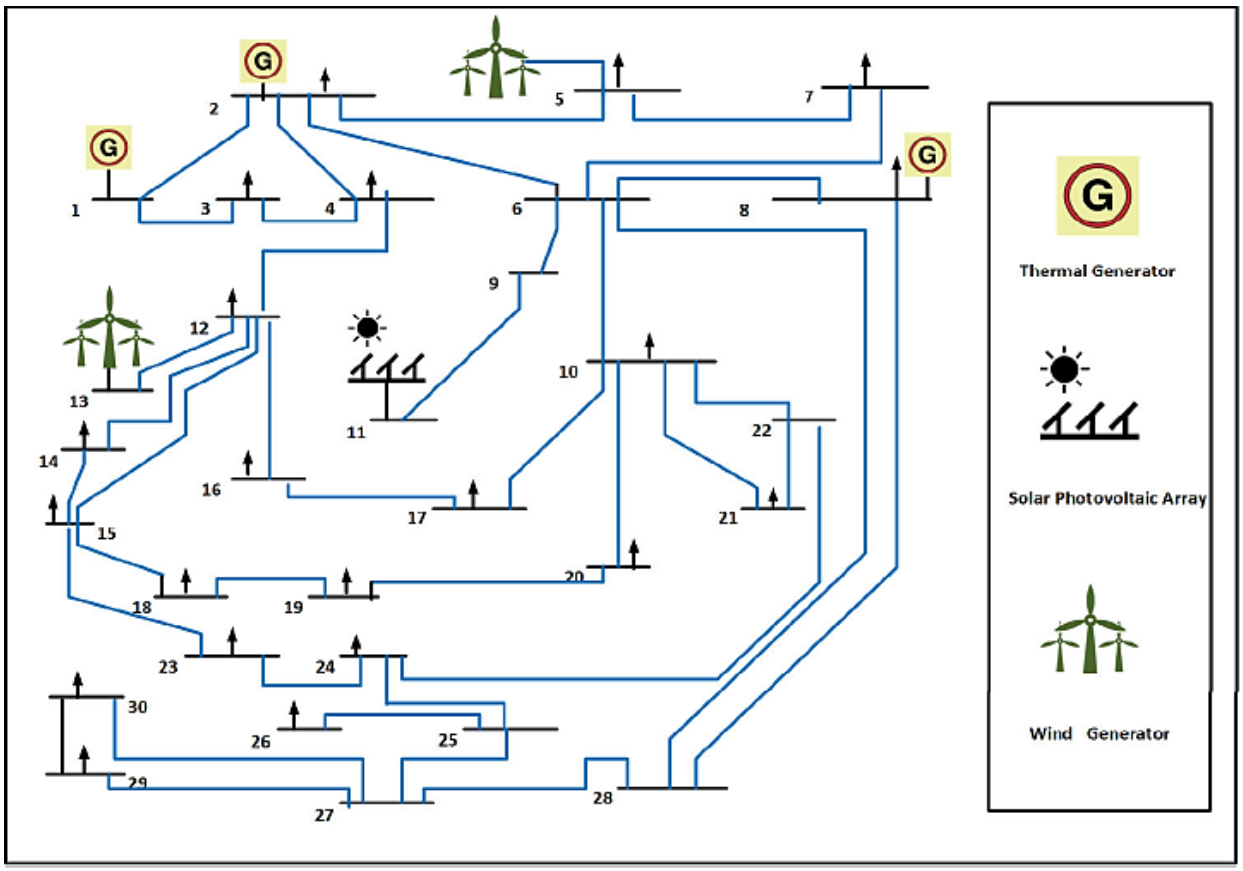

Figure V.15. Modified IEEE 30-bus network with RES integration.

The statistics from wind farms and solar power units, which are depicted in Table V.11 and V.12, reveal that each wind farm has 25 and 20 turbines, respectively, and that the rated output of each turbine is 3 MW. Within the same context, we have different wind speed values, such as 16m/s for an expected wind speed, 3m/s for a cut-in wind speed, and 25m/s for a cut-out wind speed. At specific standard conditions, the value of solar radiation for a solar power plant is 800 W/m 2, whereas the radiation point is fixed at 120 W/m 2. Regarding the thermal generators installed on Buses 1, 2, and 8, their fuel cost and emission factors remain unchanged when considering optimal power flow alone. The detailed information on wind and solar energy, as obtained from the reference [26]. The parameters of the proposed approach in this scenario are as follows:

TR=0.3, Cr=0.2, and N_min=30. In addition, there are 250 population sizes and 500 maximum iterations.

V.3.2.1 Optimization Objectives

Three primary objective functions are developed for the OPF solution in the presence of renewable energies. In the first objective function, the cost is optimized with the integration of all cost functions without incorporating the cost of emissions. The second objective function

reduces real power losses, and the final target improves overall cost with the addition of the cost of emissions.

Table V.11. PDF Parameters and Cost Coefficients of WT unit.

Wind Farm	No. of Turbines	P_{wr} (MW)	Weibull PDF Parameters	Weibull Mean, M_{wbl}	Direct Cost Coefficient	Reserve Cost Coefficient	Penalty Cost Coefficient
1 (bus 5)	25	75	$c = 9, k = 2$	$v = 7.976\, m/s$	$g_5 = 1.6$	$K_{Rw,5} = 3$	$K_{Pw,5} = 1.5$
2 (bus 11)	20	60	$c = 10, k = 2$	$v = 8.862\, m/s$	$g_{11} = 1.75$	$K_{Rw,11} = 3$	$K_{Pw,11} = 1.5$

Table V.12. PDF Parameters and Cost Coefficients of PV unit.

Solar PV Plant	P_{sr} (MW)	Lognormal PDF Parameters	Lognormal Mean, M_{lgn}	Direct Cost Coefficient	Reserve Cost Coefficient	Penalty Cost Coefficient
1 (bus 13)	50	$\sigma = 0.6, \mu = 6$	$G = 483\, W/m2$	$h_{13} = 1.6$	$K_{Rs,11} = 3$	$K_{Ps,13} = 1.5$

Case 1

Power generators have traditionally used fossil fuels in power systems, and fuel consumption is controlled by adjusting the fuel supply reservoir valves. As a result, in the context of the fuel cost function in Case 1, valve point effects (VPE) can be efficiently described using the following equation:

$$C_{TG}(P_{Gi}) = \sum_{i=1}^{NG} (a_i + b_i P_{Gi} + c_i P_{Gi}^2) + \left| d_i \times \sin\left(e_i\left(P_{TG}^{min} - P_{Gi}\right)\right)\right| \qquad (V.1)$$

where d_i and e_i are the valve point cost coefficients for unit i and P_{TG}^{min} is the minimum generation limit for the same unit.

Table V.13. Comparison of Optimal Values for Case 1.

Control variables	Min	ALO	PSO	CS	SWO	Max
Pg1(MW)	50	192.4289	194.7470	194.221	194.2694	200
Pg2(MW)	20	42.8806	48.9091	48.8770	48.1530	80
Pg5(MW)	15	18.1312	18.2540	18.5010	19.0371	50
Pg8(MW)	10	17.7207	10.0000	10.0000	10.1266	35
Pg11(MW)	10	10.1226	10.0000	10.0502	10.0001	30
Pg13(MW)	12	12.000	12.0000	12.0066	12.0385	40
Vg1(p.u.)	0.95	1.0840	1.0747	1.0830	1.0821	1.1
Vg2(p.u.)	0.95	1.0618	1.0523	1.0603	1.0597	1.1
Vg5(p.u.)	0.95	1.0296	1.0202	1.0292	1.0272	1.1
Vg8(p.u.)	0.95	1.0382	1.0277	1.0329	1.0374	1.1
Vg11(p.u.)	0.95	1.0548	1.0870	1.0699	1.0638	1.1
Vg13(p.u.)	0.95	1.0452	1.1000	1.0537	1.0564	1.1
Qc10(MVAR)	0	3.6895	0	1.74421	4.4406	5
Qc12(MVAR)	0	1.6171	5.0000	2.8712	1.0411	5

Qc15(MVAR)	0	2.5672	5.0000	3.4179	4.3334	5
Qc17(MVAR)	0	2.9652	0	5.0000	3.6847	5
Qc20(MVAR)	0	1.1569	0	5.0000	4.2978	5
Qc21(MVAR)	0	4.1000	5.0000	4.8591	4.9879	5
Qc23(MVAR)	0	2.3460	0	1.7304	2.4445	5
Qc24(MVAR)	0	4.0402	0	4.1454	4.9167	5
Qc29(MVAR)	0	2.9401	0	3.1060	2.5820	5
T11(p.u.)	0.9	0.9587	1.0231	1.0658	1.0373	1.1
T12(p.u.)	0.9	1.0435	0.9000	0.9008	0.9484	1.1
T15(p.u.)	0.9	0.9960	1.0619	0.9908	0.9823	1.1
T36(p.u.)	0.9	0.9809	0.9525	0.9814	0.9943	1.1
Fuel cost ($/h)		835.7421	834.1492	833.6002	**833.5673**	-
Emission (t/h)		0.4141	0.4236	0.4216	0.4216	-
Ploss (MW)		9.8843	10.5102	10.2562	10.2250	-
VD (p.u.)		0.6023	0.7914	0.7782	0.7461	-

Table V.13 shows the optimal control settings obtained by combining SWO, CS, PSO, and ALO approaches. This comparison analysis reveals that the SWO approach produced the best results, with a fuel cost of 833.5673($/h). This outperforms the CS (833.6002$/h), PSO (834.1492$/h), and ALO (835.7421$/h) algorithms, as described in the same table. Furthermore, Figure V.16 (a) depicts the convergence behavior of the SWO algorithm in this case. Based on the extensive dataset, it is clear that the SWO algorithm successfully found the optimal OPF solutions for the case study.

Case 2

Case 2 employs Eq. (V,2) to optimize the scheduled power of both conventional and renewable energy generators to reduce total generating costs.

$$F_1 = C_T(P_{TG}) + C_{wind} + C_{Solar} \quad (V.2)$$

The control variables, reactive power (Q), and other determined objective functions are summarized in Table V.14, where the best objective function is highlighted in bold. P_{W1} and P_{W2} signify the outgoing power of wind farms 1 and 2, respectively, while P_{s1} denotes the output power of the solar PV unit. Table V.15 shows that the proposed algorithm for spider wasp outperforms the rest of the optimization algorithms reported in the literature in terms of solution quality. The SWO algorithm achieves the lowest total generation cost of 781.0793($/h). Figure V.16 (b) shows the convergence characteristics of the proposed approach for this case.

By comparing the results obtained without the use of renewable energy sources (cost=833.5673$/h) to the results obtained with the use of renewable energy sources (cost=781.0793$/h), we can conclude that the integration of renewable energy sources results in a 53.49$/h per hour reduction in total generation costs. When calculated over a year (365*24*53.49$/h), this equates to a cost savings of 468572.4($/ h) per year is thus possible. The results of the proposed algorithm show that including renewable energy sources can significantly contribute to lowering total fuel costs when compared to the original system.

Case 3

This case focuses on optimizing the scheduling of conventional thermal generators with renewable energy sources to reduce active power losses. Table V.14 demonstrates the best results obtained by scheduling thermal generators and RES using the proposed SWO algorithm to reduce active power loss. These results show that the proposed approach effectively reduced active power loss to 1.7351 MW, with a significant decrease of 42.74% compared to the case without renewable energies, in which the active power loss value reached 3.0305 MW. These findings underline the importance of integrating renewable energy sources to reduce the problem of active power losses. Figure V.16 (c) illustrates the convergence characteristics of the proposed SWO algorithm for this case. Table V.15 displays the statistical findings for the current case. This table shows that the proposed method performed well in terms of decreasing active power losses when compared to other algorithms discussed in the literature.

Case 4

In this instance, the objective is to minimize the overall generation cost, encompassing the carbon tax applied to emissions from traditional thermal power generators. The assumed carbon tax rate, $Ctax$, stands at 20 ($/ton). Referring to Eq. (V,3), the combined cost to be minimized is expressed as follows:

$$F_2 = F_1 + C_{emi} \tag{V.3}$$

Table V.14 shows the control variables, reactive power (Q), and other calculated values (including carbon tax), with the optimal objective function highlighted in bold. It can be observed that the penetration of wind and solar power in this scenario is higher than in case 2 without incurring an emissions penalty. The extent of the increase in the optimal generating schedule for renewable resources is determined by the quantity of emissions and the rate of carbon cost applied. Table V.14 presents the statistical findings in the current case. This table illustrates that when compared to other algorithms addressed in the literature, the proposed

approach performed well in decreasing active power losses. Figure V.16 (d) shows the convergence characteristics of the proposed approach for this case.

The load bus voltage limitation is especially important in the context of the OPF, as the load bus operating voltage approaches its limits. It is essential in this study to maintain the load bus voltage within a specific range of 0.95 p.u. to 1.05 p.u. Figure V.17 illustrates the voltage profiles of the load buses used to improve Cases 1, 2, 3, and 4, and it is clear that the bus voltage as a whole remains within the specified limits.

Table V.14. Best variables obtained for cases 2 to 4.

Control variables	**Min**	**Case 2**	**Case 3**	**Case 4**	**Max**
Pg1(MW)	50	134.9078	50.0000	123.4563	200
Pg2(MW)	20	30.1744	60.6397	32.7242	80
Pw1(MW)	0	43.6619	74.9973	45.6858	75
Pg8(MW)	10	10.0010	34.9999	10.0000	35
Pw2(MW)	0	36.6794	59.9962	38.5502	60
Ps1(MW)	0	33.4864	46.7779	37.9923	50
Vg1($p.u.$)	0.95	1.0999	1.1000	1.0999	1.1
Vg2($p.u.$)	0.95	1.0885	1.1000	1.0899	1.1
Vg5($p.u.$)	0.95	1.0691	1.0909	1.0711	1.1
Vg8($p.u.$)	0.95	1.0850	1.0952	1.0975	1.1
Vg11($p.u.$)	0.95	1.0999	1.1000	1.0999	1.1
Vg13($p.u.$)	0.95	1.0870	1.1000	1.0950	1.1
Parameters	**Min**	**Case 2**	**Case 3**	**Case 4**	**Max**
Qg1(MVAR)	-20	-9.5660	-3.2120	-10.4633	150
Qg2(MVAR)	-20	17.8966	8.8367	16.6691	60
Qw1(MVAR)	-30	25.2994	22.4266	24.5717	35
Qg8(MVAR)	-15	40.0000	40.0000	40.0000	40
Qw2(MVAR)	-25	19.8602	16.5761	18.9294	30
Qs1(MVAR)	-20	19.2935	19.5931	21.5430	25
Total Cost ($/h)	-	**781.0793**	957.8031	**809.3199**	-
Emission (t/h)	-	1.76169	0.0996	0.8879	-
Carbon tax ($/h)	-	-	-	**17.7581**	-
Ploss (MW)	-	5.5112	**1.7351**	5.0089	-
DV (p.u.)	-	**0.9895**	1.3422	**1.0696**	-

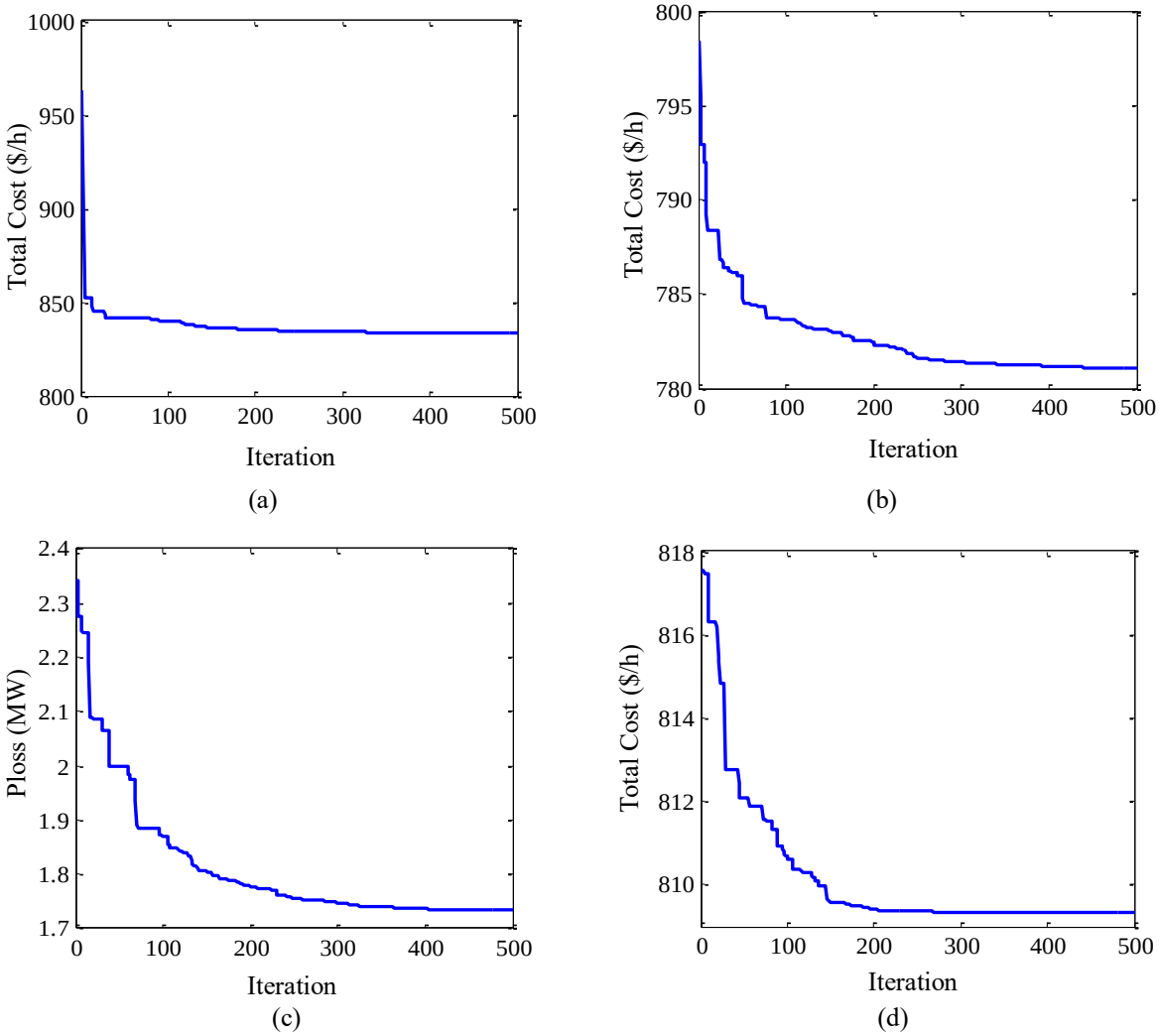

Figure V.16. The convergence characteristics of the suggested method in three different cases: Case 1 (a), Case 2 (b), Case 3 (c), and Case 4 (d).

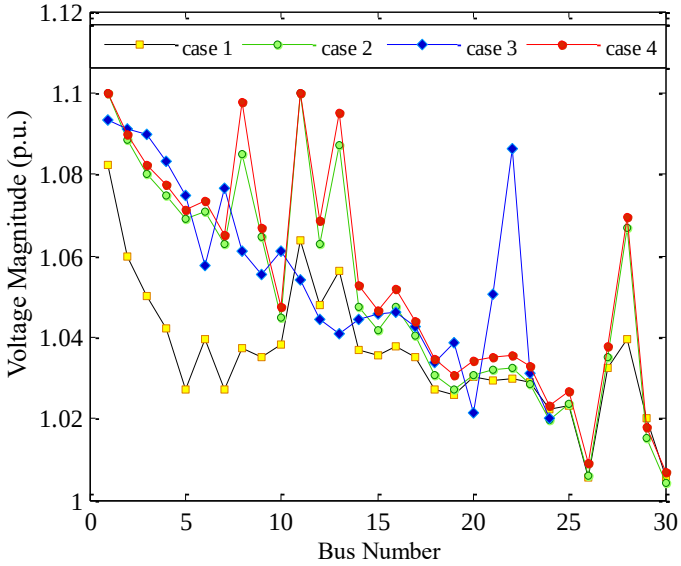

Figure V.17. System voltage profiles for three cases obtained using the SWO algorithm.

Table V.15. Comparison of optimal outcomes generated by the SWO approach with previous studies for cases 2–4.

Case	Algorithm	Total cost ($/h)	Emission (t/h)	Ploss (MW)	DV (p.u.)
Case 2	SWO	**781.0793**	1.7616	5.5112	0.9895
	PSO [27]	781.321	1.762	5.482	1.021
	CBO5 [28]	781.3524	1.7621	5.7806	0.4548
	GWO [29]	781.4	1.76	5.44	1.05
	JS [30]	781.6387	1.7619	5.7738	0.4482
	BO [28]	781.7198	1.7622	5.7826	0.4549
	TLTFWO [31]	781.9791	1.76245	5.7941	0.4654
	CGO [30]	782.195	1.76196	5.76851	0.4538
	FPA [29]	782.8596	1.762312	5.8636	0.453825
	ABC [29]	783.81	1.75	6.06	0.56
	CSA [29]	784.77	1.96	6.47	0.85
	GA [29]	787.84	2.76	6.43	0.87
Case 3	SWO	957.3135	0.0993	**1.7350**	1.3412
	CBO5 [28]	957.8938	0.099827	1.8321	0.5382
	BO [28]	958.5272	0.099828	1.8331	0.5314
Case 4	SWO	**809.3199**	0.8879	5.0089	1.0696
	GWO [29]	809.93	0.86	4.99	1.07
	JS [30]	810.1201	0.8937	5.276	0.4688
	PSO [30]	810.071	0.898	5.128	1.033
	CGO [30]	811.4568	0.9024	5.3779	0.4996
	FPA [30]	811.6664	0.9203	5.3076	0.4656
	TLTFWO [31]	810.8444	0.8814	5.318	0.4729
	ABC [29] [28]	811.26	0.89	5.31	0.47
	SHADE-SF [26]	810.346	0.891	5.276	0.469
	TLBO [31]	811.5219	0.8903	5.378	0.4915
	CSA [29]	811.53	0.92	5.44	0.49
	GA [29]	814.72	1.36	5.63	0.64

V.3.3 Optimal power flow considering SVC devices and renewable energy

To verify the performance of the proposed approach, the same scenario as before was used, and the same algorithm parameters were kept, but SVC devices were added. SVC is not connected to the PV bus, even though it can supply or absorb up to 10 MVAR of reactive power. The optimal placement and sizing of SVC devices were established to maximize the enhancement achieved for each objective function. Simulation results for this study are provided in Table V.16. Two different cases were investigated as follows:

- Case 1: Minimizing the total cost generation.
- Case 2: Minimizing active power losses.

Table V.16 displays the best control settings and SVC device locations obtained by combining the SWO, PSO, and ALO approaches. A comparison analysis reveals that the proposed algorithm significantly reduced the total energy production cost to a remarkable 780.8533 dollars per hour. As shown in the table, this solution outperforms the PSO algorithm (781.9645$/h) and the ALO algorithm (786.3530$/h). Notably, this case represents the most cost-effective solution among Case 2 and cases excluding SVC devices.

According to this table, the active power loss within the grid has reached its lowest possible value, measuring only 1.5545 MW, thanks to the use of the SWO algorithm. This result outperforms both the PSO algorithm (1.7148 MW) and the ALO approach (1.7409 MW), indicating a significant improvement in power system efficiency. Furthermore, when compared to Case 1 and cases without SVC devices, the SWO algorithm has the lowest value.

Table V.16. The findings of the SWO method for the modified IEEE 30-bus system.

Control variables	Min	Case 1			Case 2			Max
		ALO	PSO	SWO	ALO	PSO	SWO	
Pg1(MW)	50	134.9079	134.9079	134.9085	50.0000	50.0000	50.0000	200
Pg2(MW)	20	26.3120	28.2913	29.5664	75.3705	73.7773	66.5411	80
Pw1(MW)	0	44.1303	43.3299	42.6804	75.0000	75.0000	74.9999	75
Pg8(MW)	10	14.8922	10	10.0068	35.0000	35.0000	34.9997	35
Pw2(MW)	0	36.5877	36.7086	34.1839	60.0000	60.0000	59.9733	60
Ps1(MW)	0	32.1742	35.7911	37.4215	37.3672	40.0000	39.39026	50
Vg1($p.u.$)	0.95	1.0994	1.1	1.0999	1.0989	0.95	1.0988	1.1
Vg2($p.u.$)	0.95	1.0955	1.1	1.0881	1.1	1.03908	1.0998	1.1
Vg5($p.u.$)	0.95	1.0835	1.0806	1.0682	1.0921	1.1	1.08970	1.1
Vg8($p.u.$)	0.95	1.0838	1.0864	1.0737	1.0966	1.1	1.0943	1.1
Vg11($p.u.$)	0.95	1.0991	1.1	1.0998	1.0933	1.1	1.0842	1.1
Vg13($p.u.$)	0.95	1.0961	1.0354	1.0983	1.0958	1.1	1.0999	1.1
T11($p.u.$)	0.9	1.0899	1.0683	1.0113	1.0676	0.9307	1.0559	1.1
T12($p.u.$)	0.9	1.0208	1.1	0.9875	1.0898	0.9	0.9171	1.1
T15($p.u.$)	0.9	1.0538	1.1	1.0189	1.0955	0.94105	1.0476	1.1
T36($p.u.$)	0.9	1.0203	1.1	0.9946	1.07	0.9	1.0017	1.1
Parameters	**Min**	**Case 1**			**Case 2**			**Max**
		ALO	**PSO**	**SWO**	**ALO**	**PSO**	**SWO**	
Qg1(MVAR)	-20	-20.0000	-20.0000	-12.0892	-7.7733	-20.0000	-8.9183	150
Qg2(MVAR)	-20	19.2836	10.74646	10.9890	-2.4999	12.8627	4.1742	60
Qw1(MVAR)	-30	31.6166	21.61385	22.5290	20.0501	35.0000	19.3216	35
Qg8(MVAR)	-15	40.0000	26.53246	29.9588	28.3879	40.0000	31.8945	40
Qw2(MVAR)	-25	30.0000	30.0000	17.2164	30.0000	6.5685	14.5519	30
Qs1(MVAR)	-20	25.0000	22.71129	21.9526	25.0000	9.0964	22.6805	25
Q$SVC1$ (MVAR)	-10	-1.6085	10.0000	9.6696	8.3416	10.0000	9.9999	10
Q$SVC2$ (MVAR)	-10	-9.7966	9.9928	9.4099	3.4972	10.0000	9.5688	10

SVC1 bus no.	-	10	3	24	24	24	21	-
SVC2 bus no.	-	22	24	21	28	21	24	-
Total Cost ($/h)		786.3530	781.9645	**780.8533**	969.8838	988.5867	955.7309	-
Emission (t/h)		1.7615	1.76214	1.7619	0.1069	0.1028	0.1005	-
Ploss (MW)		5.6078	5.4583	5.3676	1.7409	1.7148	**1.5545**	-
DV (p.u.)		0.6949	0.89952	1.3421	0.6811	1.7544	1.56912	-

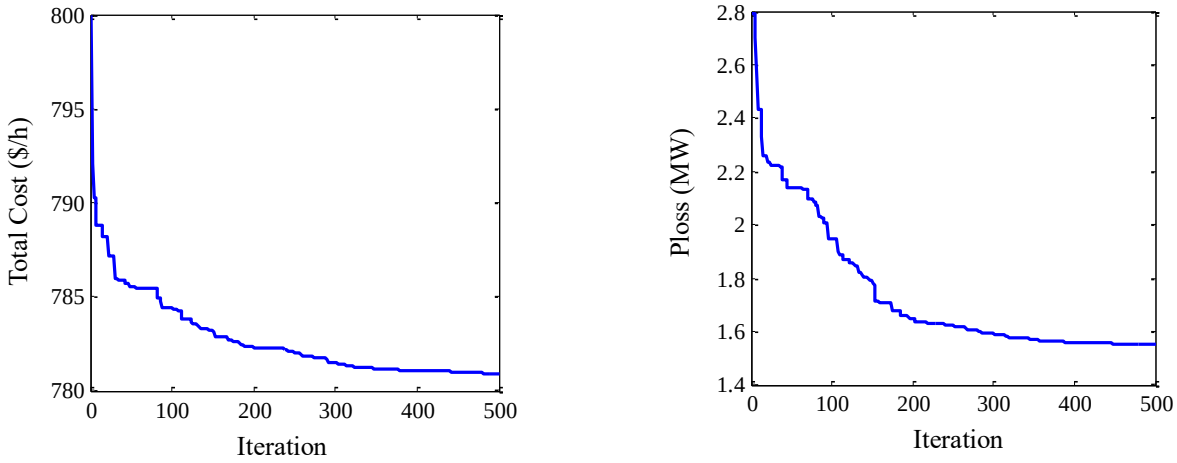

(a) (b)

Figure V.18. The convergence characteristics of the suggested method in three different cases: Case 1(a), Case 2 (b).

Buses 21 and 24 are deemed the best SVC locations acquired in reducing both situations, indicating that integrating this type of FACTS in the optimal proposed locations improves the load capacity in the power system, hence improving network performance. Figure V.18 depicts the convergence behavior of the suggested technique in both Case 1 and Case 2. The suggested technique was used to regulate the capacity of the SVC devices while keeping the voltage magnitude within an acceptable range, as shown in Figure V.19. The state variables in the modified IEEE 30-bus test system were kept within the permitted limits.

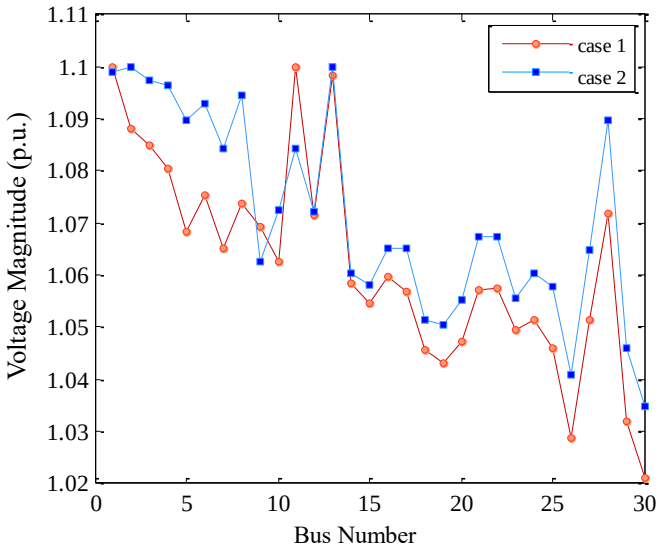

Figure V.19. System voltage profiles for three cases obtained using the SWO algorithm.

V.4. Conclusion

In this chapter, we presented a modern spider wasp optimization algorithm for solving the power flow optimization problem on an IEEE 30-bus test system while taking renewable energy sources and SVC devices into account. Initially, the performance of the proposed algorithm is evaluated on an OPF problem with a single objective, aiming to optimize various objective functions such as fuel cost, gas emissions, total active losses, and voltage deviation. This algorithm was later modified for the multi-objective spider wasp optimizer (MOSWO) algorithm, which is used to solve multi-objective problems such as minimizing fuel cost with gas emissions, minimizing fuel cost with total active losses, and minimizing fuel cost with voltage deviation. The algorithm's results for single and multi-objective optimizations are compared to those from previous studies to validate the accuracy and validity of the proposed approach.

Furthermore, the proposed approach was used to solve the OPF problem with the integration of RES. In this scenario, the algorithm focuses on optimizing single objective functions, such as reducing fuel cost while accounting for valve-point effects (VPE) without integrating renewable energy sources, reducing total active power losses and total generation cost while accounting for all generation sources, as well as reducing total generation cost while accounting for the introduction of a carbon price. The proposed SWO method provided high-quality solutions to OPF issues with random sources. To demonstrate the efficiency of the SWO algorithm, the generated results were thoroughly compared with those produced using different other approaches reported in the literature.

The optimal location and size of the SVC devices were then chosen based on achieving maximum optimization. The results of the proposed algorithm were compared to the PSO and ALO algorithms, and the comparison results for various scenarios demonstrate the proposed algorithm's strength and effectiveness in discovering high-quality solutions with optimal control variables and no constraints violations, making it an attractive tool for addressing complicated energy systems.

Reference

[1] M. Abdel-Basset, R. Mohamed, M. Jameel, and M. Abouhawwash, "Spider wasp optimizer: A novel meta-heuristic optimization algorithm," *Artificial Intelligence Review,* pp. 1-64, 2023.

[2] T. H. B. Huy, P. Nallagownden, K. H. Truong, R. Kannan, D. N. Vo, and N. Ho, "Multi-objective search group algorithm for engineering design problems," *Applied Soft Computing,* vol. 126, p. 109287, 2022.

[3] P. Jangir and I. N. Trivedi, "Non-dominated sorting moth flame optimizer: A novel multi-objective optimization algorithm for solving engineering design problems," *Engineering Technology Open Access Journal,* vol. 2, pp. 17-31, 2018.

[4] K. Lee, Y. Park, and J. Ortiz, "A united approach to optimal real and reactive power dispatch," *IEEE Transactions on power Apparatus and systems,* pp. 1147-1153, 1985.

[5] A. Meng, C. Zeng, P. Wang, D. Chen, T. Zhou, X. Zheng*, et al.*, "A high-performance crisscross search based grey wolf optimizer for solving optimal power flow problem," *Energy,* vol. 225, p. 120211, 2021.

[6] W. Warid, "A Novel Chaotic Rao-2 Algorithm for Optimal Power Flow Solution," *Journal of Electrical and Computer Engineering,* vol. 2022, 2022.

[7] M. Ahmad, N. Javaid, I. A. Niaz, I. Ahmed, and M. A. Hashmi, "An orthogonal learning bird swarm algorithm for optimal power flow problems," *IEEE Access,* vol. 11, pp. 23659-23680, 2023.

[8] P. P. Biswas, P. N. Suganthan, R. Mallipeddi, and G. A. Amaratunga, "Optimal power flow solutions using differential evolution algorithm integrated with effective constraint handling techniques," *Engineering Applications of Artificial Intelligence,* vol. 68, pp. 81-100, 2018.

[9] A. Alanazi, M. Alanazi, Z. A. Memon, and A. Mosavi, "Determining Optimal Power Flow Solutions Using New Adaptive Gaussian TLBO Method," *Applied Sciences,* vol. 12, p. 7959, 2022.

[10] S. Abd El-sattar, S. Kamel, M. Ebeed, and F. Jurado, "An improved version of salp swarm algorithm for solving optimal power flow problem," *Soft Computing,* vol. 25, pp. 4027-4052, 2021.

[11] M. Z. Islam, N. I. A. Wahab, V. Veerasamy, H. Hizam, N. F. Mailah, J. M. Guerrero*, et al.*, "A Harris Hawks optimization based single-and multi-objective optimal power flow considering environmental emission," *Sustainability,* vol. 12, p. 5248, 2020.

[12] L. Jebaraj and S. Sakthivel, "A new swarm intelligence optimization approach to solve power flow optimization problem incorporating conflicting and fuel cost based objective functions," *e-Prime-Advances in Electrical Engineering, Electronics and Energy,* vol. 2, p. 100031, 2022.

[13] M. Al-Kaabi, V. Dumbrava, and M. Eremia, "Single and multi-objective optimal power flow based on hunger games search with pareto concept optimization," *Energies,* vol. 15, p. 8328, 2022.

[14] M. Al-Kaabi, V. Dumbrava, and M. Eremia, "A slime mould algorithm programming for solving single and multi-objective optimal power flow problems with pareto front approach: A case study of the iraqi super grid high voltage," *Energies,* vol. 15, p. 7473, 2022.

[15] Z. Lan, Q. He, H. Jiao, and L. Yang, "An improved equilibrium optimizer for solving optimal power flow problem," *Sustainability,* vol. 14, p. 4992, 2022.

[16] A. Khan, H. Hizam, N. I. bin Abdul Wahab, and M. Lutfi Othman, "Optimal power flow using hybrid firefly and particle swarm optimization algorithm," *Plos one,* vol. 15, p. e0235668, 2020.

[17] M. Ghasemi, S. Ghavidel, M. M. Ghanbarian, M. Gharibzadeh, and A. A. Vahed, "Multi-objective optimal power flow considering the cost, emission, voltage deviation and power losses using multi-objective modified imperialist competitive algorithm," *Energy,* vol. 78, pp. 276-289, 2014.

[18] T. Niknam, M. Narimani, J. Aghaei, and R. Azizipanah-Abarghooee, "Improved particle swarm optimisation for multi-objective optimal power flow considering the cost, loss, emission and voltage stability index," *IET generation, transmission & distribution,* vol. 6, pp. 515-527, 2012.

[19] X. Yuan, B. Zhang, P. Wang, J. Liang, Y. Yuan, Y. Huang*, et al.*, "Multi-objective optimal power flow based on improved strength Pareto evolutionary algorithm," *Energy,* vol. 122, pp. 70-82, 2017.

[20] B. Jeddi, A. H. Einaddin, and R. Kazemzadeh, "A novel multi-objective approach based on improved electromagnetism-like algorithm to solve optimal power flow problem considering the detailed model of thermal generators," *International Transactions on Electrical Energy Systems,* vol. 27, p. e2293, 2017.

[21] M. S. Kumari and S. Maheswarapu, "Enhanced genetic algorithm based computation technique for multi-objective optimal power flow solution," *International Journal of Electrical Power & Energy Systems,* vol. 32, pp. 736-742, 2010.

[22] O. Herbadji, L. Slimani, and T. Bouktir, "Optimal Power Flow With Four Conflicting Objective Functions Using Multiobjective Ant Lion Algorithm: A Case Study of the Algerian Electrical Network," *Iranian Journal of Electrical & Electronic Engineering,* vol. 15, 2019.

[23] Z. Deng, M. D. Rotaru, and J. K. Sykulski, "A study of evolutionary based optimal power flow techniques," in *2016 51st International Universities Power Engineering Conference (UPEC)*, 2016, pp. 1-6.

[24] A. Ali, G. Abbas, M. U. Keerio, M. A. Koondhar, K. Chandni, and S. Mirsaeidi, "Solution of constrained mixed-integer multi-objective optimal power flow problem considering the hybrid multi-objective evolutionary algorithm," *IET Generation, Transmission & Distribution,* vol. 17, pp. 66-90, 2023.

[25] F. Berrouk, H. Bouchekara, A. Chaib, M. Abido, K. Bounaya, and M. Javaid, "A new multi-objective Jaya algorithm for solving the optimal power flow problem," *Journal of Electrical Systems,* vol. 14, pp. 165-181, 2018.

[26] P. P. Biswas, P. Suganthan, and G. A. Amaratunga, "Optimal power flow solutions incorporating stochastic wind and solar power," *Energy conversion and management,* vol. 148, pp. 1194-1207, 2017.

[27] M. Riaz, A. Hanif, S. J. Hussain, M. I. Memon, M. U. Ali, and A. Zafar, "An optimization-based strategy for solving optimal power flow problems in a power system integrated with stochastic solar and wind power energy," *Applied Sciences,* vol. 11, p. 6883, 2021.

[28] M. H. Hassan, S. K. Elsayed, S. Kamel, C. Rahmann, and I. B. M. Taha, "Developing chaotic Bonobo optimizer for optimal power flow analysis considering stochastic renewable energy resources," *International Journal of Energy Research,* vol. 46, pp. 11291-11325, 2022.

[29] I. U. Khan, N. Javaid, K. A. Gamage, C. J. Taylor, S. Baig, and X. Ma, "Heuristic algorithm based optimal power flow model incorporating stochastic renewable energy sources," *IEEE Access,* vol. 8, pp. 148622-148643, 2020.

[30] M. Farhat, S. Kamel, A. M. Atallah, and B. Khan, "Optimal Power Flow Solution Based on Jellyfish Search Optimization Considering Uncertainty of Renewable Energy Sources," *IEEE Access,* vol. 9, pp. 100911-100933, 2021.

[31] M. Alanazi, A. Alanazi, A. Y. Abdelaziz, and P. Siano, "Power Flow Optimization by Integrating Novel Metaheuristic Algorithms and Adopting Renewables to Improve Power System Operation," *Applied Sciences,* vol. 13, p. 527, 2022.

GENERAL CONCLUSION

General conclusion

We have recently seen a significant increase in the communities' need for energy, which has resulted in a significant increase in energy consumption. As a result, it should be emphasized that the search for sustainable and environmentally friendly energy sources has become critical in order to meet this rising demand. In this context, integrating Renewable Energy Sources (RESs) into the electrical grid is a beneficial and effective method of reducing demand for traditional energy sources.

We face additional challenges as we transition to renewable energy sources due to their random and unpredictable nature. As a result, in order to achieve economic integration of renewable energy, we must address these issues by employing optimal analysis in the development and operation of modern energy systems.

The significance of this research is to analyze the optimal power flow (OPF) problem, which takes into account random renewable energy sources, and to provide innovative solutions using modern optimization methods depend on "metaheuristic" algorithms. These recent techniques have a high success rate in resolving difficult OPF issues and achieving peak power system performance.

Furthermore, the current focus is on the development of Flexible AC Transmission Systems (FACTS) as a novel approach to improving the performance and operation of the electric transmission system. These novel solutions are critical for improving the ability of electric networks to transmit power efficiently and reducing grid power losses.

This thesis is divided into three sections. The first section discusses the use of advanced artificial intelligence approaches based on optimization algorithms to solve optimal power flow problems. The second section focuses on resolving the OPF problem while accounting for the energy of random renewables such as wind and solar. The final section addresses a solution to the OPF problem by utilizing FACTS devices and their function in assisting wind and solar energy.

The first section focuses on solving the OPF problem in the IEEE30 bus system, where an extension of the spider wasp optimization algorithm (SWO) is created to transform it into the "multi-objective spider wasp optimization algorithm (MOSWO)." Its effectiveness has been proven on seven mathematical functions, five of which are unconstrained and four of which are restricted. Using three known performance measures, the obtained results were compared

to two algorithms, MAOA and MOGOA, and the best Pareto- optimal solutions were shown. Following that, we talked about how to use single and multiple algorithms to solve single and multiple OPF problems. Thermal plant costs, emissions, active power loss, and voltage standard deviation are among the improved goal functions, which improved by 11.35%, 14.38%, 48.58%, and 92.22% in the single function, respectively. The findings were compared with the PSO, CS, and ALO algorithms, as well as other methods listed in the literature. The results showed that the single and multi-objective spider wasp algorithms beat the other comparison algorithms.

In the second part of the thesis, the spider wasp approach was employed to solve the OPF problem while taking into account the economic integration of solar and wind energy. The first of these objectives was to reduce the price while accounting for the impacts of the valve point and without including renewable energies, as the results of the proposed algorithm demonstrated its superiority over the PSO, CS, and ALO algorithms. The total cost associated with thermal costs of thermal power plants, including penalty and reserve costs, is then decreased, regardless of whether the energy is derived from solar or wind sources. Combining these random energies reduced total generating costs by $53.49, or 6.29%, when compared to the first scenario. The other objective function that was reduced was active energy losses, which were reduced by 47.42% in the absence of renewable sources. The final aim that the suggested method decreased is the total cost, which includes the cost of carbon. It is worth noting here that the rise in total cost is determined by the value of emissions and the carbon rate applied. The results of the last three objectives clearly demonstrated the spider wasp algorithm's superiority over the other methods mentioned in the literature.

In the final section of the thesis, the same scenario was used, with SVCs with optimal values inserted and routed to appropriate locations. When the results of the proposed algorithm were compared to the results of two other algorithms, PSO and ALO, the results were competitive in terms total cost and active power losses. Furthermore, when we compared these results to the absence of SVCs, we observed an important reduction in the two objective functions.

These three parts are critical to the development and improvement of sustainable energy systems, and they promote the future trend of using clean and sustainable energy. It contributes to striking a balance between meeting our energy needs and preserving our environment for future generations.

In the future, we may propose some specific research axes to supplement and improve on what we presented in this work:

- The possibility of expanding the algorithm used to solve optimal power flow problems to larger and more complex power systems, such as Algeria 114-bus power system, can be investigated.
- Studies on evaluating the investment cost of SVCs to improve power system performance and stability can be conducted.
- It's possible to explore and suggest various structures for FACTS gadgets, like TCSC, SSSC, and UPFC. These formats can potentially improve the support for renewable energy and increase the stability of the energy system.
- The impact of events caused by network disturbances, such as overloading and line outages, can be studied in order to evaluate the capacity and efficiency of the proposed control system (OPF-FACTs and REs based on SWO).

Annexe

1. Particle Swarm Optimization (PSO)

```
%_____________________________________________________________________%
%                       Particul swarm Optimization (PSO)
%
%_____________________________________________________________________%
%
%
clc
clear all
close all
tic
%-----------------     Discipline of the objective function -------------%
nom_fonction='F1';
[LB,UB,dim,fobj]=fonction_obj(nom_fonction);

%-----------------            PSO parameters values          -------------
%
n=50;           % population size
wmax=0.9;        % inertia weight
wmin=0.4;        % inertia weight
c1=2;            % acceleration factor
c2=2;            % acceleration factor

%-----------------           PSO main program (start)        -------------
%
maxite=1000;    % set maximum number of iteration
maxrun=1;       % set maximum number of runs need to be

for run=1:maxrun
    % Start PSO initialization-------------------------------------------
%
    for i=1:n
        for j=1:dim
            x0(i,j)=round(LB(j)+rand()*(UB(j)-LB(j)));
        end
    end
    x=x0;            % initial position
    v=zeros(n,dim);  % initial velocity
    % End PSO initialization---------------------------------------------
    % Start evaluating fitness-------------------------------------------
%
    for i=1:n
        f0(i,1)=fobj(x0(i,:));
    end
    % End evaluating fitness---------------------------------------------
    % Start updating pbest and gbest -------------------------------------
%
    [fmin0,index0]=min(f0);
    pbest=x0;               % initial pbest
    gbest=x0(index0,:);     % initial gbest
    % End updating pbest and gbest ---------------------------------------
%
     ite=1;
```

```
    tolerance=1;
    while ite<=maxite

          % Start update inertial weight-----------------------------------
          w=wmax-(wmax-wmin)*ite/maxite;
          % End update inertial weight-------------------------------------
          % Start updating velocity and position---------------------------
%
          for i=1:n
              for j=1:dim
                  v(i,j)=w*v(i,j)+c1*rand()*(pbest(i,j)-x(i,j))...
                                 +c2*rand()*(gbest(1,j)-x(i,j));
              end
          end
          for i=1:n
              for j=1:dim
                  x(i,j)=x(i,j)+v(i,j);
              end
          end
          % End updating velocity and position-----------------------------
          % Start handling boundary violations-----------------------------
%
          for i=1:n
              for j=1:dim
                  if x(i,j)<LB(j)
                     x(i,j)=LB(j);
                  elseif x(i,j)>UB(j)
                     x(i,j)=UB(j);
                  end
              end
          end
          % End handling boundary violations-------------------------------
          % Start evaluating fitness---------------------------------------
%
          for i=1:n
              f(i,1)=fobj(x(i,:));
          end
          % End evaluating fitness-----------------------------------------
          % Start updating pbest and gbest --------------------------------
%
          for i=1:n
              if f(i,1)<f0(i,1)
                 pbest(i,:)=x(i,:);
                 f0(i,1)=f(i,1);
              end
          end
          [fmin,index]=min(f0);    % finding out the best particle
          ffmin(ite,run)=fmin;     % storing best fitness
          ffite(run)=ite;          % storing iteration count
          if fmin<fmin0
             gbest=pbest(index,:);
             fmin0=fmin;
          end
```

```
          % End updating pbest and gbest ---------------------------------
          % Start displaying iterative results----------------------------
%
          if mod(ite,50)==0
             display(['A itération ', num2str(ite), ...
             ' global_best_fitness est ', num2str(fmin0)]);
          end
          % End displaying iterative results------------------------------

          ite=ite+1;
    end
    tim=toc;
    fvalue=fobj(gbest);
    fff(run)=fvalue;
    rgbest(run,:)=gbest;
    disp(sprintf('---------------------------------------'));
end
%-----------------          PSO main program (end)             --------------
%
affichage
%----------             PSO convergence characteristic           -----------
%
ploting
%----------                    (End)   -----------%
```

- **Objective function**

```
%_____________________________________________________________________________%
%                            The objective function %
%_____________________________________________________________________________%
%
%dim      ===>( problem sizing)
%ub and lb ===>(upper and low bounds of variables)

function [lb,ub,dim,fobj] =fonction_obj(F)
   switch F
       case 'F1'
            fobj = @F1;
            dim=10;
            lb=[-100 -100 -100 -100 -100 -100 -100 -100 -100 -100];
            ub=[ 100  100  100  100  100  100  100  100  100  100];
       case 'F2'
            fobj = @F2;
            dim=10;
            lb=[-32 -32 -32 -32 -32 -32 -32 -32 -32 -32];
            ub=[ 32  32  32  32  32  32  32  32  32  32];
       case 'F3'
            fobj = @F3;
            dim=3;
            lb=[-100 -100 -100 ];
            ub=[ 100  100  100 ];
   end
end
function o = F1(x)
```

```
        o=sum(x.^2);
end
function o = F2(x)
        dim=size(x,2);
        o=-20*exp(-.2*sqrt(sum(x.^2)/dim))-
exp(sum(cos(2*pi.*x))/dim)+20+exp(1);
end
function o = F3(x)
        of=10*(x(1)-1)^2+20*(x(2)-2)^2+30*(x(3)-3)^2;
        c0=[];
        c0(1)=x(1)+x(2)+x(3)-5;     % <=0 type constraints
        c0(2)=x(1)^2+2*x(2)-x(3);   % <=0 type constraints
        % defining penalty for each constraint
        for i=1:length(c0)
            if c0(i)>0c(i)=1;
            else c(i)=0;
            end
        end
        penalty=10000;
        % penalty on each constraint violation
        o=of+penalty*sum(c);     % fitness function
end
```

- **Show results**

```
%_____________________________________________________________________%
%                   Results Particul swarm Optimization (PSO)
%
%_____________________________________________________________________%
%
disp('  ')

fprintf('              Final Results of Fitness function by PSO
Optimization \n')
head =['               ------------------------------------------------
'
       '             ¦       Best variables      ¦          value
¦   '
       '             ¦---------------------------¦-------------------------
¦   '

];
disp(head)
k0=dim;
for n0=1:dim
      fprintf('             ¦            X%1.0f             ¦    ', n0),
      fprintf(' %e       ¦', gbest(1,n0)),
      fprintf('      \n')
      if n0==k0

  disp('             ¦------------------------------------------------
-¦ ')
  fprintf('              ¦ Fitness function value          ')
  fprintf('%e', fvalue),fprintf('       ¦')
  fprintf('      \n')
```

```
  disp('             ¦-------------------------------------------------
-¦ ')
  fprintf('              ¦ Elapsed time is           ')
  fprintf('       %1.4f seconds', tim),fprintf('      ¦')
  fprintf('      \n')
  disp('               -------------------------------------------------
-  ')

end
end
```

- **convergence characteristic**

```
%_____________________________________________________________________%
%    convergence characteristic of Particul swarm Optimization (PSO)
%
%_____________________________________________________________________%
%
[bestfun,bestrun]=min(fff);
best_variables=rgbest(bestrun,:);
  figure(1)
  plot(ffmin(1:ffite(bestrun),bestrun),'-k');
  xlabel('Iteration');
  ylabel('Fitness function value');
  title('PSO convergence characteristic')
  if nom_fonction=='F1'
  figure(2)
  xv=-100:2:100; yv=xv;
  f=[];
  Lp=length(xv);
  for i=1:Lp
  for j=1:Lp
  f(i,j)=fobj([xv(i),yv(j)]);
  end
  end
  surfc(xv,yv,f,'LineStyle','none');
  title('Test function')
  xlabel('x_1');
  ylabel('x_2');
  end
```

2. Cuckoo search algorithm (CS)

```
 % ========================================================== %
% Files of the Matlab programs included in the book:        %
% Xin-She Yang, Nature-Inspired Metaheuristic Algorithms,   %
% Second Edition, Luniver Press, (2010).   www.luniver.com  %
% ========================================================== %
% Cuckoo Search for nonlinear constrained optimization      %
% Programmed by Xin-She Yang @ Cambridge University 2009    %
% Usage: cuckoo_spring(25000) or cuckoo_spring;             %

function [bestsol,fval]=cuckoo_search_spring(time)
format long;
help cuckoo_search_spring.m
```

```
if nargin<1,
    % Number of iteraions
    time=2000;
end

disp('Computing ... it may take a few minutes.');

% Number of nests (or different solutions)
n=25;
% Discovery rate of alien eggs/solutions
pa=0.25;

% Simple bounds of the search domain
% Lower bounds and upper bounds
Lb=[0.05 0.25 2.0];
Ub=[2.0  1.3  15.0];

% Random initial solutions
for i=1:n,
nest(i,:)=Lb+(Ub-Lb).*rand(size(Lb));
end

% Get the current best
fitness=10^10*ones(n,1);
[fmin,bestnest,nest,fitness]=get_best_nest(nest,nest,fitness);

N_iter=0;
%% Starting iterations
for t=1:time,

    % Generate new solutions (but keep the current best)
     new_nest=get_cuckoos(nest,bestnest,Lb,Ub);
     [fnew,best,nest,fitness]=get_best_nest(nest,new_nest,fitness);
    % Update the counter
      N_iter=N_iter+n;
    % Discovery and randomization
      new_nest=empty_nests(nest,Lb,Ub,pa) ;

    % Evaluate this solution
      [fnew,best,nest,fitness]=get_best_nest(nest,new_nest,fitness);
    % Update the counter again
      N_iter=N_iter+n;
    % Find the best objective so far
    if fnew<fmin,
        fmin=fnew;
        bestnest=best ;
    end
end %% End of iterations

%% Post-optimization processing
%% Display all the nests
disp(strcat('Total number of iterations=',num2str(N_iter)));
fmin
```

```
bestnest

%% --------------- All subfunctions are list below ------------------
%% Get cuckoos by ramdom walk
function nest=get_cuckoos(nest,best,Lb,Ub)
% Levy flights
n=size(nest,1);
% Levy exponent and coefficient
% For details, see equation (2.21), Page 16 (chapter 2) of the book
% X. S. Yang, Nature-Inspired Metaheuristic Algorithms, 2nd Edition,
Luniver Press, (2010).
beta=3/2;
sigma=(gamma(1+beta)*sin(pi*beta/2)/(gamma((1+beta)/2)*beta*2^((beta-
1)/2)))^(1/beta);

for j=1:n,
    s=nest(j,:);
    % This is a simple way of implementing Levy flights
    % For standard random walks, use step=1;
    %% Levy flights by Mantegna's algorithm
    u=randn(size(s))*sigma;
    v=randn(size(s));
    step=u./abs(v).^(1/beta);

    % In the next equation, the difference factor (s-best) means that
    % when the solution is the best solution, it remains unchanged.
    stepsize=0.01*step.*(s-best);
    % Here the factor 0.01 comes from the fact that L/100 should the
typical
    % step size of walks/flights where L is the typical lenghtscale;
    % otherwise, Levy flights may become too aggresive/efficient,
    % which makes new solutions (even) jump out side of the design domain
    % (and thus wasting evaluations).
    % Now the actual random walks or flights
    s=s+stepsize.*randn(size(s));
   % Apply simple bounds/limits
   nest(j,:)=simplebounds(s,Lb,Ub);
end


%% Find the current best nest
function [fmin,best,nest,fitness]=get_best_nest(nest,newnest,fitness)
% Evaluating all new solutions
for j=1:size(nest,1),
    fnew=fobj(newnest(j,:));
    if fnew<=fitness(j),
       fitness(j)=fnew;
       nest(j,:)=newnest(j,:);
    end
end
% Find the current best
[fmin,K]=min(fitness) ;
best=nest(K,:);
```

```
%% Replace some nests by constructing new solutions/nests
function new_nest=empty_nests(nest,Lb,Ub,pa)
% A fraction of worse nests are discovered with a probability pa
n=size(nest,1);
% Discovered or not -- a status vector
K=rand(size(nest))>pa;

% In real world, if a cuckoo's egg is very similar to a host's eggs, then
% this cuckoo's egg is less likely to be discovered, thus the fitness
should
% be related to the difference in solutions.  Therefore, it is a good idea
% to do a random walk in a biased way with some random step sizes.
nestn1=nest(randperm(n),:);
nestn2=nest(randperm(n),:);
%% New solution by biased/selective random walks
stepsize=rand*(nestn1-nestn2);
new_nest=nest+stepsize.*K;
for j=1:size(new_nest,1)
    s=new_nest(j,:);
  new_nest(j,:)=simplebounds(s,Lb,Ub);
end

% Application of simple constraints
function s=simplebounds(s,Lb,Ub)
  % Apply the lower bound
  ns_tmp=s;
  I=ns_tmp<Lb;
  ns_tmp(I)=Lb(I);

  % Apply the upper bounds
  J=ns_tmp>Ub;
  ns_tmp(J)=Ub(J);
  % Update this new move
  s=ns_tmp;
```

- **Objective function**

```
%% Spring desgn optimization -- objective function
function z=fobj(u)
% The well-known spring design problem
z=(2+u(3))*u(1)^2*u(2);
z=z+getnonlinear(u);

function Z=getnonlinear(u)
Z=0;
% Penalty constant
lam=10^15;

% Inequality constraints
g(1)=1-u(2)^3*u(3)/(71785*u(1)^4);
gtmp=(4*u(2)^2-u(1)*u(2))/(12566*(u(2)*u(1)^3-u(1)^4));
g(2)=gtmp+1/(5108*u(1)^2)-1;
g(3)=1-140.45*u(1)/(u(2)^2*u(3));
```

```
g(4)=(u(1)+u(2))/1.5-1;

% No equality constraint in this problem, so empty;
geq=[];

% Apply inequality constraints
for k=1:length(g),
    Z=Z+ lam*g(k)^2*getH(g(k));
end
% Apply equality constraints
for k=1:length(geq),
   Z=Z+lam*geq(k)^2*getHeq(geq(k));
end

% Test if inequalities hold
% Index function H(g) for inequalities
function H=getH(g)
if g<=0,
    H=0;
else
    H=1;
end
% Index function for equalities
function H=getHeq(geq)
if geq==0,
   H=0;
else
   H=1;
end
% ----------------- end -------------------------------
```

3. Ant lion optimization algorithm (ALO)

```
%_____________________________________________________________________%
%                      Ant Lion Optimizer (ALO)                       %
%_____________________________________________________________________%
clear all
clc
Num_agr=40;          %numbre agents de recherche
Max_iter=500;        %max d'itération
nom_fonction='F1';
[lmin,lmax,dim,fobj]=Detail_fonction(nom_fonction);
% Initialisation des positions de antlions et ants
Num_Limite= size(lmax,2);
% Si un Num_Limite pour tous les variable
if Num_Limite==1
    position_AL=rand(Num_agr,dim).*(lmax-lmin)+lmin;
    position_A =rand(Num_agr,dim).*(lmax-lmin)+lmin;
end
% Si chaque variable ayant un different lmax et lmin
if Num_Limite>1
    for i=1:dim
         lmax_i=lmax(i);
```

```
            lmin_i=lmin(i);
            position_AL(:,i)=rand(Num_agr,1).*(lmax_i-lmin_i)+lmin_i;
            position_A (:,i)=rand(Num_agr,1).*(lmax_i-lmin_i)+lmin_i;
        end
    end
    % save le position d'élite,les positions antlions, courbe de
    convergence,
    % antlions fitness, et ants fitness
    classement_AL=zeros(Num_agr,dim);
    position_AL_Elite=zeros(1,dim);
    fitness_AL_Elite=inf;
    courbe_convergence=zeros(1,Max_iter);
    fitness_AL=zeros(1,Num_agr);
    fitness_A=zeros(1,Num_agr);
    % Calculer les fitness de antlions initiale et elle save
    for i=1:Num_agr
        fitness_AL(1,i)=fobj(position_AL(i,:));
    end
    % classement les fitness de antlions initiale (min ver max)
    [classement_AL_fitness,classement_indexe]=sort(fitness_AL);
    % classement les positions de antlions selon leurs fitness
    for nouvindex=1:Num_agr

    classement_AL(nouvindex,:)=position_AL(classement_indexe(nouvindex),:);
    end
    position_AL_Elite=classement_AL(1,:);
    fitness_AL_Elite=classement_AL_fitness(1);
    % Debut de la boucle à partir de 2eme iteration
    Current_iter=2;
    while Current_iter<=Max_iter
        % Boucle ants random walks
        for i=1:Num_agr
            % Selection antlions pour attraper ants base surle Roulette
            inv_fitness=(1./classement_AL_fitness);
            accumulation= cumsum(inv_fitness);
            val= rand()* accumulation(end);
            choix_index = -1;
            index=1;
            while index <= Num_agr & choix_index==-1
                if accumulation(index) > val
                   choix_index = index;
                end
                index=index+1;
            end
            Rolette_index=choix_index;
            if  Rolette_index==-1
                Rolette_index=1;
            end
            % RA est random walk autour antlion selectionne par rolette
            antlion=classement_AL(Rolette_index,:);
            if  size(lmin,1) ==1 && size(lmin,2)==1  %Vérifier si les
    limites sont scalaires
                lmin=ones(1,dim)*lmin;
```

```
            lmax=ones(1,dim)*lmax;
        end
        if  size(lmin,1) > size(lmin,2)          %Vérifier si les
vecteurs de limitessont
            lmin=lmin';                          %horizontaux ou
verticaux
            lmax=lmax';
        end
        Ira=1;                                   %Ira est le ratio
        if  Current_iter>Max_iter/10
            Ira=1+100*(Current_iter/Max_iter);
        end
        if  Current_iter>Max_iter/2
            Ira=1+1000*(Current_iter/Max_iter);
        end
        if  Current_iter>Max_iter*(3/4)
            Ira=1+10000*(Current_iter/Max_iter);
        end
        if  Current_iter>Max_iter*(0.9)
            Ira=1+100000*(Current_iter/Max_iter);
        end
        if  Current_iter>Max_iter*(0.95)
            Ira=1+1000000*(Current_iter/Max_iter);
        end
        % Diminution les limites pour converger vers l'antlion
        lmind=lmin/(Ira);
        lmaxd=lmax/(Ira);
        % nouvelle intervalle autour de l'antlion Elite
        if  rand<0.5
            lminR=lmind+antlion;
        else
            lminR=-lmind+antlion;
        end
        if  rand>=0.5
            lmaxR=lmaxd+antlion;
        else
            lmaxR=-lmaxd+antlion;
        end
        % Cette fonction crée n Random walk et normalise selon lmin
etlmax
        for j=1:dim
            X = [0 cumsum(2*(rand(Max_iter,1)>0.5)-1)'];
            a = min(X);
            b = max(X);
            c = lminR(j);
            d = lmaxR(j);
            X_norm=((X-a).*(d-c))./(b-a)+c;
            RWs(:,j)=X_norm;
        end
        RA=RWs;

        % RE est random walk autour antlion Elite
        antlion=position_AL_Elite;
```

```
        if  rand<0.5
            lminE=lmind+antlion;
        else
            lminE=-lmind+antlion;
        end
        if  rand>=0.5
            lmaxE=lmaxd+antlion;
        else
            lmaxE=-lmaxd+antlion;
        end
        % Cette fonction crée n Random walk et normalise selon lmin
etlmax
        for j=1:dim
            X = [0 cumsum(2*(rand(Max_iter,1)>0.5)-1)'];
            a = min(X);
            b = max(X);
            c = lminE(j);
            d = lmaxE(j);
            X_norm=((X-a).*(d-c))./(b-a)+c;
            RWs(:,j)=X_norm;
        end
        RE=RWs;


        position_A (i,:)= (RA(Current_iter,:)+RE(Current_iter,:))/2; %
position Ants

    end

    %--------------------------   Fin Random walk   --------------------
---
    for i=1:Num_agr
        % Vérification des limites et ramenez les antlions et ants dans
        % l'espace de recherche
        Flag4lmax=position_A(i,:)>lmax;
        Flag4lmin=position_A(i,:)<lmin;

position_A(i,:)=(position_A(i,:).*(~(Flag4lmax+Flag4lmin)))+lmax.*Flag4l
max+lmin.*Flag4lmin;
        fitness_A(1,i)=fobj(position_A(i,:));
    end
   % Mettre à jour les positions et fitness de l'antlion base sur ants
   % si ant devient plus proche antlion nous supposons qu'il a été
attrapé
   % par l'antlion (la mise à jour des positions de l'antlion defini
comme
   % la construire de nouvelle piège.
    double_population=[classement_AL;position_A];
    double_fitness=[classement_AL_fitness fitness_A];

    [classement_double_fitness Ind]=sort(double_fitness);
    classement_double_population=double_population(Ind,:);
```

```
        fitness_AL=classement_double_fitness(1:Num_agr);
        classement_AL=classement_double_population(1:Num_agr,:);
        % Actualiser la position de l'élite si des antlinons deviennent plus
    mieux
        if fitness_AL(1)<fitness_AL_Elite
        position_AL_Elite=classement_AL(1,:);
        fitness_AL_Elite=fitness_AL(1);
        end
       % Garder l'élite dans la population
        classement_AL(1,:)=position_AL_Elite;
        fitness_AL(1)=fitness_AL_Elite;
        % Affiche l'itération et le meilleur optimum obtenus jusqu'à présent
        if mod(Current_iter,1)==0
            display(['A itération ', num2str(Current_iter), ...
            ' le fitness d elite est ', num2str(fitness_AL_Elite)]);
        end
        Convergence_curve(Current_iter)=fitness_AL_Elite;
        Current_iter=Current_iter+1;
    end
    %--------------------       plot fonction      -------------------------
    ---

    figure('Position',[350 350 660 290])
    subplot(1,2,1);
    xv=-100:2:100; yv=xv;
    f=[];
    Lp=length(xv);
    for i=1:Lp
        for j=1:Lp
            f(i,j)=fobj([xv(i),yv(j)]);
        end
    end
    surfc(xv,yv,f,'LineStyle','none');
    title('Test function')
    xlabel('x_1');
    ylabel('x_2');
    subplot(1,2,2);
    semilogy (Convergence_curve,'r')
    axis tight
```

- **Objective function**

```
% Ce fiche containt information de la fonction objective
%dim                dimensionnement de probleme
%lmax               limite max de variable
%lmin               limite min de variable

function [lb,ub,dim,fobj] = Detail_fonction(F)
        switch F
                case 'F1'
                fobj = @F1;
                lb=-100;
                ub=100;
                dim=10;
```

```
                case 'F2'
                    fobj = @F2;
                    lb=-32;
                    ub=32;
                    dim=10;

        end
end
% F1
function o = F1(x)
o=sum(x.^2);
end
% F2
function o = F2(x)
dim=size(x,2);
o=-20*exp(-.2*sqrt(sum(x.^2)/dim))-exp(sum(cos(2*pi.*x))/dim)+20+exp(1);
end
```

4. Spider wasp optimizer (SWO)

```
clear all
clc
SW_no=100; % Number of search agents (Spider Wasps)
Tmax=50000; % Maximum number of Function evaluations
RUN_NO=30; %% Number of independent runs
Fun_id=[1,2,3,4,5,6,7,8,9,10,11,12,13,14,15,16,17,18,19,20,21,22,23,24,2
5,26,27,28,29,30];
fhd=str2func('cec17_func'); %%Default Benchmark
cec=2;
if cec==1 %% CEC-2014
    fhd=str2func('cec14_func');
    benchmarksType='cec14_func';
elseif cec==2 %% CEC-2017
    fhd=str2func('cec17_func');
    benchmarksType='cec17_func';
elseif cec==3 %% CEC-2020
    fhd=str2func('cec20_func');
    benchmarksType='cec20_func';
elseif cec==4 %% CEC-2022
    fhd=str2func('cec22_func');
    benchmarksType='cec22_func';
end
for i=1:30
 for j=1:RUN_NO
  if cec==2 && i==2
       continue;
  elseif cec==3 && i>10
       return
  elseif cec==4 && i>12
       return
  end
  [lb,ub,dim]=Get_Functions_detailsCEC(Fun_id(i));
  fobj=Fun_id(i);
```

```
   [Best_score,Best_pos,Convergence_curve]=SWO(100,Tmax,ub,lb,dim,fobj,fhd)
   ;
     fitness(1,j)=Best_score;
   end
   fprintf(['benchmark
   \t',num2str(cec),'\t','Function_ID\t',num2str(i),'\tAverage
   Fitness:',num2str(mean(fitness(1,:)),20),'\n']);
   %% Drawing Convergence Curve %%
   figure(i)
   h=semilogy(Convergence_curve,'-<','MarkerSize',8,'LineWidth',1.5);
   h.MarkerIndices = 1000:1000:Tmax;
   xlabel('Iteration');
   ylabel('Best Fitness obtained so-far');
   axis tight
   grid off
   box on
   legend({'SWO'});
   end


%_____________________________________________________________________%
%  Spider Wasp Optimizer (SWO) source codes demo 1.0                  %
%                                                                     %
%  Developed in MATLAB R2019A                                         %
%                                                                     %
%  Author and programmer: Reda Mohamed (E-mail: redamoh@zu.edu.eg) &
Mohamed Abdel-Basset (E-mail: mohamedbasset@ieee.org)
%
%                                                                     %
%   Main paper: Abdel-Basset, M., Mohamed, R.
%
%               Spider Wasp Optimizer: A Novel Meta-Heuristic Optimization
Algorithm,                          %
%               Artificial Intelligence Review, in press              %
%                  %
%                                                                     %
%_____________________________________________________________________%
% The Spider Wasp Optimizer
function
[Best_score,Best_SW,Convergence_curve]=SWO(SearchAgents_no,Tmax,ub,lb,dim,f
obj,fhd)
%%%%-------------------Definitions--------------------------%%
%%
Best_SW=zeros(1,dim); % A vector to include the best-so-far spider
wasp(Solution)
Best_score=inf; % A Scalar variable to include the best-so-far score
Convergence_curve=zeros(1,Tmax);
%%-------------------Controlling parameters--------------------------%%
%%
TR=0.3; %% Representing the trade-off probability between hunting and
mating behaviours.
Cr=0.2; %% The Crossover probability
N_min=20; %% Representing the minimum population size.
```

```
%%---------------Initialization----------------------%%
%%
Positions=initialization(SearchAgents_no,dim,ub,lb); % Initialize the
positions of spider wasps
t=0; %% Function evaluation counter
%%---------------------Evaluation-----------------------%%
for i=1:SearchAgents_no
    %% Test suites of CEC-2014, CEC-2017, CEC-2020, and CEC-2022
    SW_Fit(i)=feval(fhd, Positions(i,:)',fobj);
    % Update the best-so-far solution
    if SW_Fit(i)<Best_score % Change this to > for maximization problem
       Best_score=SW_Fit(i); % Update the best-so-far score
       Best_SW=Positions(i,:); % Update te best-so-far solution
    end
end
% Main loop
while t<Tmax
    %%
    a=2-2*(t/Tmax); % a decreases linearly from 2 to 0
    a2=-1+-1*(t/Tmax); % a2 linearly dicreases from -1 to -2 to calculate l
in Eq. (8)
    k=(1-t/Tmax); %% k decreases linearly from 1 to 0 (Eq. (13))
    JK=randperm(SearchAgents_no); %% A randomly-generated permutation of
the search agent's indices
    if rand<TR %% 3.2   Hunting and nesting behavior
       % Update the Position of search agents
       for i=1:SearchAgents_no
          r1=rand(); % r1 is a random number in [0,1]
          r2=rand(); % r2 is a random number in [0,1]
          r3=rand(); % r3 is a random number in [0,1]
          p = rand();  % p is a random number in [0,1]
          C=a*(2*r1-1);  % Eq. (11) in the paper
          l=(a2-1)*rand+1;   % The parameter in Eqs. (7) and (8)
          L=Levy(1); %% L is a Levy-based number
          vc = unifrnd(-k,k,1,dim); %% The vector in Eq. (12)
          rn1=randn; %% rn1 is a normal distribution-based number
          %%
          O_P=Positions(i,:); %% Storing the current position of the ith
solution
          %%
          for j=1:size(Positions,2)
            if i<k*SearchAgents_no
               if p<(1-t/Tmax) %% 3.2.1   Searching stage (Exploration)
                   if r1<r2
                      m1=abs(rn1)*r1; %% Eq. (5)
                      Positions(i,j)=Positions(i,j)+m1*(Positions(JK(1),j)-
Positions(JK(2),j)); %% Eq. (4)
                   else
                      B=1/(1+exp(l)); %% Eq. (8)
                      m2=B*cos(l*2*pi); %% Eq. (7)

Positions(i,j)=Positions(JK(i),j)+m2*(lb(j)+rand*(ub(j)-lb(j))); %% Eq. (6)
                   end %% End If
```

```
                else %% 3.2.2  Following and escaping stage (exploration and
exploitation)
                    if r1<r2

Positions(i,j)=Positions(i,j)+C*abs(2*rand*Positions(JK(3),j)-
Positions(i,j)); %% Eq. (10)
                    else
                       Positions(i,j)=Positions((i),j).*vc(j); %% Eq. (12)
                    end %% End If
                end
             else
                 if r1<r2
                    Positions(i,j)=Best_SW(j)+cos(2*l*pi)*(Best_SW(j)-
Positions(i,j));      % Eq. (16)
                 else

Positions(i,j)=Positions(JK(1),j)+r3*abs(L)*(Positions(JK(1),j)-
Positions(i,j))+(1-r3)*(rand>rand)*(Positions(JK(3),j)-Positions(JK(2),j));
% Eq. (17)
                 end %% End if
           end %% End if
         end %% End Inner If
         %% Return the search agents that exceed the search space's bounds
         for j=1:size(Positions,2)
             if  Positions(i,j)>ub(j)
                  Positions(i,j)=lb(j)+rand*(ub(j)-lb(j));
             elseif  Positions(i,j)<lb(j)
                  Positions(i,j)=lb(j)+rand*(ub(j)-lb(j));
             end
         end
         SW_Fit1=feval(fhd, Positions(i,:)',fobj); %% The fitness value of
the newly generated spider
         % Memory Saving and Updating the best-so-far solution
         if SW_Fit1<SW_Fit(i) % Change this to > for maximization problem
              SW_Fit(i)=SW_Fit1; % Update the local best fitness
              % Update the best-so-far solution
              if SW_Fit(i)<Best_score % Change this to > for maximization
problem
                Best_score=SW_Fit(i); % Update best-so-far fitness
                Best_SW=Positions(i,:); % Update best-so-far position
              end
         else
              Positions(i,:)=O_P; %% Return the last best solution
obtained by the ith solution
         end
         t=t+1;
         if t>Tmax
             break;
         end
         Convergence_curve(t)=Best_score;
       end %% Enter Outer For
       %% Mating behavior
    else
```

```
        % Update the Position of search agents
        for i=1:SearchAgents_no
            l=(a2-1)*rand+1;    %% The parameter in Eqs. (7) and (8)
            SW_m=zeros(1,dim);  %% including the spider wasp male
            O_P=Positions(i,:); %% Storing the current position of the ith
solution
          %% The Step sizes used to generate the male spider with a high
quality
            if SW_Fit(JK(1))<SW_Fit(i)  %Eq. (23)
               v1=Positions(JK(1),:)-Positions(i,:);
            else
               v1=Positions(i,:)-Positions(JK(1),:);
            end
            if SW_Fit(JK(2))<SW_Fit(JK(3)) %Eq. (24)
               v2=Positions(JK(2),:)-Positions(JK(3),:);
            else
               v2=Positions(JK(3),:)-Positions(JK(2),:);
            end
            %%
            rn1=randn; %% rn1 is a normal distribution-based number
            rn2=randn; %% rn1 is a normal distribution-based number
            for j=1:size(Positions,2)
                SW_m(j)= Positions(i,j)+(exp(l))*abs(rn1)*v1(j)+(1-
exp(l))*abs(rn2)*v2(j);      % Eq. (22)
                if(rand<Cr) %% Eq. (21)
                   Positions(i,j)=SW_m(j);
                end
            end
            %% Return the search agents that exceed the search space's
bounds
            for j=1:size(Positions,2)
               if  Positions(i,j)>ub(j)
                    Positions(i,j)=lb(j)+rand*(ub(j)-lb(j));
               elseif  Positions(i,j)<lb(j)
                    Positions(i,j)=lb(j)+rand*(ub(j)-lb(j));
               end
            end
            SW_Fit1=feval(fhd, Positions(i,:)',fobj);; %% The fitness value
of the newly generated spider
            % Memory Saving and Updating the best-so-far solution
            if SW_Fit1<SW_Fit(i) % Change this to > for maximization problem
                SW_Fit(i)=SW_Fit1; % Update the local best fitness
                % Update the best-so-far solution
                if SW_Fit(i)<Best_score % Change this to > for maximization
problem
                  Best_score=SW_Fit(i); % Update best-so-far fitness
                  Best_SW=Positions(i,:); % Update best-so-far position
                end
            else
                Positions(i,:)=O_P; %% Return the last best solution
obtained by the ith solution
            end
            t=t+1;
```

```
            if t>Tmax
               break;
            end
            Convergence_curve(t)=Best_score;
        end %% End For
    end %% End If
    %% Population reduction %%
    SearchAgents_no=fix(N_min+(SearchAgents_no-N_min)*((Tmax-t)/Tmax)); %%
Eq. (25)
end %% End While
Convergence_curve(t-1)=Best_score;
end
% Draw n Levy flight sample
function L=Levy(d)
beta=3/2;
sigma=(gamma(1+beta)*sin(pi*beta/2)/(gamma((1+beta)/2)*beta*2^((beta-
1)/2)))^(1/beta);
u=randn(1,d)*sigma;
v=randn(1,d);
step=u./abs(v).^(1/beta);
L=0.05*step;
end
%_____________________________________________________________________%
%  Spider Wasp Optimizer (SWO) source codes demo 1.0               %
%                                                                     %
%  Developed in MATLAB R2019A                                      %
%                                                                     %
%  Author and programmer: Reda Mohamed (E-mail: redamoh@zu.edu.eg) &
Mohamed Abdel-Basset (E-mail: mohamedbasset@ieee.org)
%
%                                                                     %
%   Main paper: Abdel-Basset, M., Mohamed, R.
%
%               Spider Wasp Optimizer: A Novel Meta-Heuristic Optimization
Algorithm,                          %
%               Artificial Intelligence Review, in press              %
%                  %
%                                                                     %
%_____________________________________________________________________%


 % This function initialize the first population of search agents

function Positions=initialization(SearchAgents_no,dim,ub,lb)
Boundary_no= length(ub); % numnber of boundaries
% If the boundaries of all variables are equal and user enter a signle
% number for both ub and lb
if Boundary_no==1
     Positions=rand(SearchAgents_no,dim).*(ub-lb)+lb;
end
% If each variable has a different lb and ub
if Boundary_no>1
    for i=1:dim
        ub_i=ub(i);
```

```
        lb_i=lb(i);
         Positions(:,i)=rand(SearchAgents_no,1).*(ub_i-lb_i)+lb_i;
    end
end

%_____________________________________________________________________%
%  Spider Wasp Optimizer (SWO) source codes demo 1.0                  %
%                                                                     %
%  Developed in MATLAB R2019A                                         %
%                                                                     %
%  Author and programmer: Reda Mohamed (E-mail: redamoh@zu.edu.eg) &
Mohamed Abdel-Basset (E-mail: mohamedbasset@ieee.org)
%
%                                                                     %
%   Main paper: Abdel-Basset, M., Mohamed, R.
%
%               Spider Wasp Optimizer: A Novel Meta-Heuristic Optimization
Algorithm,                          %
%               Artificial Intelligence Review, in press              %
%                  %
%_____________________________________________________________________%
% This function containts full information and implementations of the
benchmark
% functions in Table 1, Table 2, and Table 3 in the paper
% lb is the lower bound: lb=[lb_1,lb_2,...,lb_d]
% up is the uppper bound: ub=[ub_1,ub_2,...,ub_d]
% dim is the number of variables (dimension of the problem)
function [lb,ub,dim] = Get_Functions_detailsCEC(F)
switch F
    case 1
        dim=10;
        lb=-100*ones(1,dim);
        ub=100*ones(1,dim);

    case 2
       dim=10;
        lb=-100*ones(1,dim);
        ub=100*ones(1,dim);

    case 3
      dim=10;
        lb=-100*ones(1,dim);
        ub=100*ones(1,dim);

    case 4
        dim=10;
        lb=-100*ones(1,dim);;
        ub=100*ones(1,dim);;

    case 5
         dim=10;
        lb=-100*ones(1,dim);;
        ub=100*ones(1,dim);;
```

```
    case 6
         dim=10;
        lb=-100*ones(1,dim);;
        ub=100*ones(1,dim);;
    case 7
        dim=10;
        lb=-100*ones(1,dim);;
        ub=100*ones(1,dim);;

    case 8
       dim=10;
        lb=-100*ones(1,dim);;
        ub=100*ones(1,dim);;

    case 9
dim=10;
        lb=-100*ones(1,dim);;
        ub=100*ones(1,dim);;

    case 10
         dim=10;
        lb=-100*ones(1,dim);;
        ub=100*ones(1,dim);;

    case 11
       dim=10;
        lb=-600*ones(1,dim);;
        ub=600*ones(1,dim);;

    case 12
        dim=10;
        lb=-100*ones(1,dim);;
        ub=100*ones(1,dim);;

    case 13
        dim=10;
        lb=-100*ones(1,dim);;
        ub=100*ones(1,dim);;

    case 14
         dim=10;
        lb=-100*ones(1,dim);;
        ub=100*ones(1,dim);;

    case 15
         dim=10;
        lb=-100*ones(1,dim);;
        ub=100*ones(1,dim);;

    case 16
         dim=10;
        lb=-100*ones(1,dim);;
```

```
    ub=100*ones(1,dim);;

 case 17
      dim=10;
    lb=-100*ones(1,dim);;
    ub=100*ones(1,dim);;

 case 18
      dim=10;
    lb=-100*ones(1,dim);;
    ub=100*ones(1,dim);;

 case 19
      dim=10;
    lb=-100*ones(1,dim);;
    ub=100*ones(1,dim);;


 case 20
      dim=10;
    lb=-100*ones(1,dim);;
    ub=100*ones(1,dim);;


 case 21
      dim=10;
    lb=-100*ones(1,dim);;
    ub=100*ones(1,dim);;


 case 22
      dim=10;
    lb=-100*ones(1,dim);;
    ub=100*ones(1,dim);;


 case 23
      dim=10;
    lb=-100*ones(1,dim);;
    ub=100*ones(1,dim);;

       case 24
   dim=10;
    lb=-100*ones(1,dim);;
    ub=100*ones(1,dim);;

      case 25
      dim=10;
    lb=-100*ones(1,dim);;
    ub=100*ones(1,dim);;

case 26
    dim=10;
```

```
        lb=-100*ones(1,dim);;
        ub=100*ones(1,dim);;

    case 27
        dim=10;
        lb=-100*ones(1,dim);;
        ub=100*ones(1,dim);;

    case 28
         dim=10;
        lb=-100*ones(1,dim);;
        ub=100*ones(1,dim);;

    case 29
         dim=10;
        lb=-100*ones(1,dim);;
        ub=100*ones(1,dim);;

    case 30
         dim=10;
        lb=-100*ones(1,dim);;
        ub=100*ones(1,dim);;

  end
end
```